GL01245

University of Utah Research Institute

Magnetotelluric Data Acquisition System

by

Steven L. Olsen, John A. Stodt, Philip

E. Wannamaker and Gerald W. Hohmann

It is convenient to consider the present state of our MT instrumentation in terms of its hardware and its operating software.

a) **MT System Hardware.** - Our MT system is currently a five-channel, single-station unit, with the capability to handle either coils or a SQUID magnetometer. Data acquisition and processing is under control of a Digital Equipment Corporation (DEC) LSI 11/23 computer operating under control of RT-11. The computer system currently consists of the 11/23 processor with floating point unit, 192 Kbytes of RAM memory, an 8 Mbyte Winchester disk, two DEC TU 58 tape drives, a DEC VT 100 video text terminal, and a DEC LA-50 printer. This equipment is mounted in a half-ton 4 X 4 pickup with a camper shell.

Analog equipment consists of preamplifiers and signal conditioning hardware to handle the electric and magnetic field data, analog-to-digital conversion hardware, and an 8-channel strip chart recorder.

Electric fields are measured with a 5-electrode configuration utilizing low-noise, lead-lead chloride electrodes of our own design. Our standard configuration is 100 meter lengths in a cross configuration, located approximately 100 meters from the recording truck. Connections are made at the central ground electrode to a remote programmable electric field signal conditioner consisting of low noise differential preamplifiers, high-pass and notch filters, offset control, and line drivers. The gain in this box is a maximum of 64 dB and is programmable. The high-pass filter is in/out selectable and has three programmable cutoffs. The 60/180 Hz notch filter is in/out selectable and can be tuned over five percent of the center frequency at 60 Hz or 180 Hz for maximum rejection of both harmonics. The offset control is independently programmable in each channel to

provide SP buck-out for DC coupled operation. These options provide control to handle a wide range of field conditions. Constant-current line drivers are utilized for low-noise transmission of data to the recording truck.

We have currently achieved an overall instrument noise floor of 40 $nV/Hz^{1/2}$ at 1 Hz in the electric field measurement, with a 10 K-ohm source resistance. This is more than a factor of two better than the figure of 100 $nV/Hz^{1/2}$ recently reported by Clarke et al. (1983a) for the intrinsic noise of the electric field preamplifiers in their remote reference MT system. Furthermore, the intrinsic resistance of our custom-fabricated lead-lead chloride electrodes is approximately 30 ohms. They have been designed with a large metal-electrolyte surface area to reduce intrinsic noise, and a large ground contact surface area to minimize contact resistance. We have obtained electrode ground resistances as low as 50 ohms with these electrodes.

Our system was initially designed to utilize a SQUID magnetometer. However, a recent donation by the Mobil Oil Co. of Geotronics coils and associated hardware, combined with an instrument failure in our SQUID magnetometer, has prompted us to modify our system so that it is capable of collecting magnetic field data using either coils or a SQUID magnetometer. Coils for the horizontal field measurement have a peak sensitivity of 140 mV/gamma at approximately 100 Hz. Coils for the vertical field measurement are smaller, with a peak sensitivity of 60 mV/gamma at 100 Hz. The coils came with chopper-stabilized preamplifiers designed by Mobil Oil Co. having an intrinsic noise of 60 nV peak-to-peak in a 100-Hz bandwidth. In-house modifications to their circuitry has resulted in a reduction of intrinsic noise to 40 nV peak-to-peak in a 100-Hz bandwidth.

The magnetic field sensors are located near the center of the electric field sensor array. Signals from the SQUID magnetometer are transmitted over the manufacturer's transmission cables, and are processed at the recording truck with the manufacturer's

signal conditioning and control units, which provide switch-selectable gain, low-pass, and notch filter control. Alternatively, signals from the induction coils are fed immediately into a preamplifier in the coil head and then to a control box for transmission to the recording truck. The coil control box contains remote switching control, line drivers, and battery power. A high- or low-gain circuit in the coil preamps is switch selectable from the recording truck. The high-gain circuit provides an additional 20 dB of gain and incorporates a single pole low-pass filter with a cutoff at 4 Hz to provide attenuation at the high frequencies.

At the recording truck, high-level signals are passed through line receivers to programmable signal conditioning cards that prepare the signals for digitization. The signal conditioning cards (one for each channel) plug into the backplane of the computer and provide programmable anti-alias and high-pass filtering options, and a final programmable gain stage. The output of these cards is fed to a card that contains sample-and-hold circuitry and a programmable time base to control sampling rates. Digitization is performed by a Data Translation 14-bit A/D converter. The programmable time base and A/D cards also plug into the backplane of the computer and are controlled directly by software. Measurements have shown that the noise in the programmable signal conditioning cards is sufficiently low that the full dynamic range of the 14 bit A/D is utilized; the limiting system noise is the noise of the sensors and the first stage preamplifiers.

Power for the system, with the exception of the battery powered coil preamplifiers and control box, is supplied by a 4 KVA gasoline motor generator. Power for the computer system and analog hardware is fed through an uninterruptable power supply which provides regulation and battery backup in case of generator failure. The power system is trailer mounted and is operated approximately 30 meters from the recording truck, in the opposite direction from the measurement sensors. The power supply is well

isolated and does not interfere with the measurements.

b) **MT System Software.** - The software which controls data acquisition and reduction in real time is menu driven under control of an operator at the video terminal. Two-letter commands are typed to execute subroutines which accomplish specific tasks. These tasks include hardware set up, data collection, computation of spectra with archiving, computation of impedance and tipper functions and other related parameters, file manipulation, and system calibration.

Our MT system is set up to acquire data in three bands. Data below 2.5 Hz are acquired in two bands using a modified version of the real-time decimation algorithm developed by Weight et al. (1977) and Bostick and Smith (1979). This algorithm computes spectra at the sixth and eighth harmonics of 32-point data sequences. The sampling rate is thus four points per cycle of the eighth harmonic. An appropriate analog low-pass filter is employed initially to avoid aliasing. Correlations with sine and cosine sequences to which a Hanning window has been applied are performed on 32-point segments of the incoming data to compute a set of periodograms at the two harmonics. The data are then filtered digitally and decimated by two. A filtered 32-point data segment with a sampling frequency half that of the initial data sequence is created from two of these decimated data segments. Correlations with the windowed sine and cosine sequences are performed on the filtered data, and periodograms are computed at the sixth and eighth harmonics of the decimated data sequences. The filtering, decimation, and correlation process is continued to obtain sixth and eighth harmonic spectral estimates an octave apart to as low a frequency as desired. The filtering and decimation process must continue uninterrupted until data acquisition is terminated. However, all periodogram estimates from individual 32-point data sequences at a given level need not be incorporated into the spectral averages, as described shortly.

Data from 2.5 Hz to .25 Hz are recorded with a two-pole, high-pass filter having a

cutoff at .3 Hz to limit the bandwidth, allowing high gain settings to be utilized. Data below .25 Hz are recorded with this filter out. We intend to modify this filter to have a low-frequency cutoff at 0.1 Hz. A four-pole, anti-alias filter with a knee at 2.5 Hz or .25 Hz, respectively, has been chosen for low-frequency runs. Additional pre-whitening filters with appropriate cutoffs can be selected to provide proper spectral shaping with either coils or SQUID magnetometer.

Program control is identical for data acquisition in the mid and low bands. The operator first configures the hardware appropriately, enters data file header information, and computes the response of the hardware configuration. The hardware configuration and response factors are stored as part of the spectral data file header. The operator then calls a program which initiates A/D conversion and storage of raw data into a circular data buffer in memory via direct memory transfers (DMA). This program is an interrupt service routine to handle "data ready" interrupts from the A/D converter by initiating a DMA transfer. At other times, the processor is free to carry out other tasks under control of the operator.

The primary task during a data run is to compute and archive spectra. The operator calls a subroutine that automatically carries out these tasks. This routine is interruptable from the keyboard to allow the operator to check the status of a run by computing coherencies or impedance and tipper quantities. Incoming data are buffered during the interrupt. The buffer is 32,767 samples long and provides 1.4 hours of buffering for five channels of data at a 1-Hz sample rate, which is the sample rate of our low-band run. A run is terminated under operator control, or if the circular data buffer is overrun. Data can be acquired and spectra computed and archived indefinitely in both the mid and low bands.

Data above 2.5 Hz are acquired differently, because the processor becomes 100 percent occupied by the data acquisition, decimation, spectral computation, and

archiving algorithms at a data frequency between 2.5 Hz and 5 Hz. If the decimation algorithm is used at higher frequencies, data are acquired only until the buffer is overrun. The remaining data in the buffer can be processed and a new run initiated, but this is not efficient because of the large amount of time spent processing data compared to the time spent collecting data. In particular, a large amount of time is spent by the decimation algorithm performing digital filtering.

At these higher frequencies, it is more efficient to avoid digital filtering and decimation. Instead, data are acquired in 32-point buffers, and windowed sixth and eighth harmonic sine and cosine correlations are performed on the 32-point data sequences. The eighth harmonic lies at the 3-dB knee of the analog anti-alias filter, which in turn is selectable from the keyboard. Spectra are then computed and archived in the same manner as for the low and mid bands. A new data set is acquired as soon as the processor is free and the cycle repeats. Data are thus acquired one pair of frequencies at a time. The operator can interrupt the collection process from the keyboard to select a different analog anti-alias filter cutoff and sampling rate and thus change frequencies, to change data selection criteria which controls archiving procedures, or to compute coherencies or impedance and tipper functions from the currently archived spectra. We intend to test the utility of 64- or 128-point data sequences for eliminating spectral leakage from nearby frequencies due to the strongly non-stationary character of the natural fields, especially in the high band.

Data are processed according to selection and archiving procedures described below. These combined procedures are to our knowledge unique and are designed to exploit nonstationary behavior of the signal or noise components of the measured fields.

Note that at each level of decimation, periodogram estimates are obtained each time a 32-point data segment is processed. The option exists at this point to incorporate these estimates into a spectral average. Our software allows the operator to set an

amplitude cutoff value which is compared to the amplitude of the digitized fields. Data sets for which the sum of the amplitudes of the horizontal electric or magnetic field components is less than the specified cutoff are immediately rejected. The operator is presented with a continuously updated display informing him of the percentage of data being kept at each level to guide the selection of a cutoff value. The operator may change the cutoff value at any time.

Periodogram estimates which pass the cutoff criteria are averaged in a temporary array to generate spectral estimates. The number of averages in the spectral estimates at each level is set by the operator at the start of a run. When the specified number of averages is reached, multiple coherence functions are computed and the spectra in the temporary array at that level are archived on disk storage in two separate data files. In one data file, the spectra are sorted and accumulated into one of ten bins based on the multiple coherence values. All spectral data are accumulated in this file. In a second data file, only the ten best data sets are retained in separate bins, based on the computed multiple coherence values. These two data files allow selection of the best data to compute impedance and tipper functions. We intend to incorporate additional weighted averaging procedures as described by Stodt (1983).

In Figures 1 and 2, example results of a field test in August, 1985 show what we have achieved in MT instrumentation thus far. Tensor apparent resistivities ρ_{xy} and ρ_{yx} and impedance phase ϕ_{xy} and ϕ_{yx}, with x-north, y-east, z-down, obtained in the Western Cascades Range of Oregon near U.S. Highway 20, are plotted as measured by five academic institutions on successive days as part of the mini-EMSLAB test traverse. The systems of Utah and Michigan are without remote reference sensors, that of Oregon carries a local coil reference with analog wire communications, while a complete dual-station telemetry systems is implemented by CICESE/San Diego State. The long period measurements by J. Booker of Washington required time series recording of about a week

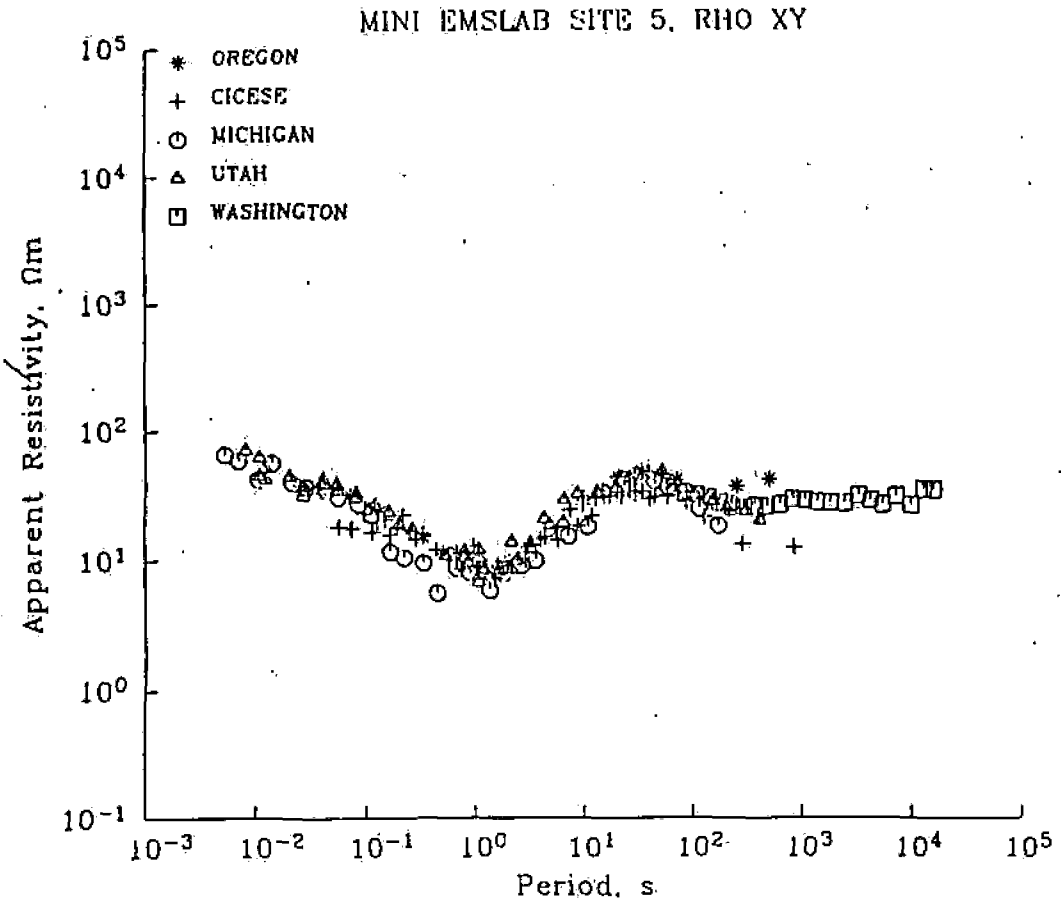
MINI EMSLAB SITE 5, RHO XY
OREGON
CICESE
MICHIGAN
UTAH
WASHINGTON
Apparent Resistivity, Ωm
Period, s

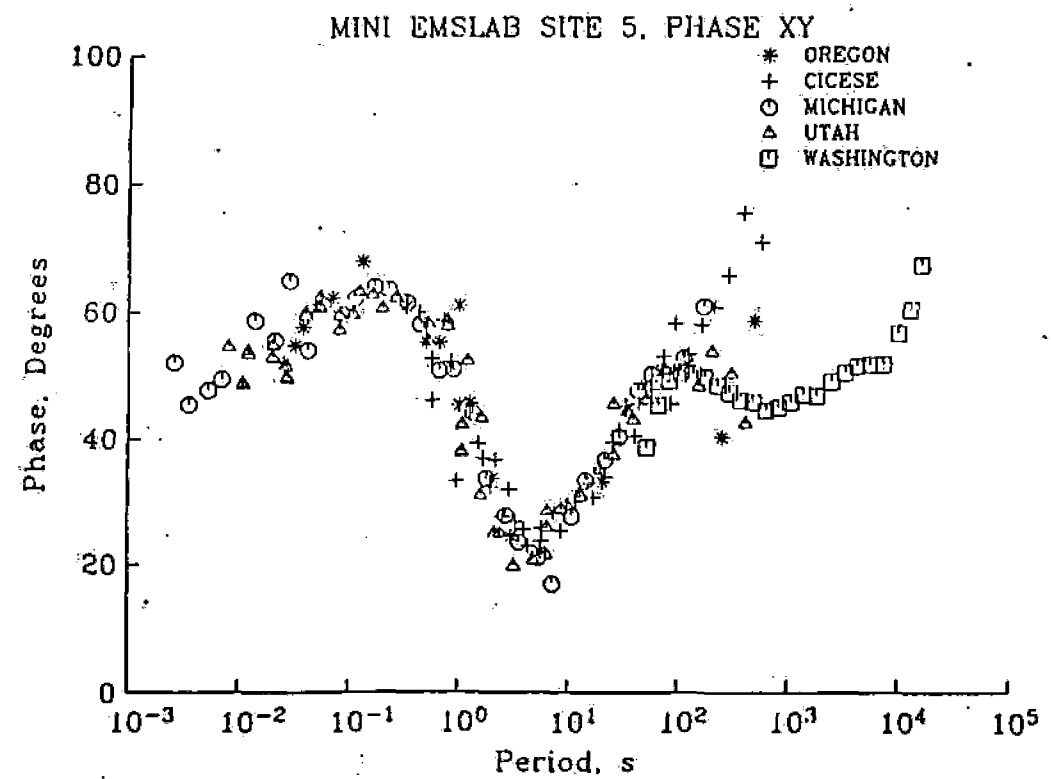
MINI EMSLAB SITE 5, PHASE XY
OREGON
CICESE
MICHIGAN
UTAH
WASHINGTON
Phase, Degrees
Period, s

Figure 1

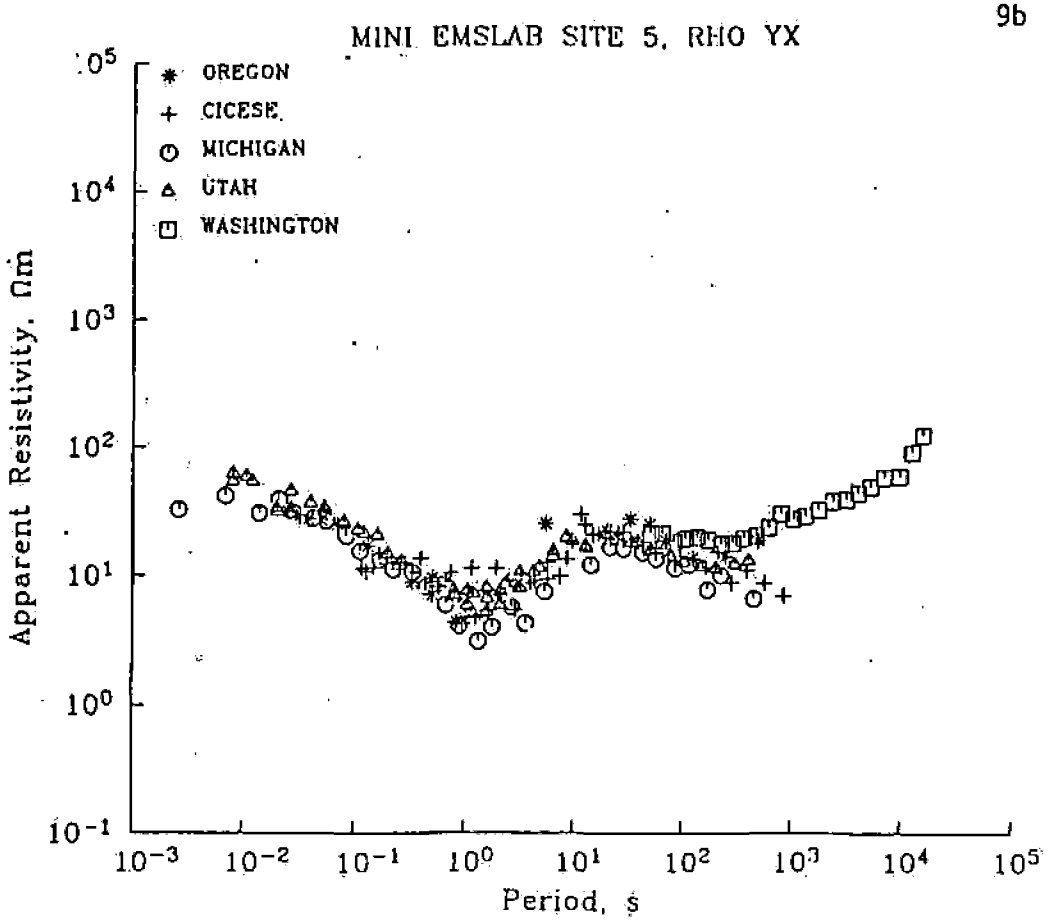
MINI EMSLAB SITE 5, RHO YX
OREGON
CICESE
MICHIGAN
UTAH
WASHINGTON
Apparent Resistivity, Ωm
Period, s

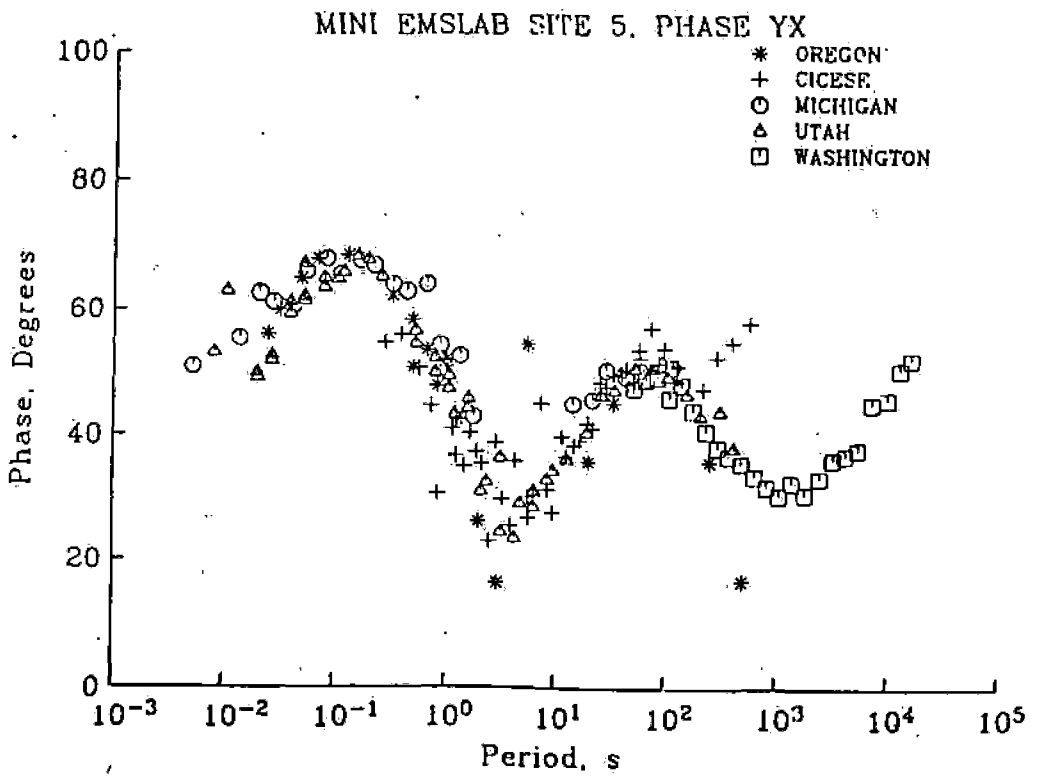
MINI EMSLAB SITE 5, PHASE YX
OREGON
CICESE
MICHIGAN
UTAH
WASHINGTON
Phase, Degrees
Period, s

Figure 2

and used a battery powered system without a reference. Of relevance to this proposal, the Utah data scatter is as small as that of any of the systems, and our data show good agreement in the region of overlap with the long-period measurements of Booker.

Parallel Research Efforts.

Substantial advances in the interpretation of MT data and in the understanding of deep resistivity have been achieved with NSF and other funding to date. These have resulted in a number of papers, either in press, submitted, or presented at scientific meetings.

For example, theoretical development and 3D computer simulations in the paper by Wannamaker et al. (1984b) have addressed the applicability of 1D and 2D MT interpretation schemes in 3D environments and have provided methods of circumventing the troublesome effects of near-surface extraneous resistivity structure (geological noise). Most of the 3D model studies appearing in this paper were supported by DOE, but a significant portion of the modeling, as well as preparation of the final manuscript for publication, were performed under NSF sponsorship. This paper has been cited as an "important contribution" and "of major benefit to the MT community" by the reviewers.

These 3D model results were computed using our newly-developed integral equation algorithm for simulating the MT responses of 3D bodies in layered earths (Wannamaker et al., 1984a). We believe this to be a uniquely versatile and accurate algorithm for modeling this class of problem. While this program was developed to fulfill contracts for DOE, it exemplifies the capabilities of our research group in the numerical simulation of inhomogeneous resistivity structure.

Principally under NSF sponsorship, Wannamaker (1983) has carried out a review of the resistivity structure of the northern Basin and Range. Emphasis was placed on the effects of upper crustal lateral inhomogeneity upon estimates of deep resistivity

structure. Many if not most published models of deep resistivity from both natural and artificial source methods suffer some, and often large, bias toward erroneously low resistivity at depth. Much of the speculation about a free water phase in the lower crust may result from this bias.

Thermodynamic principles governing the equilibrium existence of fluid phases affecting resistivity in the lower crust have been discussed by Wannamaker (1985), under NSF funding. In high-grade, intermediate to mafic rocks common to the lower crust, a free-water-rich fluid at $P_f = P_t$ appears improbable at temperatures below those of melting. However, it is possible for a conductive CO_2-rich fluid to evolve through joint decomposition of carbonate and amphibole. Moreover in this paper, conductivity of partial melts produced under water-undersaturated conditions has been quantified using the H_2O activity model of Burnham (1979). As melting proceeds in the presence of fixed amounts of water, melt phase conductivity drops sharply due to dilution of water in spite of increasing temperature. Therefore, when typical Archie's Law mixing models are relevant, bulk conductivity varies only weakly for melt fractions greater than about 0.2.

Recent progress has been achieved in finite element modeling of 2-D MT responses with DOE and NSF support. Developments include capability to model topographic variations as well as direct calculation of secondary field responses (i.e., those just due to the inhomogeneity). One conclusion of the topographic modeling is that a horizontal placement of the sensors (coils or SQUID) for H_x and H_y will reduce topographic effects at low frequencies relative to a placement of sensors parallel to the slope. Implementation of the secondary field formulation has circumvented difficulties with computer word length at low frequencies observed in total field solutions for the TM mode especially, but also for the TE mode. Two manuscripts on this work are in preparation for publication by Wannamaker.

Stodt (1983), primarily with DOE support, has provided a rigorous error analysis for

conventional and remote reference magnetotellurics under the assumption that noise in the E- and H-field measurements is governed by a complex normal distribution. He found that the standard unweighted least squares estimates of the impedence and tipper functions (e.g., Gamble et al., 1979) are not minimum-variance when the measured fields are non-stationary. Furthermore, the weighted least squares estimate

$$Z_i = (R\ ^{*T}V_o^{-1}H)^{-1}\ R\ ^{*T}V_o^{-1}E_i,$$

where $Z_i^T = (\ Z_{ix}\ Z_{iy})$, and $R = \ A\ B\ $ is the matrix of N-dimensional column vectors of harmonics computed from two reference (not necessarily remote) field measurements A and B, is minimum variance provided only the E-fields are noisy. Here V_o is the covariance matrix for the column vector E_i. However, because errors in the tensor MT estimates depend on the noise power in E_i, and on the noise to signal ratios in H and R, generalized weights which reflect this behavior can be estimated from subsets of the data using the appropriate multiple coherence functions (Stodt, 1983). Three manuscripts have returned from journal review and are undergoing revision for publication by Stodt.

Proposed Upgrade of MT System

Because of the low instrument noise levels we had achieved we initially were optimistic about the possibility of acquiring high quality data without employing a remote reference in areas where correlated cultural noise was insignificant. Unfortunately, at this time we are near a minimum in solar activity. During our initial field tests in southern Utah, we observed magnetic field signal strengths averaging approximately .005 gamma peak-to-peak in a 1-Hz bandwidth. This is roughly an order of magnitude decrease in the average strength of the natural fields compared to that observed during a survey conducted in 1977. However, we have not achieved an order magnitude of improvement in signal to noise ratio compared with instrumentation available in 1977.

Our field tests, especially the one in Oregon where signals were higher, have been

encouraging because we can acquire good quality data in all three frequency bands. The data selection and archiving techniques described above have proved valuable in editing for high quality data. We have found, however, as corroborated in conversations with commercial MT contractors, that precise data remains most difficult to obtain in the mid-band (0.1 - 1. Hz), and not at low frequencies. A remote reference is required to utilize effectively measurements having low signal contents. The weighted averaging techniques proposed by Stodt (1983) are expected to be most advantageous when applied to remote reference data.

Funds are requested to upgrade our current magnetotelluric data acquisition system by incorporating a local "remote" reference. The local reference will consist of an additional pair of horizontal magnetic field measurements obtained simultaneously with measurements from the base station sensor array. Goubau et al. (1984) showed that a separation of only 200 m was sufficient to eliminate bias errors at their test locations. This approach represents a good and economical way for us to field a state-of-the-art system with separate reference capability, and it should be very advantageous for the field work of our proposals.

Our MT system was built and is maintained by S. L. Olsen electronics engineer, and J. A. Stodt, Ph.D. geophysicist, of the Earth Science Laboratory, University of Utah Research Institute. They have a fully equipped, state-of-the-art electronics laboratory at their disposal. The amount we are requesting for upgrading the MT system is divided between equipment cost and support for Olsen and Stodt.

Bibliography

Bostick, F. X., Jr., and Smith, H. W., 1979, Development of real-time, on-site methods for analysis and inversion of tensor magnetotelluric data: Technical Report No. 206, Elec. Geop. Res. Lab., Univ. of Texas at Austin.

Clarke, J., Gamble, T. D., Goubau, W. M., Koch, R. H., and Miracky, R. F., 1983, Remote-reference magnetotellurics: equipment and procedures: Geop. Prosp., 31, 149-170.

Gamble, T. D., Goubau, W. M., and Clarke, J., 1979, Magnetotellurics with a remote reference: Geophysics, 44, 53-68.

Goubau, W. M., Maxton, P. M., Koch, R. H., and Clarke, J., 1984, Noise correlation lengths in remote reference magnetotellurics: Geophysics, 4, 433-438.

Park, S. K., 1983, Three-dimensional magnetotelluric modeling and inversion: Ph.D. Thesis, Mass. Inst. Tech.

Stodt, J. A., 1983, Error analysis for conventional and remote reference magnetotellurics: Ph.D. Thesis, Univ. of Utah.

Wannamaker, P. E., 1983, Resistivity structure of the northern Basin and Range, In The Role of Heat in the Development of Energy and Mineral Resources in the Northern Basin and Range Province, Geothermal Resources Council Special Rept. 13, 345-362.

____, 1985, Electrical conductivity of water-undersaturated crustal melting: submitted to J. Geophys. Res.

Wannamaker, P. E., Hohmann, G. W., and San Filipo, W. A., 1984a, Electromagnetic modeling of three-dimensional bodies in layered earths using integral equations: Geophysics, 49, 60-74.

Wannamaker, P. E., Hohmann, G. W., and Ward, S. H., 1984b, Magnetotelluric responses of three-dimensional bodies in layered earths: Geophysics, 49, 1517-1533.

Wright, D. E., Bostick, F. X., Jr., and Smith, H. W., 1977, Real time Fourier transformation of magnetotelluric data: Technical Report of the Elec. Geop. Res. Lab., Univ. of Texas at Austin.

Scheduled for July/85
in Geophysics

ON THE DETECTABILITY OF CRUSTAL MAGMA CHAMBERS USING THE MAGNETOTELLURIC METHOD

by

Gregory A. Newman*, Philip E. Wannamaker+ and Gerald W. Hohmann*

Presented at the 53rd Annual International SEG Meeting September 14, 1983, in Las Vegas

*Department of Geology and Geophysics, University of Utah, Salt Lake City, Utah 84112-1183

+Earth Science Laboratory, University Research Institute, 391 Chipeta Way, Suite C, Salt Lake City, Utah 84108

ABSTRACT

We have utilized resistivity models of silicic magma chambers to explore effects that layering can have on three-dimensional (3-D) magnetotelluric (MT) responses. Model simulations show that MT detection of magma may depend strongly on its one-dimensional (1-D) host. The 3-D responses of a model juvenile magma body which is connected electrically to deeper less resistive crust of regional extent were very subdued. However, intermediate and mature magmatic systems leaving magma no longer in contact with lower less resistive crust may be detectable with the MT method. Further, the release and ascent of volatiles from crystallizing melt may lead to fracturing above the chamber, thereby establishing electrical contact of the magma with shallow conductive crust and thereby amplifying its MT response.

INTRODUCTION

This paper is concerned with some factors that characterize magnetotelluric (MT) responses of three dimensional (3-D) structures embedded in layered media. We have emphasized, for practical application, resistivity models of silicic magma chambers. The MT responses studied here were computed using the algorithm of Wannamaker et al. (1984a). This algorithm is based on the method of integral equations and is suited for one or a few 3-D bodies in layered hosts. The MT method has been applied to detect magma bodies beneath geothermal systems because of its potentially large depth of exploration (Ward, 1983).

Dissolved water strongly affects magma resistivity (Lebedev and Khitarov, 1964). Concentrations of dissolved water within magma have been inferred to range from about 1 to 5 wt% (cf., Crecraft et al., 1981; Hildreth, 1981). Burnham (1975) has shown that siliceous melts composed of 4 to 1 wt% dissolved water have corresponding resistivities between 1 and 100 ohm-m at 1000°C. A resistivity of 4 Ω·m could represent a silicic liquid in the middle crust possessing 2.5 wt% of dissolved water at 1000°C. Burnham (1979) proposes that such liquid originates from vapor-absent fusion of hornblende-bearing rocks in the lower continental crust.

The resistivity structure of the 1-D host for the magma chambers we consider resembles that of the Basin and Range as interpreted by Brace (1971). In Brace's interpretation, the increase in the resistivity in the upper 15 km of the crust reflects a decrease with depth in rock porosity; bulk resistivity in this region is controlled by electrolytic conduction. Below 15 km depth, resistivity decreases as solid-state electrical conduction in minerals becomes more important. This resistivity structure is shown in Figure 1 with an upper mantle resistivity of 40 Ω·m below 35 km depth.

MODEL RESPONSES OF A JUVENILE MAGMA BODY

Figure 1 displays a simplified resistivity structure that could be associated with a juvenile magma chamber in the western United States. The magma chamber has a resistivity of $4\,\Omega \cdot m$ and is represented in an early stage of its development, i.e., before it has risen completely from its site of generation in the lower crust (Hildreth, 1981).

Apparent resistivity and impedance phase pseudosections for the 3-D model of Figure 1 are compared to pseudosections of a 2-D structure of identical cross-section in Figures 2 and 3. These pseudosections are calculated at the center cross-profile of the magma chamber model. Note that the x axis of Figure 1 is the strike direction of the magma chamber. Only half of each pseudosection is shown in these figures since the model is symmetric across the x-axis. The 2-D results were calculated with a finite element program written by Rijo (1977). Note that 2-D apparent resistivity ρ_{yx} and impedence phase ϕ_{yx} (Figure 2) correspond to the TM or $E_{\perp}$ mode of excitation, while apparent resistivity ρ_{xy} and phase ϕ_{xy} (Figure 3) correspond to the TE or $E_{\parallel}$ mode of excitation.

For both modes, the 3-D pseudosections (Figures 2 and 3) illustrate very subdued departures from the layered host response. This subdued response would be especially difficult to recognize in the presence of any extraneous structure nearer to the surface (Wannamaker et al., 1984b). The results for the 2-D TM mode and corresponding 3-D results agree closely since current channeling figures prominently in both responses. This agreement indicates that an increased strike length for the magma body will not amplify its signature in the $E_{\perp}$ mode, so that detection of the body in this mode will be very difficult. Current channeling is caused by a boundary polarization charge at discontinuities in the normal component electric field along resistivity boundaries. The current channeling responses of a 2-D (TM mode) or 3-D structure will affect the apparent resisitivity to arbitrarily low frequencies. However, at low frequencies the

impedance phase response of the structure will not be distinguishable from that of its layered host (Wannamaker, et al., 1984b).

As expected there is disagreement between 2-D TE mode results and corresponding 3-D results. Current channeling is a strong source of the 3-D $E_{||}$ mode response due to the limited strike extent of the magma body. On the other hand, volume currents alone are the source of the 2-D TE mode response. Responses in apparent resistivity and phase due to volume currents are band-limited in frequency and vanish as frequency falls (Wannamaker et al., 1984b).

In order to understand how the layered host affects the MT response of the magma body, the layered host was removed and replaced with a 400Ω·m half-space. This calculation showed that the response of the magma chamber in both (ρ_{xy}, ϕ_{xy}) and (ρ_{yx}, ϕ_{yx}) was much stronger in the half-space than in the layered host. The sensitivity of the response of the magma chamber to its host is important and demonstrates that detection of magma depends strongly on its 1-D host.

Physical understanding of current channeling is important if we are to explain this sensitivity in detecting magma for different 1-D hosts. The specific effects of layering upon current channeling can be demonstrated in section view. Figures 4a and 4b illustrate the distortion of the electric field due to the magma chamber for the layered host of Figure 1 and a 400Ω·m half space. The centrally located longitudinal section shows polarization ellipses of electric field at 0.01 Hz. In Figures 4a and 4b the polarization ellipses are normalized to the layered host and half-space electric field magnitudes, respectively, at the earth's surface. The polarization of the incident electric field in both figures is parallel to strike. Also included in these figures are profiles of normalized real and imaginary total electric field (E) at the earth's surface.

Figures 4a and 4b show that the electric field at this low frequency is essentially linearly polarized and in phase with the incident electric field since the polarization

ellipses of electric field have degenerated into line segments. The linearly polarized electric field (distorted with respect to the direction and strength of the incident electric field) demonstrates the current channeling response of the magma body in both 1-D hosts. The overshoot-to-undershoot behavior in normalized total electric field drawn at the top of these figures gives another view of the current channeling phenomenon. These profiles also show how much more subdued is the 3-D response at the surface for the layered host than for the half-space.

The interesting point in comparing Figure 4a to 4b is the manner and the degree to which the electric field is altered by the body for different 1-D hosts. In Figure 4a, the electric field alteration is stronger below the body in the layered host than in the half-space (Figure 4b). However, above the body the opposite is true; the electric field is distorted more strongly in the half-space. We interpret this discrepancy as being caused by current channeling in layered media. Two factors could be at work here. First, the scattered currents due to charges on the body are short circuited into the lower less resistive crust. Second, the conductive overburden in the shallow crust (the top 400 Ω.m layer) reduces the scattered electric fields that do reach the earth's surface.

We determined which part of the layering was causing the attenuated responses by removing the layering beneath the magma body. The 1-D structure now corresponds to a 2 km thick, 400 Ω.m top layer overlying a 4000 Ω.m basal half-space. We emphasize that the 3-D body now is connected neither to a less resistive layer at its base nor to the less resistive layer at the surface. The 3-D pseudosections of apparent resistivity and phase are shown in Figure 5. The response of the magma body is now distinguishable in both apparent resistivities, ρ_{yx} and ρ_{xy}, but is much stronger for the $E_{||}$ polarization. We conclude that the lower 400 Ω·m layer in the mid-crust, directly beneath the magma body, is mainly responsible for the attenuated 3-D responses in Figures 2 and 3.

MODEL RESPONSES OF A MATURE MAGMA BODY

This physical insight into current channeling is helpful in predicting the MT responses of more evolved magmatic systems that are conductive. We believe that these bodies with the 1-D host of Figure 1 may be detectable with the MT method. Consider uprise of silicic magma from depth continuing to the point where the magma chamber is disconnected electrically from the lower less resistive layers in the deep crust (Hildreth, 1981). Furthermore, the release and ascent of volatiles with melt crystallization may lead to sufficient crustal fracturing above the magma (Burnham, 1979) so as to establish electrical contact with the shallow conductive crust. Thus, current channeling in the shallow crust may cause a substantial MT response for the more mature magmatic system.

A simplified model of a mature silicic magmatic system is illustrated in Figure 6. The 400 $\Omega\cdot$m cap directly above the magma represents a zone of crustal fractures filled with fluids. This zone connects electrically with the shallow conductive crust. Note that we have assigned 10 $\Omega\cdot$ m resistivity to the magma instead of 4 $\Omega\cdot$m. This assignment is intended to aid convergence in the algorithm of Wannamaker et al. (1984a) for receiver stations over the body.

Pseudosections in apparent resistivity and impedance phase of this model are compared to those of a 2-D structure of identical cross-section in Figures 7 and 8. These pseudosections are located on the y axis at x = 0. Once again only half of each pseudosection is shown due to symmetry.

The response of the magma body is now quite distinguishable in the 3-D apparent resistivities (ρ_{yx} and ρ_{xy}), but less so in the 3-D phases (ϕ_{yx} and ϕ_{xy}). The 3-D $E_{\perp}$ (ρ_{yx} and ϕ_{yx}) mode results are verified by direct comparison with the 2-D TM mode results. As expected, there is poor agreement between the 2-D TE (ρ_{xy} and ϕ_{xy}) and 3-D $E_{\parallel}$ (ρ_{xy} and ϕ_{xy}) modes. Since the 3-D and 1-D phase responses nearly coincide, the

secondary magnetic fields induced by the magma body are very weak and we are looking once again at a current channeling phenomenon.

We cannot say, however, that the apparent resistivity responses of the magma body would be distinguishable in the presence of severe near-surface geological noise. We are only pointing out the effect of layering on the response of the magma body.

A comparison of the 3-D $E_{||}$ mode to the $E_{\perp}$ mode illustrates that the $E_{||}$ mode is more sensitive to the magma body. For receiver stations located more than 4 km from its center, the magma body is undetectable in the $E_{\perp}$ mode. However, in the $E_{||}$ mode, the magma body is detectable with stations within 8 km of its center.

We interpret the spatially weak response in the $E_{\perp}$ mode as being caused by the physical dimensions of the magma body. The weak response in the $E_{\perp}$ mode is observed when the depth to the magma is greater than or equal to the cross-width of the magma chamber (cf. Wannamaker et al., 1984b). On the other hand the stronger response in the $E_{||}$ mode is due to the magma chamber's strike extent being large compared to its depth. It is then apparent that 3-D $E_{\perp}$ mode results may be too weak to show the magma body, even though these are the results which can be modeled rigorously with a 2-D TM algorithm (ibid.).

CONCLUSIONS

From our limited model simulations we conclude that the detection of silicic magma with the MT method depends strongly on the 1-D resistivity host. Current channeling is the dominant source of MT responses from the magma bodies we have studied due to their limited strike extent. Therefore, physical insight into current channeling in layered media is important if we are to understand some of the factors that determine the detectability of silicic magma.

An analysis of the current channeling response of a juvenile magma body was

presented. The analysis has shown that when the chamber is in electrical contact with the lower less resistive crust, current flow in the body is short-circuited into the lower crust. This short-circuiting of the scattering currents strongly inhibits detectability of the MT response of the magma body at the earth's surface for both $E_{||}$ and $E_{\perp}$ modes.

We have shown that conductive intermediate and mature magmatic systems can be detected with the MT method. Electrical contact with the shallow conductive crust may be established for these magma bodies. A detectable MT response at the earth's surface especially in the $E_{||}$ results may occur for such magmas because of current channeling in the shallow crust and disconnection electrically of these magmas with the lower less resistive crust.

In summary, our 3-D MT model simulations suggest that a dike-like magma chamber may, depending upon its relation to its layered host, be detectable in the $E_{||}$ mode, but that generally the response in the $E_{\perp}$ mode is rather weak. The spatially weak response in the $E_{\perp}$ mode is interpreted as being caused by the physical dimensions of the magma body. Apparently this weak response is observed when the depth to the magma is greater than or equal to the cross-width of the magma chamber. Therefore, 2-D TM mode modeling of $E_{\perp}$ field data may not distinguish such magmatic systems. However, while the $E_{||}$ response may be stronger, a fully 3-D modeling program is necessary for its rigorous interpretation.

ACKNOWLEDGEMENTS

We are grateful to Francis Bostick, Jr., John Maas and Bill SanFilipo for stimulating discussion concerning this work. Funding was provided by the U.S. Department of Energy under contract DE-AC07-80-ID079, and by the following companies: Amoco Production Co., ARCO Oil and Gas Co., Chevron Resources Company, Conoco Inc., CRA Exploration Pty. Ltd., SOHIO Petroleum Co., Union Oil Co. of California, and Utah International Inc.

REFERENCES

Brace, W. F., 1971, Resistivity of saturated crustal rocks to 40 km based on laboratory measurements, In The Structure and Physical Properties of the Earth's Crust, ed. by J. G. Heacock, American Geophysical Union Mono. 14, p. 243-256.

Burnham, C. W., 1975, Water and magmas; a mixing model: Geochemica et Cosmochemica Acta, 39, p. 1077-1084.

_____, 1979, Magmas and hydrothermal fluids, In Geochemistry of Hydrothermal Ore Deposits, ed. by H. L. Barnes, John Wiley and Sons, New York, p. 71-136.

Crecraft, H. R., Nash, W. P., and Evans, S. H., Jr., 1981, Late Cenozoic volcanism at Twin Peaks Utah: Geology and Petrology: Journal of Geophysical Research, 86(B11), p. 10303-10320.

Hildreth, W., 1981, Gradients in silicic magma chambers: implications for lithospheric magmatism: Journal of Geophysical Research, 86(B11), p. 10153-10199.

Lebedev, E. B., and Khitorov, N. I., 1964, Dependence on the beginning of melting of granite and the electrical conductivity of its melt on high water vapor pressure: Geokhimiya, 3, p. 195-201.

Rijo, L., 1977, Modeling of electrical and electromagnetic data: Ph.D. thesis, Dept. of Geology and Geophysics, Univ. of Utah.

Wannamaker, P. E., Hohmann, G. W., and SanFilipo, W. A., 1984a, Electromagnetic modeling of three-dimensional bodies in layered earths using integral equations: Geophysics, v. 49(1), p. 60-74.

Wannamaker, P. E., Hohmann, G. W., and Ward, S. H., 1984b, Magnetotelluric responses of three-dimensional bodies in layered earths: Geophysics, . 49(9), p. 1517-1533.

Ward, S. H., 1983, Geophysical studies of active geothermal systems in the northern Basin and Range, in The role of heat in the development of energy and mineral resources in the northern Basin and Range province, Geothermal Resources Council Special Report 13, p. 121-158.

List of Figures

Figure 4. b. This illustration shows the longitudinal-section of the magma chamber (Figure 1) enclosed in a 400 Ω·m resistivity half-space. The section view is again of polarization ellipses of electric field at .01 Hz.

Figure 5. Pseudosections of apparent resistivity (ρ_{yx}, ρ_{xy}) and phase (ϕ_{yx}, ϕ_{xy}) for magma chamber model and 1-D host of 2 km thick 400 Ω·m overburden and 4000 Ω·m basal half-space.

Figure 6. A highly simplified, mature magmatic system in a Basin and Range environment. The 400 Ω·m zone that caps the magma body represents crustal fractures filled with fluids that connect electrically with the conductive upper crust. The MT response of this magma body is detectable in the $E_{\parallel}$ mode, but spatially weak in the $E_{\perp}$ mode.

Figure 7. These pseudosections of apparent resistivity (ρ_{yx}) and phase (ϕ_{yx}) are calculated for the magma chamber model of Figure 6 and its corresponding 2-D version at the earth's surface.

Figure 8. These pseudosections of apparent resistivity (ρ_{xy}) and phase (ϕ_{xy}) are calculated for the magma chamber model of Figure 6 and its corresponding 2-D version at the earth's surface.

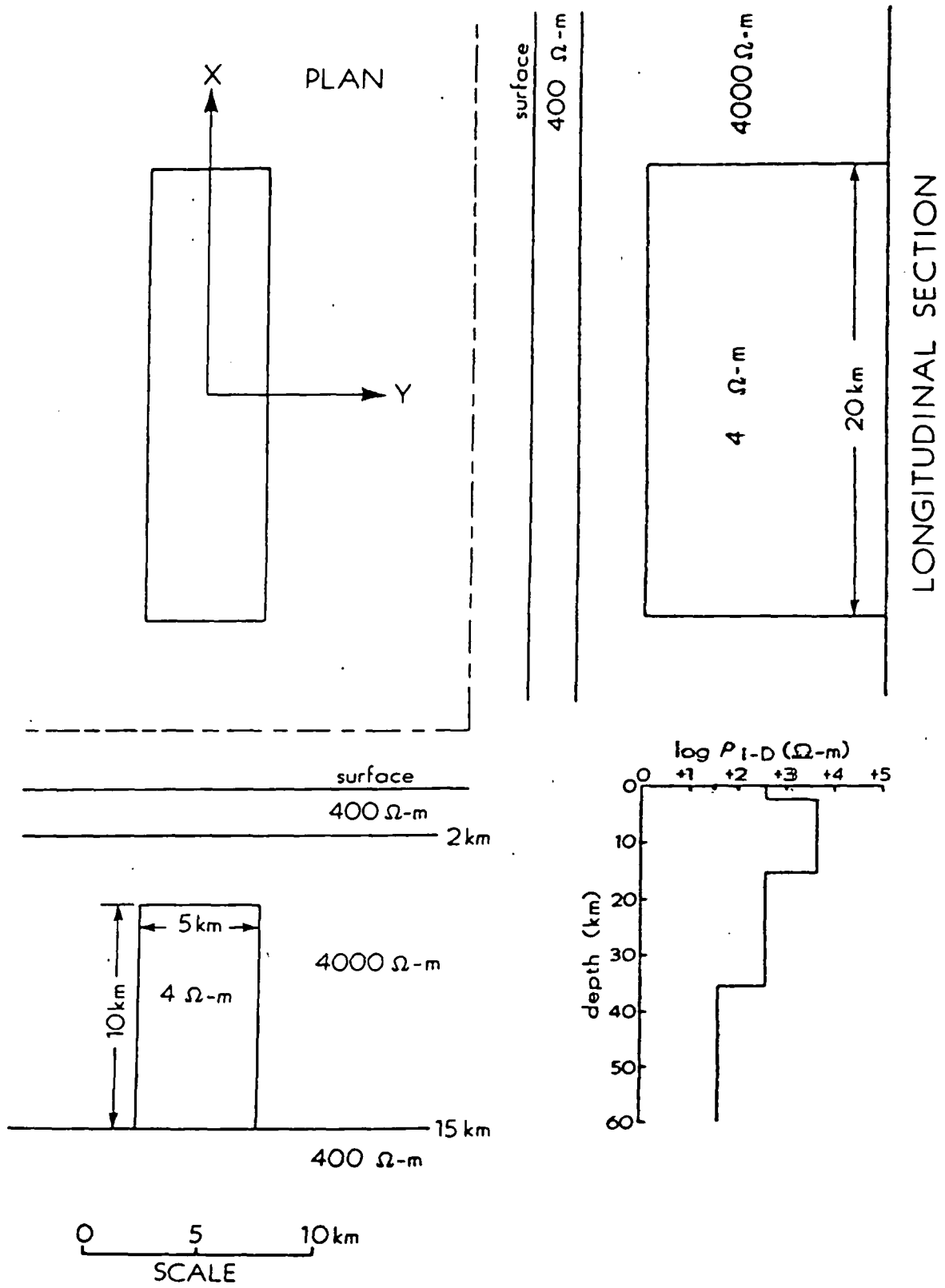

CROSS - SECTION

Figure 1.

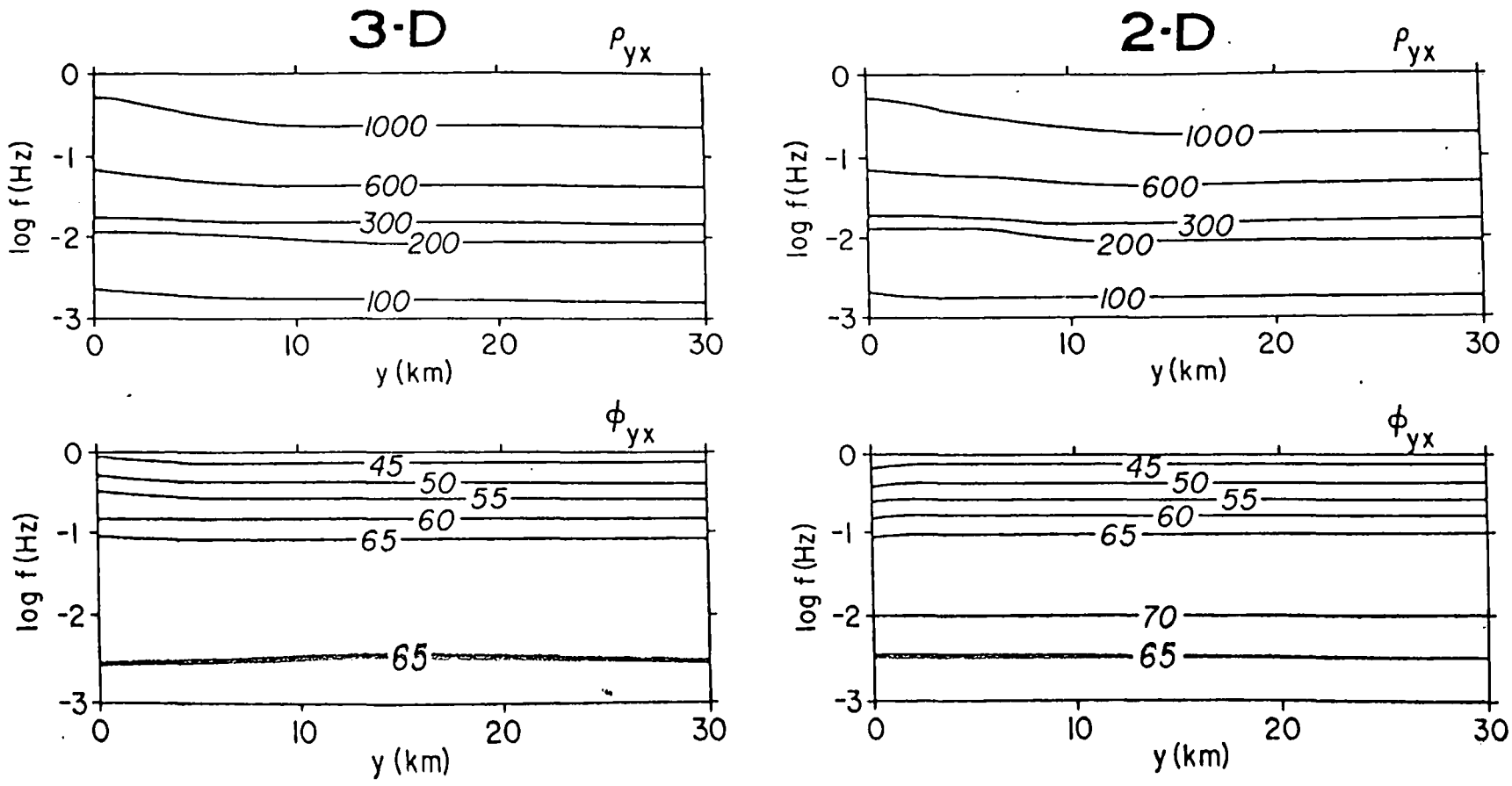
3-D
ρ_{yx}
1000
600
300
200
100
log f (Hz)
y (km)
ϕ_{yx}
45
50
55
60
65
65
2-D
ρ_{yx}
1000
600
300
200
100
log f (Hz)
y (km)
ϕ_{yx}
45
50
55
60
65
70
65

Figure 2.

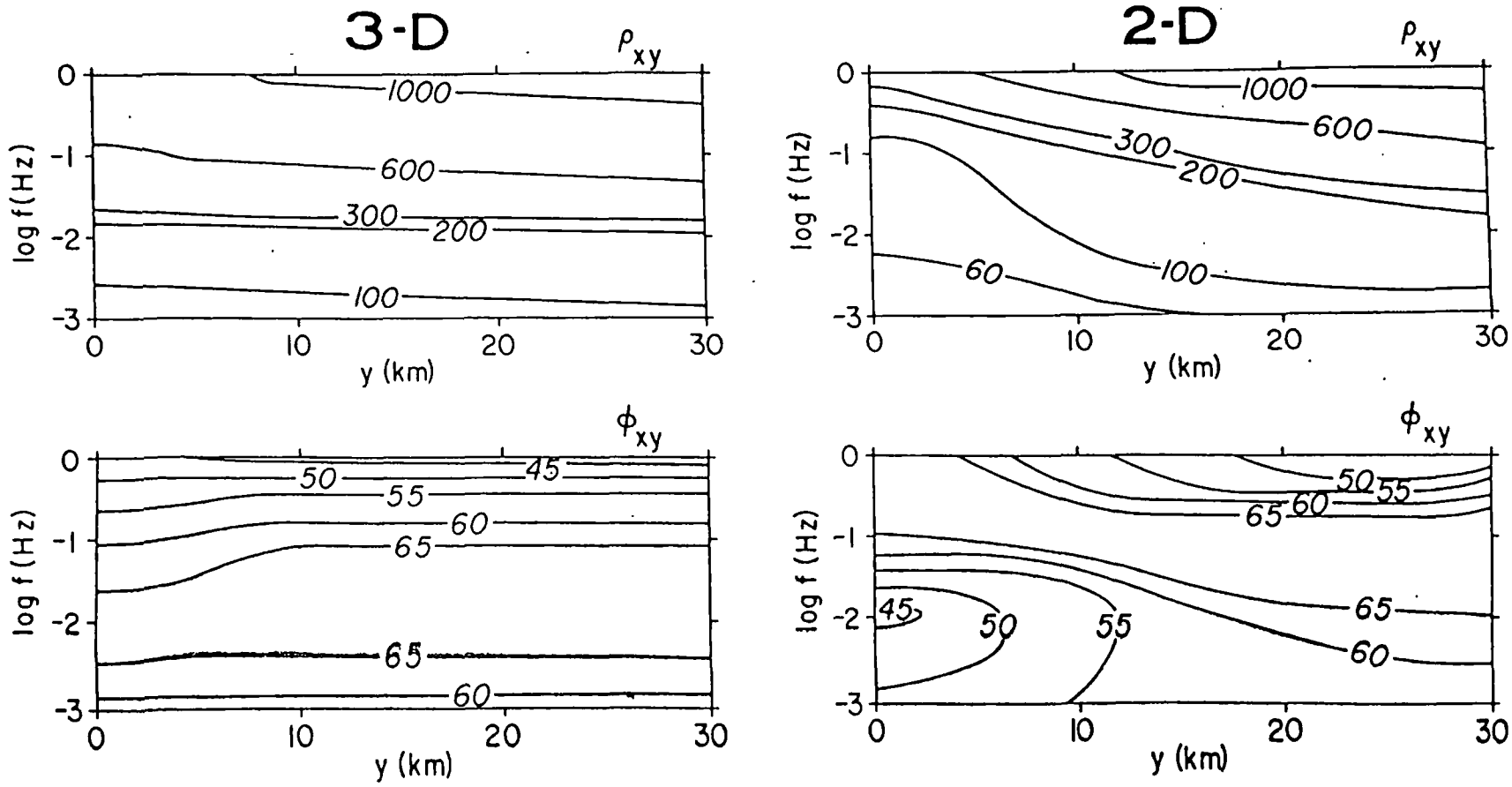
3-D
ρ_{xy}
1000
600
300
200
100
log f (Hz)
y (km)
ϕ_{xy}
50
45
55
60
65
2-D
ρ_{xy}
1000
600
300
200
60
100
log f (Hz)
y (km)
ϕ_{xy}
50
55
65
60
45
50
55
65
60
log f (Hz)
y (km)

Figure 3.

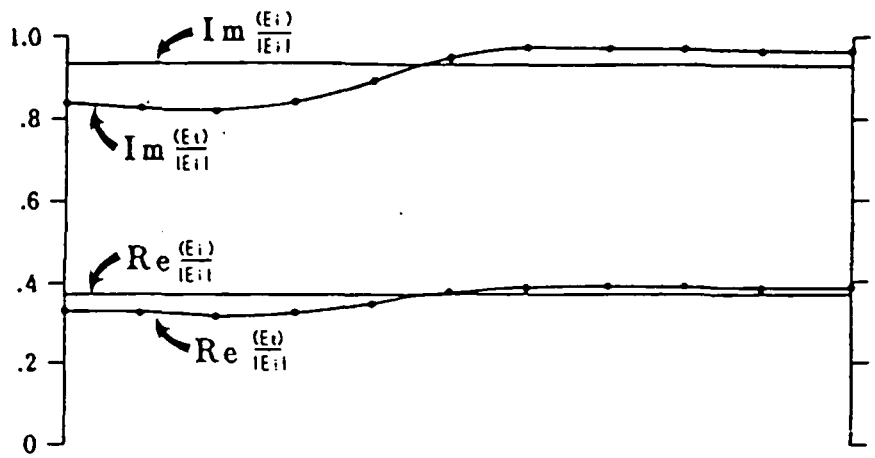
1.0
.8
.6
.4
.2
0
Im (Ei)/|Ei|
Im (Et)/|Ei|
Re (Ei)/|Ei|
Re (Et)/|Ei|

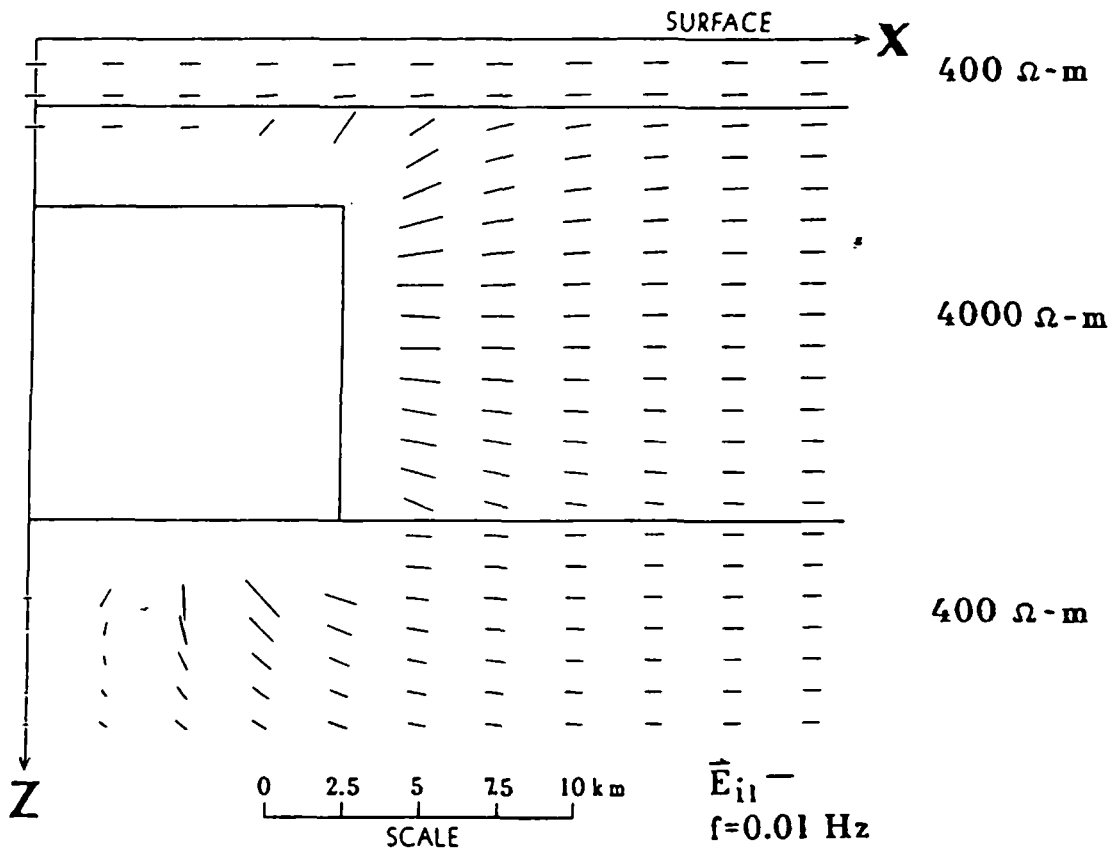
SURFACE
X
Z
400 Ω-m
4000 Ω-m
400 Ω-m
0
2.5
5
7.5
10 km
SCALE
Ei
f=0.01 Hz

Figure 4a.

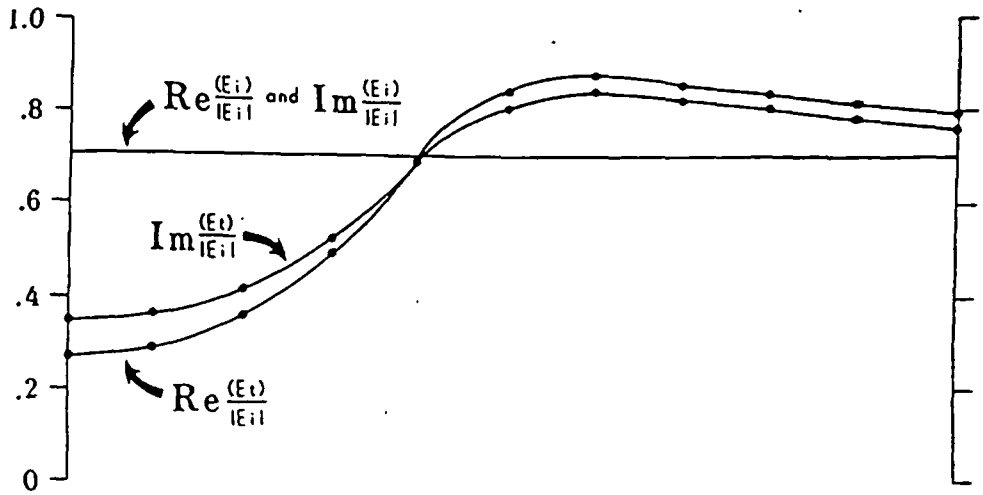
1.0
.8
.6
.4
.2
0
Re (Ei)/|Ei| and Im (Ei)/|Ei|
Im (Et)/|Ei|
Re (Et)/|Ei|

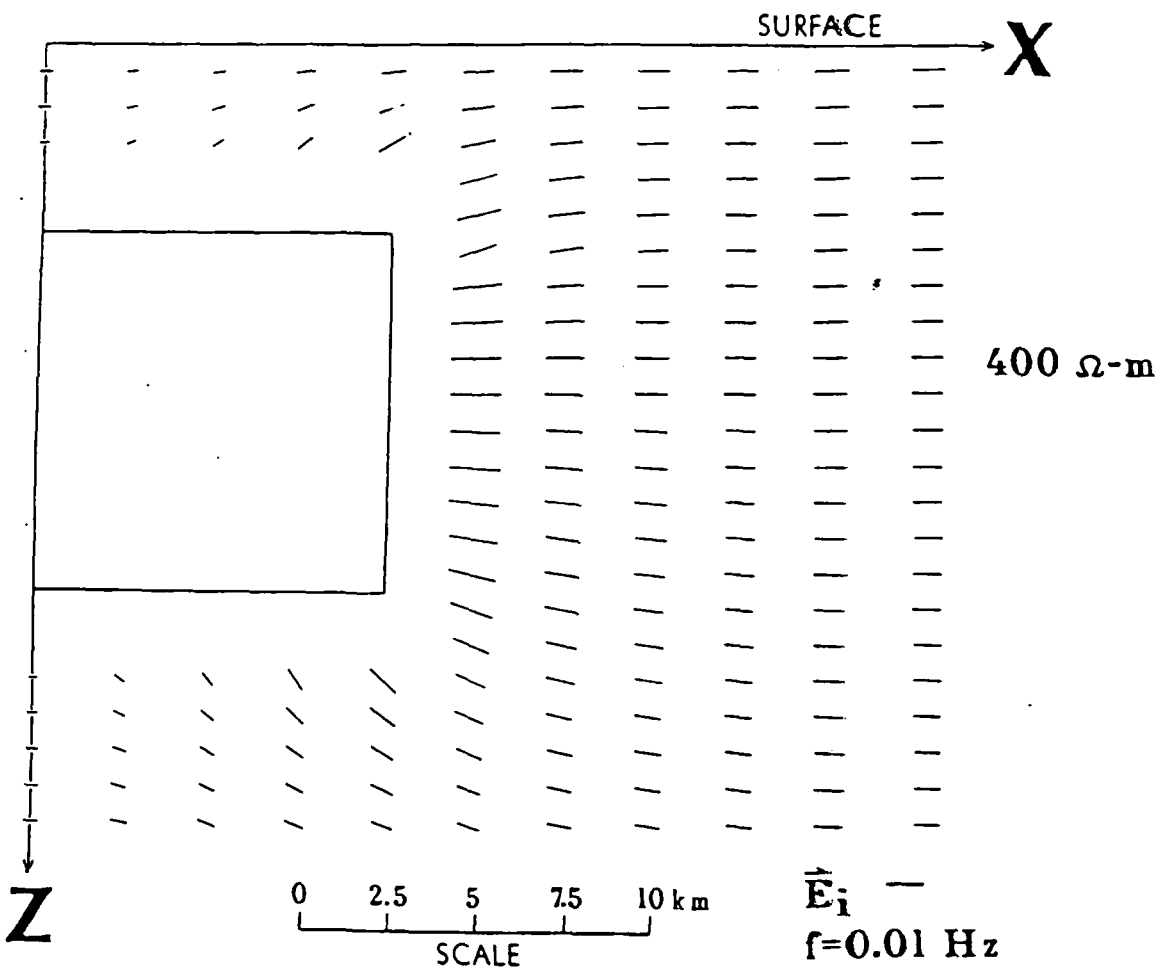
SURFACE
X
400 Ω-m
Z
0 2.5 5 7.5 10 km
SCALE
Ei
f=0.01 Hz

Figure 4b.

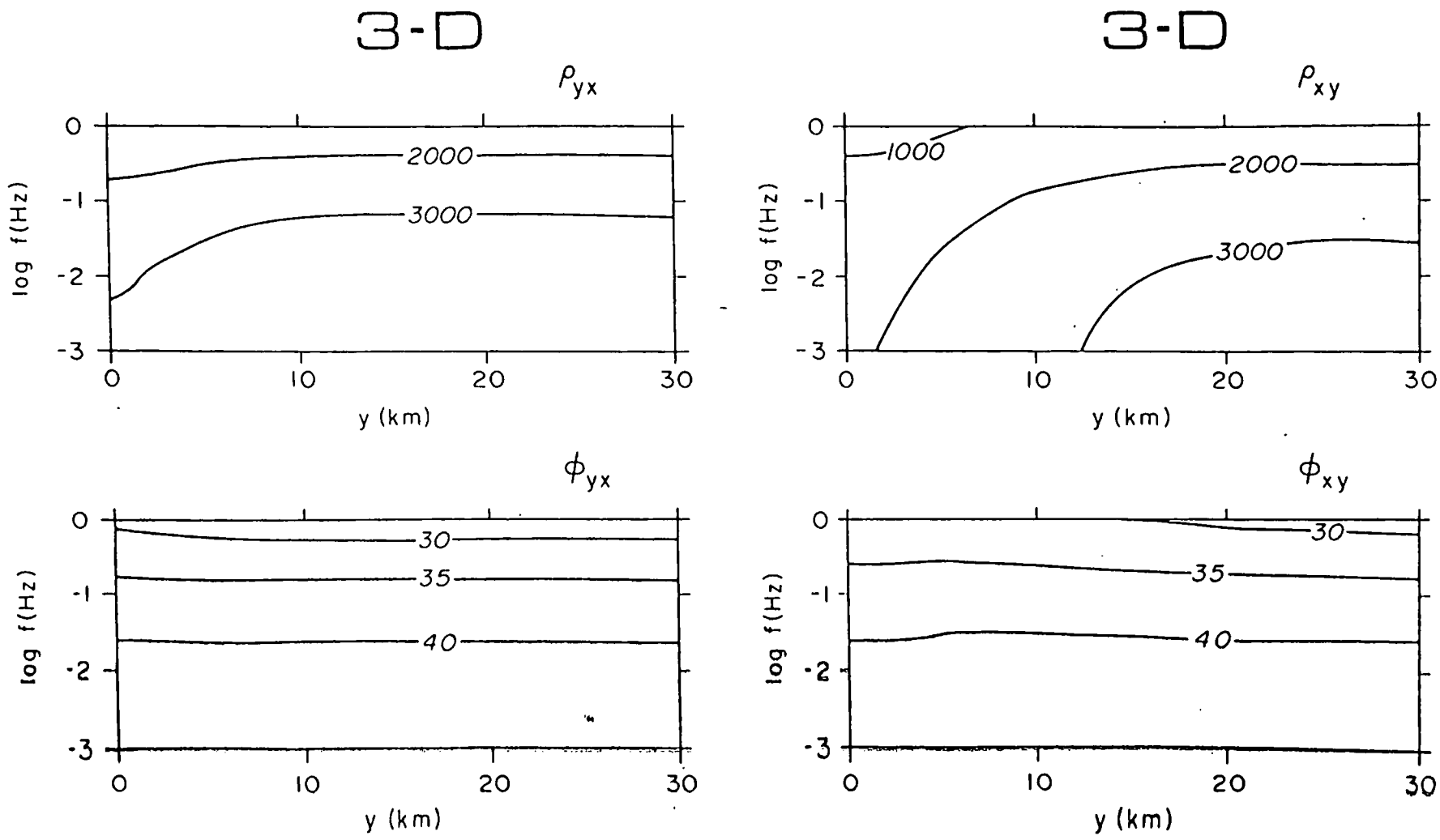
3-D
ρ_{yx}
2000
3000
log f(Hz)
y (km)
3-D
ρ_{xy}
1000
2000
3000
log f(Hz)
y (km)
ϕ_{yx}
30
35
40
log f(Hz)
y (km)
ϕ_{xy}
30
35
40
log f(Hz)
y (km)

Figure 5.

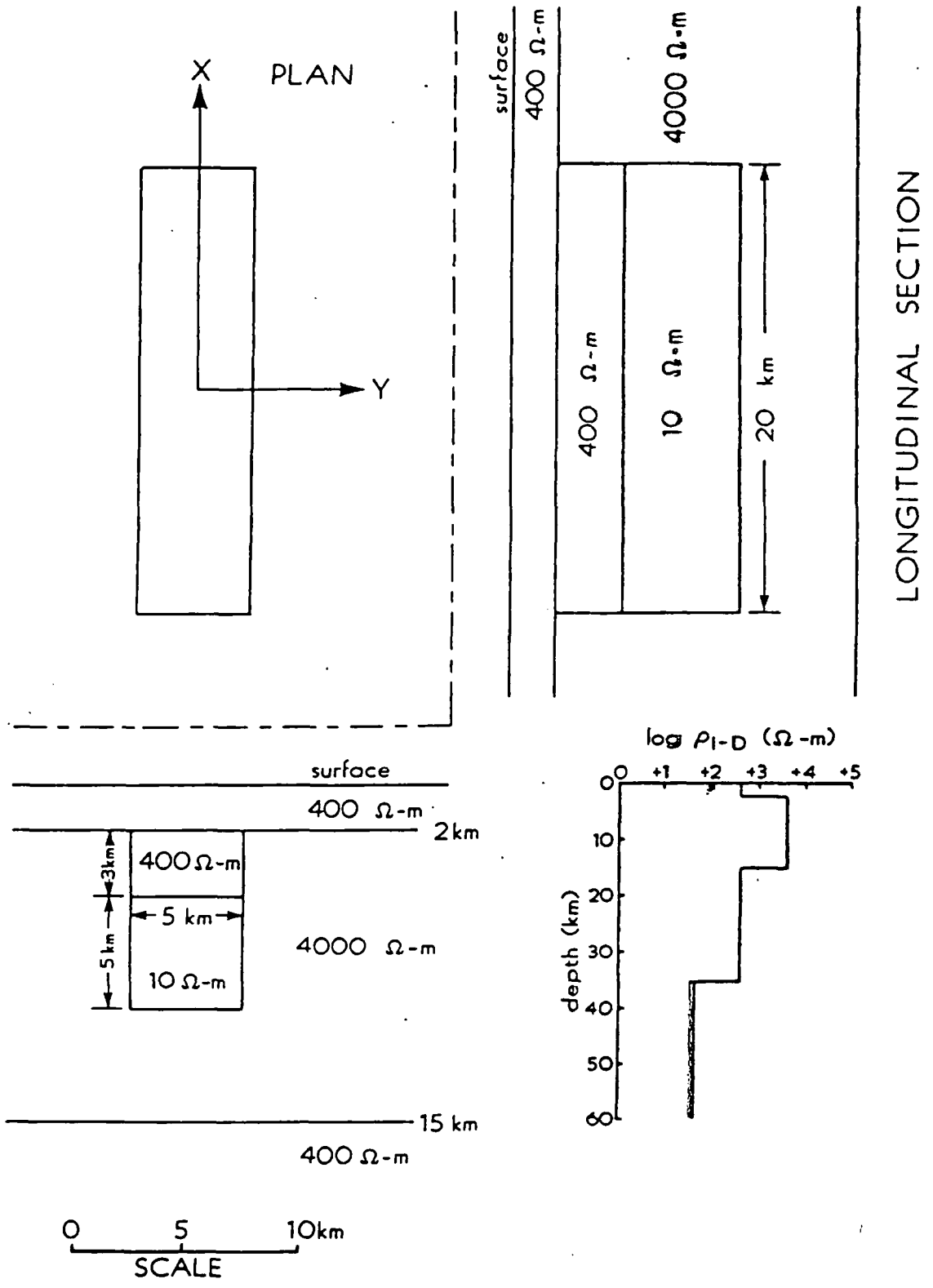
X
PLAN
Y
surface
400 Ω-m
4000 Ω-m
400 Ω-m
10 Ω-m
20 km
LONGITUDINAL SECTION
surface
400 Ω-m
2km
3km
400 Ω-m
5 km
5 km
4000 Ω-m
10 Ω-m
15 km
400 Ω-m
log ρI-D (Ω-m)
0 +1 +2 +3 +4 +5
0
10
20
30
40
50
60
depth (km)
0 5 10km
SCALE
CROSS - SECTION

Figure 6.

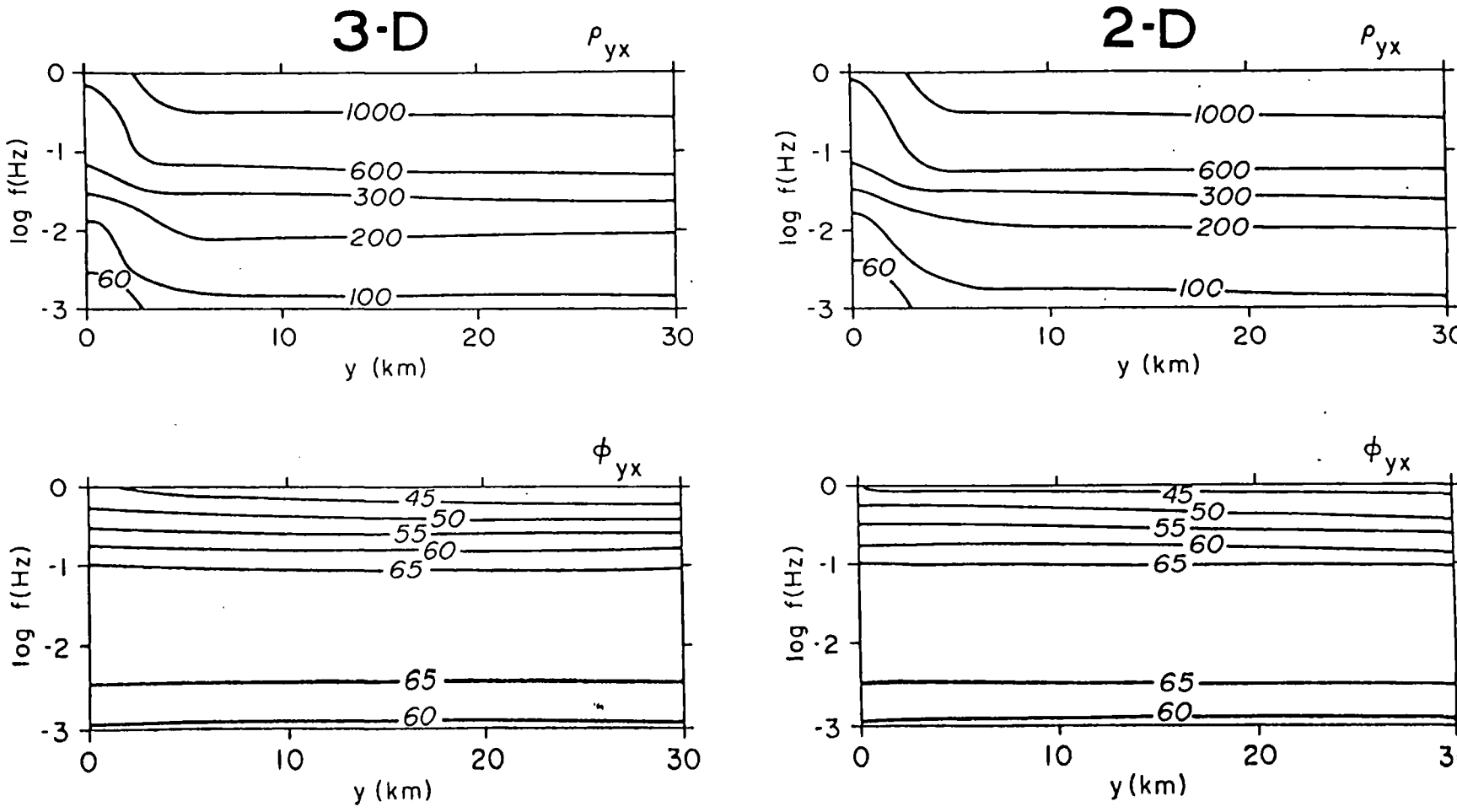
3-D
ρ_{yx}
1000
600
300
200
100
60
log f(Hz)
y (km)
2-D
ρ_{yx}
ϕ_{yx}
45
50
55
60
65

Figure 7.

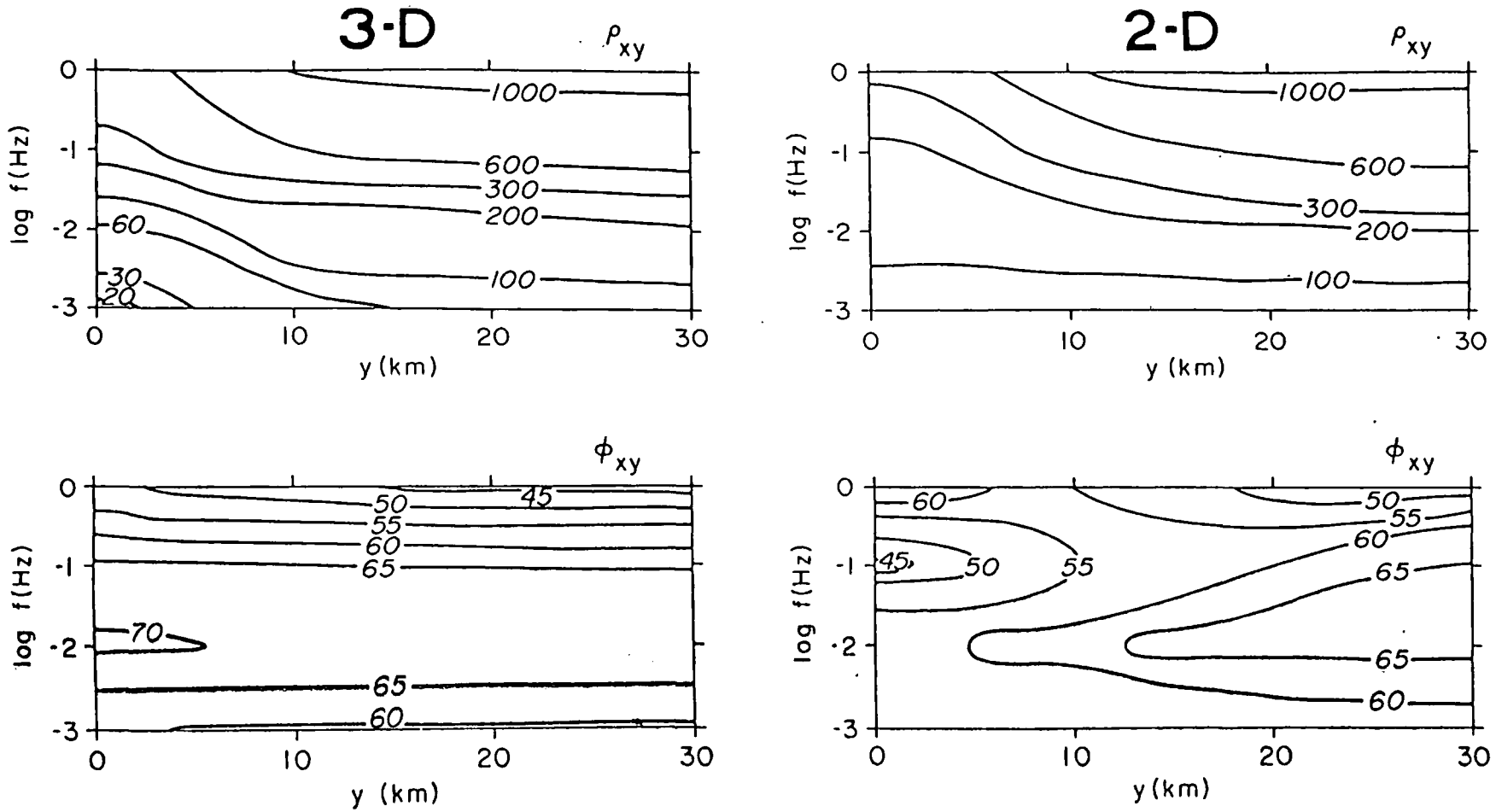
3-D
ρ_{xy}
1000
600
300
200
100
60
30
20
log f(Hz)
y (km)
2-D
ρ_{xy}
1000
600
300
200
100
log f(Hz)
y (km)
ϕ_{xy}
45
50
55
60
65
70
65
60
log f(Hz)
y (km)
ϕ_{xy}
60
50
55
60
65
45
50
55
65
60
log f(Hz)
y (km)

Figure 8.

Submitted to JGR
(Revised Version)

ELECTRICAL CONDUCTIVITY OF WATER-UNDERSATURATED CRUSTAL MELTING

Philip E. Wannamaker

Earth Science Laboratory

University of Utah Research Institute

391 Chipeta Way, Suite C

Salt Lake City, Utah 84108

Short Title: Conductivity of Water-Undersaturated Melting

July, 1985

ABSTRACT

Water-undersaturated melting in the crust can occur at lithostatic pressure in the presence of an H_2O-CO_2 fluid, of no CO_2 or fluid but with all H_2O bound structurally in hydrous minerals, or of an insufficient amount of H_2O fluid to saturate a melt at liquidus temperatures. The composition of any fluid in equilibrium with possible source rocks depends on the metamorphic grade of the rocks; the fluid at lithostatic pressure in ductile granulite facies rocks would be CO_2-rich while an increased fraction of H_2O in a fluid is probable in lithologies of lower metamorphic grade or in rocks of the brittle regime. With limited amounts of pore fluid and hydrous minerals, melting is a highly non-linear function of temperature and may extend over a broad temperature range. Electrical conductivity of the resultant feldspathic liquids can be estimated to first order from early conductivity measurements on granite under conditions of excess water and recent theories on dissolution of H_2O in aluminosilicate magmas. According to the model, melt phase conductivity falls with increased melt fraction due to dilution of water in spite of increased temperature. Melt fraction and temperature estimates for the lower crust derived from field electrical surveys are complicated seriously by melt phase tortuousity in the crystalline matrix, by H_2O content of the source rock, and by the possibility of a conductive CO_2-H_2O fluid. However, if the upper levels of a crustal magma chamber are near liquidus temperatures and if depth and confining pressure can be inferred from geophysical surveys, then electrical conductivity theoretically could provide both temperature and mole fraction of water for mole fractions less than about one-half.

INTRODUCTION

To explain high electrical conductivities inferred for the lower continental crust of high heat flow areas, researchers often have considered partial melting (Stanley et al., 1977; Olhoeft, 1981). In the way of laboratory calibrations of partial melt conductivity, one may consult measurements of dry, intermediate to silicic melts (Tyburczy and Waff, 1985) or the study of Lebedev and Khitarov (1964) on water-saturated granitic melt. In nature, silicic magmas typically possess calculated pre-eruptive water contents in the range of 1 to 5 wt. %, and thus should not have originated in either dry or water-saturated melting events at depths below about 5 km (Wyllie, 1977; Burnham, 1979a,b; Hildreth, 1981). To the extent that silicic magmas reaching shallow levels originate from middle or lower crustal melting, conditions of melting at these greater depths should be water-undersaturated.

That the availability of H_2O for melting in the lower crust is limited appears likely on other observational and experimental grounds. Although only grossly layered in composition, the crust most often shows a near-horizontal disposition of metamorphic grade, with greenschist facies in supracrustal rocks through amphibolite grade at middle levels to granulite facies in the deepest crust (Fountain and Salisbury, 1981; Kay and Kay, 1981; Windley, 1984). Seismic and geological evidence points to upper and middle levels in the crust containing the greater abundances of sedimentary and felsic magmatic rocks (Smithson et al., 1977; Oliver et al., 1983). Intermediate composition igneous rocks (diorites to tonalites) of granulite metamorphic grade comprise the commonest lower crustal sample, but with mafic and felsic lithologies, including sedimentary granulites, commonly interspersed and locally dominating (Smithson et al., 1977; Kay and Kay, 1981; Padovani et al., 1982; Windley,

1984). Laboratory experiments imply that H_2O fluid at lithostatic pressure in high-grade lower crustal rocks reacts with anhydrous silicates to form hydrous minerals, particularly amphibole (Burnham, 1979b). Fluid inclusion compositions, volcanic lava and gas chemistries and carbonate minerals in xenoliths moreover indicate a strong CO_2 component to fluids present in the deep crust (Newton et al., 1980; Kay and Kay, 1981; Touret, 1981; Wendlandt, 1981; Bailey, 1983; Menzies and Wass, 1983).

In this paper I consider water-undersaturated melting and electrical conductivity in the presence of an H_2O-CO_2 fluid, of no CO_2 or fluid but with all H_2O bound in hydrous minerals, and of an inadequate quantity of H_2O fluid to saturate a melt at liquidus temperatures (Robertson and Wyllie, 1971). Discussion centers upon a dioritic to tonalitic granulite composition, but compared also are mafic and felsic rocks and rocks of lower metamorphic grade. Equilibrium conditions are assumed, although the persistence of disequilibrium needs more study. Defining the existence of H_2O-CO_2 fluid as temperatures approach and exceed those of melting is important because fluids are expected to be conductive also and may obscure detection of melt. Estimating conductivity of subsequent H_2O-undersaturated melts combines the early water-saturated study of Lebedev and Khitarov (1964) with the theory and experiment principally of Burnham (1979a) on dissolution of H_2O in aluminosilicate melts. The available data indicates a substantial dependence of melt phase conductivity on water concentration and temperature, but large uncertainties in bulk conductivity remain regarding lower crustal water content and melt tortuousity.

FLUID-PRESENT AND FLUID-ABSENT MELTING

Even in lower crustal rocks of high metamorphic grade, water-undersaturated conditions for melting are not necessarily fluid-absent. H_2O diluted by the relatively inert agent CO_2, as well as being the most commonly inferred fluid state for the lower crust, is employed in the laboratory to demonstrate stability and fusion of crustal materials at partial pressures of water less than lithostatic.

Lower Crustal Fluids and Melting at Constant Pressure

In Figure 1 appear a tonalite solidus (Wyllie, 1977; Wendlandt, 1981) and equilibrium boundaries of an amphibole-in and a carbonate-in reaction as a function of temperature (T) vs. mole fraction of water $X^f_{H_2O}$ in an excess H_2O-CO_2 fluid phase. These are defined for fluid pressure (P_f) equal to total pressure (P_t) of 8 kbar. Amphibole-producing reactions principally involve pyroxene, feldspar and water (Eggler and Burnham, 1973; Holloway, 1973; Burnham, 1979b; Thompson, 1983). The carbonate-in reaction shown specifically consumes diopside, but other CO_2-consuming reactions in the lower crust involving olivine, pyroxene or plagioclase appear to have similar $T - X^f_{H_2O}$ topologies (Wyllie, 1979; Newton et al., 1980; Jacobs and Kerrick, 1981). Shown also is a downward-sloping univariant curve U projecting out of the diagram. Curve U is the intersection of downward-sloping amphibole-in and carbonate-in surfaces in $T - X^f_{H_2O} - P_f/P_t$ space.

Consider invariant point I in Figure 1 at a temperature $T_I \approx 700°C$ (perhaps 50-100°C lower if CO_2 is buffered by plagioclase and carbonate; Jacobs and Kerrick, 1981). In a lower crust containing pyroxene and feldspar, the boundaries of Figure 1 imply that the condition $P_f = P_t$ cannot be maintained at $T < T_I$ unless sufficient volumes of H_2O-C_2O fluid are introduced to exhaust one or both of the aforesaid volatile-free silicates. Such deple-

tion has not occurred for the granulite facies, intermediate composition model of the lower crust. Specifically, diorite-tonalite compositions can absorb nearly 1 wt. % of H_2O as hornblende (Wyllie, 1977; Burnham, 1979b). Therefore, through production of amphibole and carbonate, $P_f < P_t$ obtains at $T < T_I$ along the univariant curve U for the high-grade rocks. Finite pore volume at $P_f < P_t$ may be supported in rocks of a brittle mechanical regime (Brace, 1980; Chen and Molnar, 1983). In a lower crust which deforms ductilely in response to stress, however pore space at $P_f < P_t$ should collapse to a vanishingly small volume (Richter and Simmons, 1977; Brace, 1980; Thompson, 1983). In this case, there remains only a residual grain boundary population of volatiles. It is noted that the CO_2-rich fluid inclusions from presumably lower crustal samples are intracrystalline and isolated from carbonate-producing silicate reactants (Touret, 1981).

If a lower crust bearing amphibole and carbonate mineral is subjected to $T > T_I$, for instance with the onset of lithospheric extension or magmatism (Lachenbruch and Sass, 1978), a CO_2-rich fluid ($X^f_{H_2O} \simeq 0.1$ with amphibole) may evolve at lithostatic pressure starting at I through joint decomposition of carbonate and amphibole and exist with $P_f = P_t$ at temperatures below those of melting (cf. Thompson, 1983). In the presence of hornblende, approximately 1 vol. % CO_2-rich fluid is produced per vol. % of carbonate mineral in the rock (Glassley, 1983). Theoretically, depending on temperature and initial ratios of carbonate and hydrate, this free vapor may exist anywhere within the ruled region F. The volume abundance of amphibole must exceed that of carbonate by about a factor of two for carbonate to be consumed first and for the fluid to evolve from I toward M (melting) as temperature increases (Glassley, 1983). With sufficient amphibole, continued input of heat effects melting at M with activity of water in the melt and in any ambient fluid being

determined by hornblende breakdown (Burnham, 1979a,b).

Wherever CO_2 is absent in the lower crust, a diagram analogous to Figure 1 is relevant except that $X^f_{H_2O}$ is replaced by P_{H_2O}/P_t and carbonate reactions are not applicable. Fusion in the presence of amphibole essentially would occur at the same temperature as that of M and yield a melt of similar composition and water content (~ 3 wt. %) since activity of H_2O again is buffered by the hydrate. Introduction of CO_2 tends to increase alkalinity and decrease silica content of the melt somewhat (Wendlandt, 1981). Still in ductile granulite rocks no aqueous fluid evolves at temperatures below melting since $P_f = P_{H_2O} < P_t$. The H_2O supplied by amphibole in the absence of carbonate minerals is taken up directly by the melt at M until amphibole is depleted (Thompson, 1983). A relatively inert substance such as CO_2 is needed to dilute water for a finite volume of fluid to exist in lower crustal granulites at lithostatic pressure. Stabilization of amphibole to temperatures higher than that of M as given by the suprasolidus boundary in Figure 1 requires that water be supplied in excess of that from amphibole decomposition (e.g., Eggler and Burnham, 1973).

P_t-T Relations of Fluids and Melting

Water-undersaturated melting in the presence of several hydrate minerals is illustrated in Figure 2, a more familiar pressure-temperature projection of melting relations for tonalite. In this diagram appears the H_2O-saturated solidus, the dry liquidus, and stability boundaries for amphibole, biotite, muscovite and Mg-chlorite in the presence of quartz (Bird and Fawcett, 1973; Eggler and Burnham, 1973; Wyllie, 1977). At P_t-T values below the wet solidus, the stability boundaries mark breakdown of hydrous minerals yielding anhydrous silicates and H_2O fluid at lithostatic pressure. At P_t-T values greater than the wet solidus, the boundaries mark H_2O fluid-absent fusion of

hydrous and anhydrous minerals producing H_2O-undersaturated melt and represent the trace of point M in Figure 1 for amphibole and analogous traces for the other hydrous minerals. Low-grade chlorite forms from amphibole after depletion of pyroxene if feldspar is present and water added (Beach, 1980). Moving on, the trace of point I for amphibole from Figure 1 appears in Figure 2 as a dashed line over the pressure interval 4 to 10 kb. Corresponding traces for the other hydrate minerals are schematic but drawn assuming depletion of pyroxene, reduced activity of anorthite in plagioclase, and that the stabilities of the other hydrates in CO_2-H_2O fluids are similar to amphibole but lie at lower temperatures and higher $X^f_{H_2O}$ (Beach, 1980; Jacobs and Kerrick, 1981; Wendlandt, 1981). Finally, geotherms of Wyllie (1977) for a shield regime and of Lachenbruch and Sass (1978) for a magmatically-underplated lithosphere (reduced heat flow of 1.6 HFU) are drawn in Figure 2 with dots.

If the geotherm progresses from that of the stable environment to that of the hot tectonic regime, an H_2O-CO_2 fluid at lithostatic pressure should evolve as the traces of I are intersected provided any carbonate minerals are present. From the assumptions of Figure 2, such fluid forms at lower temperatures and higher $X^f_{H_2O}$ for the rocks of lesser metamorphic grade than for those greater. This may explain in part the observations of Touret (1981) that fluid inclusions in granulites are CO_2-rich but become H_2O-rich in greenschist and lower amphibolite assemblages. Moreover, the ability of these fluids to dissolve solids and form electrolytes relative to pure H_2O is proportional to $X^f_{H_2O}$ (Burnham, 1979a). Possible formation of a CO_2-H_2O fluid thus may contribute to the intracrustal high conductivities inferred at temperatures below those of melting by Shankland and Ander (1983).

As temperature continues to rise, melting in the lower crust may commence near the H_2O-saturated solidus of Figure 2 only in rocks of formerly low

metamorphic grade where an H_2O-rich fluid has been provided, for instance by breakdown of greenschist minerals at lower temperatures, in amounts greatly exceeding CO_2. Further melting requires temperatures in excess of the water-saturated solidus and becomes increasingly water-undersaturated. The rising temperature profile next would intersect one or more H_2O vapor-absent melting boundaries involving a hydrous mineral, depending upon metamorphic grade (water content) of the rock. Finally, liquidus temperatures are depressed below the dry curve of Figure 2 also depending upon bulk water content, (Wyllie, 1977, and next section).

Figures 1 and 2 are applicable fundamentally to rocks ranging in composition from granodiorite to gabbro because these rocks all contain some pyroxene with feldspar. Although a modest dependence of hydrous mineral stability on bulk composition is noted (Wyllie, 1977), variation in mineral abundances primarily determines the buffering capacity of a particular volume of rock to incoming H_2O and CO_2 volatile components (Thompson, 1983). Felsic compositions would be the first to allow existence of an H_2O-rich fluid if high-grade lower crust were subjected to a thorough retrograde metamorphism. Carbon dioxide, on the other hand, through dilution of water could allow electrically conductive fluid at lithostatic pressure at temperatures below melting in rocks felsic through mafic with any amounts of carbonate and hydrate minerals. A water-rich fluid appears likelier thermodynamically in the more brittle and felsic, lower-grade, middle and upper crust.

DEGREE OF MELTING WITH TEMPERATURE

Volumes and water contents of melts generated from crustal source rocks in the presence of free water or hydrate minerals may be predicted as a function of temperature to first order from the model of Burnham (1979a,b) for dissolution of H_2O in such melts. The approximation is possible because these magmas all are fundamentally aluminosilicate (feldspathic) in composition, i.e., water in the source rock leads to preferential incorporation of feldspar and quartz in the melt. A manifestation of this effect is that minimum melting temperatures in the presence of free water for compositions from granite to gabbro (amphibolite) are all very close (Wyllie, 1977, 1979). In the model, melt compositions are expressed by equivalent molal content of albite, for which thermodynamic relations in the presence of water are well established by experiment (Burnham and Davis, 1971, 1974). While much of the H_2O dissolves in molecular form (Stolper, 1982), it is the water dissolved through hydrolysis and melt depolymerization reactions which most importantly affects melt viscosity and electrical conductivity (Burnham, 1979a). The model has predicted successfully the solubility of water in magmas of composition from pegmatite to quartz tholeiite (Burnham, 1979a; Day and Fenn, 1982).

Under the assumption that crystal-hydrous melt equilibria in the crust can be approximated by those of albite, Figure 3 was constructed for total pressure of 8 kbar showing melt volume fraction ϕ as a function of T and $X^m_{H_2O}$ in a source rock of intermediate composition with 1 wt. % water provided either as a fluid or from muscovite, biotite or amphibole. To start, albite-hydrous melt equilibria at constant $X^m_{H_2O}$ (Burnham, 1979a) simply are mapped uniformly from the interval of minimum melting with free H_2O to the dry liquidus for albite onto the very similar corresponding interval for tonalite (Wyllie, 1977). Next, from the definition of mole fraction of water in the

melt (Burnham, 1979a), one may show that the weight of hydrous melt W^m formed per gram of H_2O contributed by the source rock is

$$W^m = [\frac{M_{als}}{M_{H_2O}} (1 - X^m_{H_2O})/X^m_{H_2O}] + 1 \quad . \qquad (1)$$

In (1), M_{H_2O} and M_{als} are molecular weights of water and aluminosilicate (albite). We are led from (1) to the volume fraction ϕ of hydrous aluminosilicate produced, given by

$$\phi = \frac{W^m \overset{o}{V}^m}{W^m \overset{o}{V}^m + W^r \overset{o}{V}^r} \quad , \qquad (2)$$

where W^m and W^r are the weights and $\overset{o}{V}^m$ and $\overset{o}{V}^r$ are the specific volumes of the hydrous melt phase as a function of $X^m_{H_2O}$ and T and of the crystal residuum respectively (albite values of Burnham and Davis, 1971, 1974). With 1 wt. % H_2O constituting about 2.9 gm per 100 cm^3 source rock, equations (1) and (2) were evaluated at numerous $X^m_{H_2O}$ to derive the melting curve of Figure 3.

Equation (1) for W^m is linear in source rock water content so that liquidus temperatures can be estimated by varying this water content. Because of the dependence of $\overset{o}{V}^m$ on $X^m_{H_2O}$, melt fraction is not exactly but nearly linear with water content. That a simple mapping of albite values can predict the water-undersaturated liquidi of granite compositions at various pressures within experimental uncertainty has been confirmed by Day and Fenn (1982). Therefore, while some dependence of H_2O solubility on feldspar composition has been observed (op. cit.), the dependence should not be so strong as to obscure the basic character of the melting curve for felsic to intermediate crustal rocks. In fact, even with pyroxene in substantial quantities and a generous 2 wt. % H_2O in a lower crustal source rock, liquidus temperatures determined experimentally exceed those given by equation (1) by only about 50°C for

tonalite and 75-100°C for gabbro (Wyllie, 1977). The shape of the melting curve thus is expected to resemble that in Figure 3 for a wide range of lower crustal compositions with limited amounts of water.

Temperature stability boundaries of muscovite, biotite and amphibole have been plotted in Figure 3 showing at what temperatures the water content of the rock, if it is contained in each of these minerals, promotes melting. These boundaries correspond to point M in Figure 1 and the traces of M in Figure 2. Observe that melting of intermediate composition rocks of high metamorphic grade in the presence of hornblende is calculated to yield undersaturated feldspathic melts containing 3 to 4 wt. % water. That agrees well with the experimental determinations of Eggler and Burnham (1973) and is within the range of pre-eruptive water contents inferred for silicic magmas (Burnham, 1979b; Hildreth, 1981). Indeed, a number of the least evolved silicic melts appearing in extensional environments imply pre-eruptive water contents as low as 1 to 2 wt. % (Nash, 1982), which seemingly require melting temperatures in the lower crust of 1000 to 1100°C. A favored source for high melting temperatures is introduction of mafic melts derived from the upper mantle (Hildreth, 1981). Equation (1) probably becomes inaccurate at high melt fractions in rocks bearing pyroxene component and with large water contents (>4 wt. %) since hornblende then may exist at temperatures beyond that at M in Figure 1 or may even constitute the liquidus phase (Wyllie, 1977; Burnham, 1979b).

ESTIMATES OF ELECTRICAL CONDUCTIVITY

The conductivity data of Lebedev and Khitarov (1964) obtained under conditions of water-saturation and the T - $X^m_{H_2O}$ - P_{H_2O} relations provided by Burnham and Davis (1974) may be combined to estimate conductivity of H_2O-undersaturated aluminosilicate melts as a function of temperature. The strong dependence of melt conductivity on $X^m_{H_2O}$ and T through the melting interval which is demonstrated carries through to effective medium conductivity of melt-rock mixtures.

T- $X^m_{H_2O}$ Dependence of Melt Conductivity

In Figure 4, albite-equivalent values of $X^m_{H_2O}$ are assigned to the P_{H_2O} isobars of saturated conductivity to give $X^m_{H_2O}$ isopleths. To the $X^m_{H_2O}$ values correspond temperatures at which hydrous melts exist in equilibrium with the source rocks, and these temperatures are taken from Figure 3. The intersection of said temperatures with the $X^m_{H_2O}$ isopleths of conductivity defines the dashed curve for P_t = 8 kb in Figure 4 (note that experimental conductivity requires some extrapolation, depicted by dots, below saturated liquidus temperatures). It should be emphasized that the dashed trajectory does not depend directly upon the shape of the melting curve (Figure 3) but that both the conductivity trajectory and the melting curve are functions of the T - $X^m_{H_2O}$ relations. Dashed curves shown in Figure 4 for P_t = 4, 2.5 and 1 kb were derived similarly, allowing estimation of conductivity of undersaturated felsic melts at various depths.

Olhoeft (1981) in his review noted that electrical conductivity of water-undersaturated granitic melt at constant temperature shows the greatest variation at low H_2O contents. In this paper, the effects of temperature as well as of H_2O content on conductivity are accounted for in an equilibrium model of crustal melting with limited amounts of water in the source rock. Specific-

ally, at large values of $X^m_{H_2O}$ in Figure 4, melt phase conductivity is not sensitive to temperature. With more melting and dilution of water, however, conductivity at constant P_t drops markedly despite higher temperature. The model liquid conductivity also is independent of source rock water content but, from the prior section, the melt fraction ϕ grows almost linearly with this parameter.

Some approximations inherent to the model conductivity should be discussed at this point. First, the slight dependence of H_2O solubility on temperature alone is disregarded (Burnham, 1979a). Second, the effect of P_t on melt phase conductivity for a given T and $X^m_{H_2O}$ is not accounted for. The compressibilities of hydrous aluminosilicate melts are much greater than that of dry melt (Burnham and Davis, 1971) suggesting correspondingly greater activation volumes and decreases in conductivity at greater pressure (Tyburczy and Waff, 1985). Acting to the contrary, whatever H_2O in the melt may be present as a larger molecular species (Stolper, 1982) could be driven toward dissociated form at higher P_t, thus promoting alkali exchange and conductivity. The third model uncertainty admitted is the accuracy of the data of Lebedev and Khitarov (1964) for all aluminosilicate melts at all $X^m_{H_2O}$ and T. For example, the conductivity trends in Figure 4 for $X^m_{H_2O} = 0.27$ and $X^m_{H_2O} \approx 0$ appear to cross if extrapolated subliquidus at a temperature around 1150°C. Data of Tyburczy and Waff (1985) on dry rhyodacite at 1 bar and 8 kb are included for comparison. Further experimental determinations at small $X^m_{H_2O}$ and of possible pressure and compositional effects are desirable.

Two-Phase Medium Conductivity

Jurewicz and Watson (1985) recently concluded through experiment that dry silicic melt collects along grain intersections for melt fractions of a few percent but that subsequent melt forms isolated pools throughout the sample.

The data of Lebedev and Khitarov (1964) simply suggest that melt interconnection may occur within a few degrees of the solidus under water-saturated conditions. At this time only crude bounds can be provided to deep crustal conductivity due to H_2O-undersaturated partial melting. Examples of two-phase conductivity computations for lower crustal rocks with 1 wt. % H_2O have been presented in Figure 5 as a function of melt fraction and temperature (from Figure 3) at a total pressure of 8 kbar. The two-phase models considered in Figure 5 are the Hashin-Shtrikman upper and lower bounds (Waff, 1974), the geometric mean of the melt and solid conductivities (Madden, 1976), and the Archie's Law with tortuousity coefficient of two used by Hermance (1979). Included also are conductivity of the melt phase (dashed curve for P_t = 8 kb redrawn from Figure 4) and the solid-state conductivity of a gabbroic rock host (Kariya and Shankland, 1983). Since melt fraction at a particular T varies almost linearly with bulk H_2O content, and melt conductivity is a function of $X^m_{H_2O}$, the relationships in Figure 5 between melt conductivity and effective conductivity for all two-phase geometries are specific to the 1 wt. % H_2O content adopted.

For melt fractions less than about 0.2, the two-phase models range over about three orders of magnitude in conductivity. For $\phi > 0.2$, bulk conductivity according to the Hashin-Shtrikman upper bound or the Archie's Law ranges only from 0.2 to 0.4 S/m. At the higher melt fractions with those models it would be difficult for field electromagnetic measurements to ascertain ϕ quantitatively, apart from inferring simply the absence or presence of melt. Under assumption of a prevailing hydrous mineralogy, e.g., amphibole versus biotite, such inferences would at least provide bounds on temperature at depth. The geometric mean and the Hashin-Shtrikman lower limit show a stronger dependence of conductivity on melt fraction throughout the

melting range but also show conductivity remaining below 10^{-2} S/m until melt fractions of 20 to 30% are reached. In comparison, Olhoeft (1981) and Shankland and Ander (1983) propose that conductivities approaching the prior value could arise from hot aqueous brines present in quantities on the order of 0.1 vol. %. According to my arguments, CO_2-H_2O fluids in only moderately greater amounts might effect similar conductivities.

Uncertainty over an appropriate two-phase geometry may be less for silicic magma chambers which result from melt coalescence and diapiric uprise from the lower crust (Hildreth, 1981). The higher regions of these chambers appear phenocryst-poor and their temperatures probably are close to the granite liquidus for the particular pressure and $X^m_{H_2O}$ (Hildreth, 1981; Fenn and Day, 1982). Electrical conductivity of the crystal-poor regions of these chambers therefore would be given directly by the conductivity trajectories of Figure 4. Moreover, if P_t can be constrained through geophysical observations and the magma is near liquidus temperatures, field conductivity estimates theoretically could provide T and $X^m_{H_2O}$ independently especially if mole fraction of water is less than about one-half. Before the $T - X^m_{H_2O}$ characteristics of a magma chamber can be described using electromagnetic surveys however, geophysicists have to unravel the measured field responses which must be precise, are certainly three-dimensional and may entail complex electrical interaction of the chamber with its environment (Hermance and Neumann, 1985; Newman et al., 1985).

CONCLUSIONS

Three modes of water-undersaturated melting at lithostatic pressure have been discussed in this paper: melting in the presence of an H_2O-CO_2 fluid, of no CO_2 or fluid but with all H_2O bound structurally in hydrous minerals, and of an insufficient amount of H_2O fluid to saturate a melt at liquidus temperatures. In the high-grade lower crust frequently hypothesized as the principal site of crustal melting, it is a CO_2-rich fluid at lithostatic pressure, and not an H_2O-rich one, which would exist at equilibrium for temperatures below or at those of melting. An H_2O-rich fluid can persist in rocks at low metamorphic grade or in rocks of the brittle mechanical regime. With limited amounts of pore fluid and hydrous minerals in any of the above modes, melting is a highly non-linear function of temperature and may occur over a broad temperature range.

The water-saturated conductivity experiments commonly used to interpret lower crustal fusion represent melts which, on a mole fraction basis, are more water than silicate. Water-undersaturated melts in equilibrium with residua of their source rocks are of lower conductivity than corresponding water-saturated melts even though the latter occur at much lower temperatures. Melt fractions from 10 to 50 volume percent may be needed for bulk conductivity to exceed 0.1 S/m. In addition to melt phase tortuousity, melt fraction and temperature estimates for the deep crust derived from field electrical measurements are complicated seriously by H_2O content of the source rocks and by the possible existence of a conductive CO_2-H_2O fluid phase. Conductivity in theory might tell about water concentration and temperature in crystal-poor magma chambers, but this assumes reliable estimates of conductivity structure from the field surveys.

ACKNOWLEDGEMENTS

Thoughtful reviews and criticisms of this work by J. R. Bowman, R. L. Bruhn and W. P. Nash are gratefully recognized. Technical assistance came from Sandra Bromley and Joan Pingree.

This work was supported by NSF contracts EAR-8116602 and EAR-8417765.

REFERENCES

Bailey, D. K., The chemical and thermal evolution of rifts: Tectonophysics, 94, 585-597, 1983.

Beach, A., Retrogressive metamorphic processes in shear zones with special reference to the Lewisian complex: J. Struct. Geol., 2, 257-263, 1980.

Brace, W. F., Permeability of crystalline and argillaceous rocks: Int. J. Rock Mech. Min. Sci. & Geomech. Abstr., 17, 241-251, 1980.

Burnham, C. W., and Davis, N. F., The role of H_2O in silicate melts I. P-V-T relations in the system $NaAlSi_3O_8$-H_2O to 10 kilobars and 1000°C: Amer. J. Sci., 270, 54-79, 1971.

_____, The role of H_2O in silicate melts II. Thermodynamic and phase relations in the system $NaAlSi_3O_8$ - H_2O to 10 kilobars, 700° to 1100°C: Amer. J. Sci., 274, 902-940, 1974.

Burnham, C. W., The importance of volatile constituents, In The Evolution of the Igneous Rocks: Fiftieth Anniversary Perspectives, ed. by H. S. Yoder, Jr., Princeton Univ. Press, 439-482, 1979a.

_____, Magmas and hydrothermal fluids, In Geochemistry of Hydrothermal Ore Deposits, ed. by H. L. Barnes, John Wiley and Sons, New York, 71-136, 1979b.

Chen, W. P., and Molnar, P., Focal depths of intracontinental and intraplate earthquakes and their implications for the thermal and mechanical properties of the lithosphere: J. Geophys. Res., 88, 4183-4214, 1983.

Day, H. W., and Fenn, P. M., Estimating the P-T-X_{H_2O} conditions during crystallization of low calcium granites: J. Geol., 90, 485-507, 1982.

Eggler, D. H., and Burnham, C. W., Crystallization and fractionation trends in the system andesite-H_2O-CO_2 at pressures to 10 kb: GSA Bull., 84, 2517-2532, 1973.

Fountain, D. M., and Salisbury, M. H., Exposed cross-sections through the continental crust: implications for crustal structure, petrology, and evolution: Earth Planet. Sci. Lett., 56, 263-277, 1981.

Glassley, W. E., Deep crustal carbonates as CO_2 fluid sources: Evidence from metasomatic reaction zones: Contr. Mineral Petrol., 84, 15-24, 1983.

Hermance, J. F., The electrical conductivity of materials containing partial melt: a simple model from Archie's Law: Geophys. Res. Lett., 6, 613-616, 1979.

Hermance, J. F., and Neumann, G. A., Refined analysis of telluric, magneto-telluric and magnetic variation data in Long Valley caldera (abstract): EOS Trans. AGU, 66, 392, 1985.

Holloway, J. R., The system paragasite-H_2O-CO_2: a model for melting of a hydrous mineral with a mixed-volatile fluid - I. experimental results to 8 kbar: Geochim. Cosmochim. Acta, 37, 651-666, 1973.

Jacobs, G. K., and Kerrick, D. M., Devolatilization equilibria in H_2O-CO_2 and H_2O-CO_2-NaCl fluids: an experimental and thermodynamic evaluation at elevated pressures and temperatures: Amer. Mineral., 66, 1135-1153, 1981.

Jurewicz, S. R., and Watson, E. B., The distribution of partial melt in a granitic system: the application of liquid phase sintering theory: Geochim. Cosmochim. Acta, 49, 1109-1121, 1985.

Kariya, K. A., and Shankland, T. J., Interpretation of electrical conductivity of the lower crust: Geophysics, 48, 52-61, 1983.

Kay, R. W., and Kay, S. M., The nature of the lower continental crust: inferences from geophysics, surface geology, and crustal xenoliths: Rev. Geophys. Space Phys., 19, 271-297, 1981.

Lachenbruch, A. H., and Sass, J. H., Models of an extending lithosphere and heat flow in the Basin and Range province, In Cenozoic tectonics and regional geophysics of the western Cordillera, ed. by R. B. Smith and G. P. Eaton, GSA Mem. 152, 209-250, 1978.

Lebedev, E. B., and Khitarov, N. I., Dependence on the beginning of melting of granite and the electrical conductivity of its melt on high water vapor pressure: Geochem. Int., 1, 193-197, 1964.

Madden, T. R., Random networks and mixing laws: Geophysics, 41, 1104-1125, 1976.

Menzies, M. A., and Wass, S. Y., CO_2- and LREE-rich mantle below eastern Australia: a REE and isotopic study of alkaline magmas and apatite-rich mantle xenoliths from the Southern Highlands province, Australia: Earth Planet. Sci. Lett., 65, 287-302, 1983.

Nash, W. P., Late Cenozoic silicic volcanism in the eastern Basin and Range province, Utah and Idaho (abstract): EOS Trans. AGU, 63, 1149, 1982.

Newman, G. A., Wannamaker, P. E., and Hohmann, G. W., On the detectability of crustal magma chambers using the magnetotelluric method: Geophysics, 50, in press, 1985.

Newton, R. C., Smith, J. V., and Windley, B. F., Carbonic metamorphism, granulites and crustal growth: Nature, 288, 45-50, 1980.

Olhoeft, G. R., Electrical properties of granite with implications for the lower crust: J. Geophys. Res., 86, 931-936, 1981.

Oliver, J., Cook, F., and Brown, L., COCORP and the continental crust: J. Geophys. Res., 88, 3329-3347, 1983.

Padovani, E. R., Hall, J., and Simmons, G., Constraints on crustal hydration below the Colorado Plateau from V_p measurements on crustal xenoliths: Tectonophysics, 84, 313-328, 1982.

Richter, D., and Simmons, G., Microcracks in crustal igneous rocks: microscopy, In The Earth's Crust, ed. by J. G. Heacock, AGU Mono. 20, 149-180, 1977.

Robertson, J. K., and Wyllie, P. J., Rock-water systems, with special reference to the water-deficient region: Amer. J. Sci., 271, 252-277, 1971.

Shankland, T. J., and Ander, M. E., Electrical conductivity, temperatures, and fluids in the lower crust: J. Geophys. Res., 88, 9475-9484, 1983.

Smithson, S. B., Shive, P. N., and Brown, S. K., Seismic velocity, reflections, and the structure of the crystalline crust, In The Earth's Crust, ed. by J. G. Heacock, AGU Mono. 20, 254-270, 1977.

Stanley, W. D., Boehl, J. E., Bostick, F. X., Jr., and Smith, H. W., Geothermal significance of magnetotelluric soundings in the Snake River Plain-Yellowstone region: J. Geophys. Res., 82, 2501-2514, 1977.

Stolper, E., The speciation of water in silicate melts: Geochem. Cosmochem. Acta, 46, 2609-2620, 1982.

Thompson, A. B., Fluid-absent metamorphism: J. Geol. Soc. London, 140, 533-547, 1983.

Touret, J. L. R., Fluid inclusions in high grade metamorphic rocks, In Fluid inclusions: applications to petrology: Mineral. Assoc. Canada Short Course Handbook, 182-208, 1981.

Tyburczy, J. A., and Waff, H. S., High pressure electrical conductivity in naturally occuring silicate liquids, in Point Defects in Minerals, ed. by R. N. Schock, AGU Mono. 31, 78-87, 1985.

Waff, H. S., Theoretical considerations of electrical conductivity in a partially molten mantle and implications for geothermometry: J. Geophys. Res., 79, 4003-4010, 1974.

Wendlandt, R. F., Influence of CO_2 on melting of model granulite assemblages: a model for the genesis of charnockites: Amer. Mineral., 66, 1164-1174, 1981.

Windley, B. F., The Evolving Continents: Second Edition, John Wiley & Sons, New York, 339, 1984.

Wyllie, P. J., Crustal anatexis: an experimental review: Tectonophysics, 43, 41-71, 1977.

_____, Petrogenesis and the physics of the earth, In The Evolution of the Igneous Rocks: Fiftieth Anniversary Perspectives, ed. by H. S. Yoder, Jr., Princeton Univ. Press, 483-520, 1979.

FIGURES

1. Tonalite melting and devolatilization reactions as a function of temperature T and of mole fraction of water $X^f_{H_2O}$ in an excess H_2O-CO_2 fluid at 8 kbar. Unless the rock is depleted in pyroxene or plagioclase, equilibrium fluid at lithostatic pressure and temperatures below those of melting is restricted to ruled region F. H_2O fluid-absent melting in the presence of amphibole occurs at M. Partly schematic but based on work of Eggler and Burnham (1973), Holloway (1973), Burnham (1979b), Wyllie (1979), Jacobs and Kerrick (1981), and Thompson (1983).

2. Pressure-temperature projections of melting and fluid production in tonalite for various degrees of water-undersaturation. Traces of invariant points I (dashed lines) represent first appearance of H_2O-CO_2 fluid in the presence of chlorite (chl), muscovite (ms), biotite (bi), or amphibole (am). H_2O-saturated solidus and dry liquidus are drawn as heavy solid lines. Breakdown of hydrous minerals yielding H_2O fluid below the wet solidus, or else incongruent melting of hydrous minerals with anhydrous components above the wet solidus, is depicted with medium solid lines. Dotted curves are geotherms of shield and magmatically-underplated regions.

3. Approximate model of melt volume fraction ϕ vs. temperature for production of aluminosilicate melts with 1 wt. % H_2O in lower crustal tonalitic rocks at 8 kb. Temperature of first appearance of melt depends upon the phase bearing the H_2O, i.e., free water, muscovite (ms), biotite (bi) or amphibole (am). The volume of melt created is approximately linear with bulk H_2O content, but mole fraction of water in the melt is essentially independent of such.

4. Trajectories in electrical conductivity (dashed lines) of water-undersaturated aluminosilicate liquids produced at P_t = 8, 4, 2.5 and 1 kb with fixed amounts of H_2O in the source rock. The trajectories are superimposed upon the water-saturated conductivity data of Lebedev and Khitarov (1964) shown with solid lines. Values of P_{H_2O} considered by Lebedev and Khiterov are labeled towards the right of the solid curves. Mole fraction of water in the melt for each P_{H_2O} is specified at the upper left. Dotted lines are extrapolation of saturated melt phase conductivity subliquidus to the wet solidus. Shown also is conductivity of a dry rhyodacite by Tyburczy and Waff (1985) at 1 bar (open circles) and at 8 kb (solid circles).

5. Conductivity of hydrous melt phase at 8 kb total pressure, replotted from the dashed curve of Figure 4, and of dry gabbro in the solid state (Kariya and Shankland, 1983) as a function of T compared to bulk conductivity estimates from two-phase medium theory. Two-phase models are the Hashin-Strickman upper and lower bounds (HSU and HSL, Waff, 1974), the geometric mean of melt and solid conductivities (GM, Madden, 1976), and an Archie's Law with tortuousity coefficient of two (A, Hermance, 1979). Bulk conductivities are specific to a source rock water content of 1 wt. %. Uncertainty in the data of Lebedev and Khitarov leads to uncertainty in melt and two-phase conductivity at high melt fractions. Also note the nonlinear temperature scale.

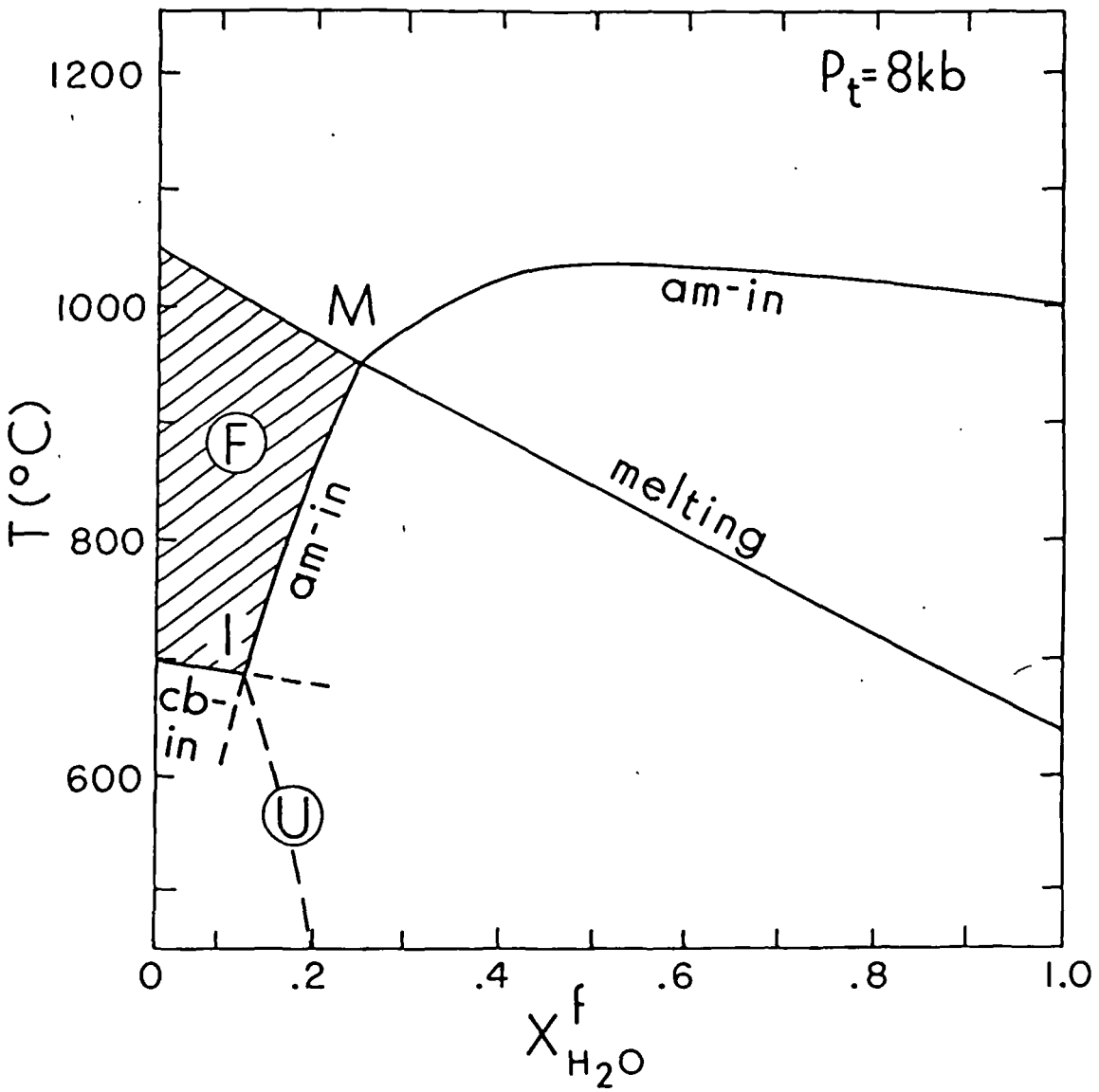
1200
1000
800
600
T (°C)
P_t=8kb
M
am-in
melting
F
I
am-in
cb-in
U
0
.2
.4
.6
.8
1.0
$X^f_{H_2O}$

Fig. 1

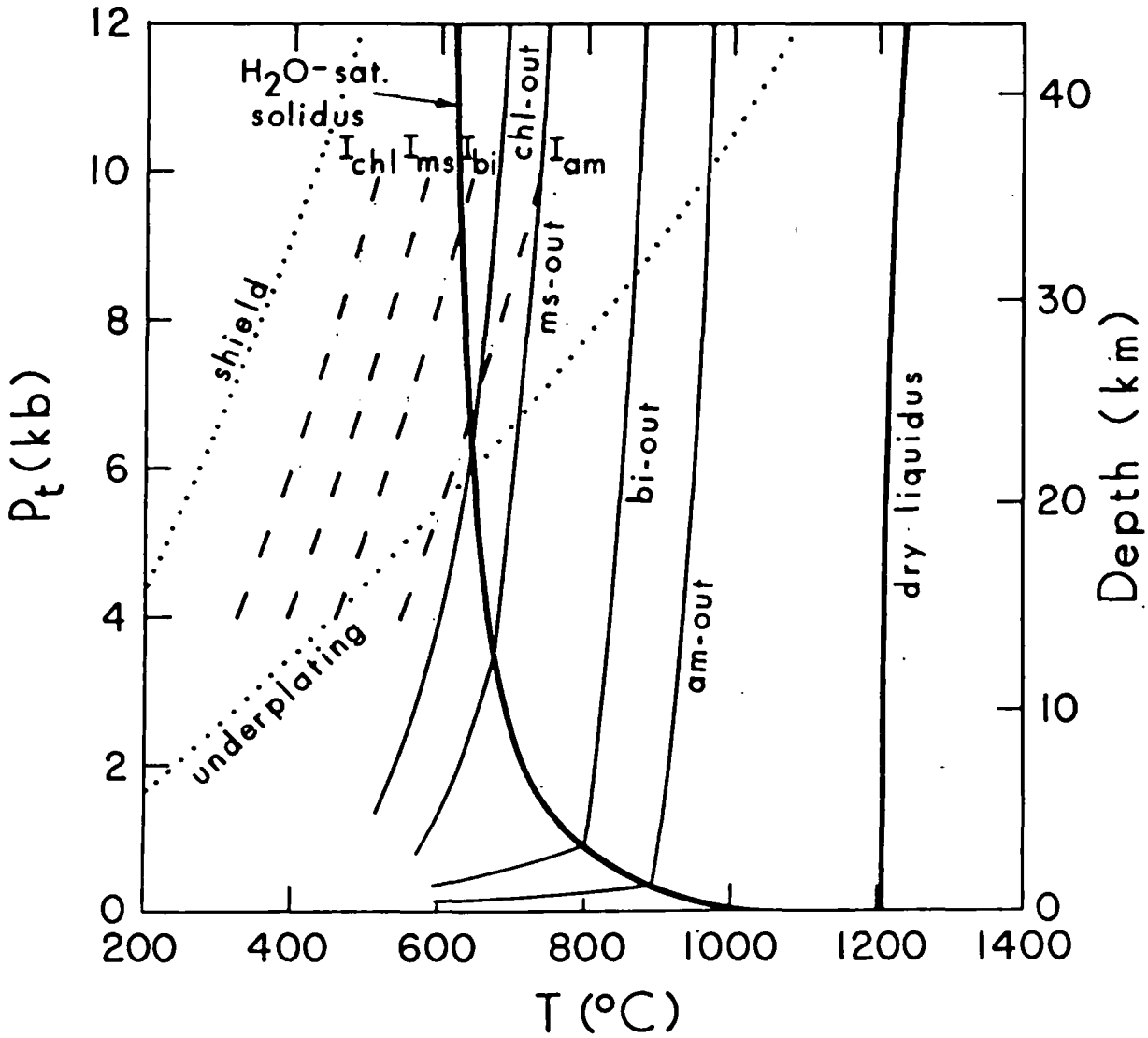
12
10
8
6
4
2
0
P_t(kb)
H_2O-sat.
solidus
I_{chl} I_{ms} I_{bi} I_{am}
chl-out
ms-out
bi-out
am-out
dry liquidus
shield
underplating
200
400
600
800
1000
1200
1400
T (°C)
40
30
20
10
0
Depth (km)

Fig. 2

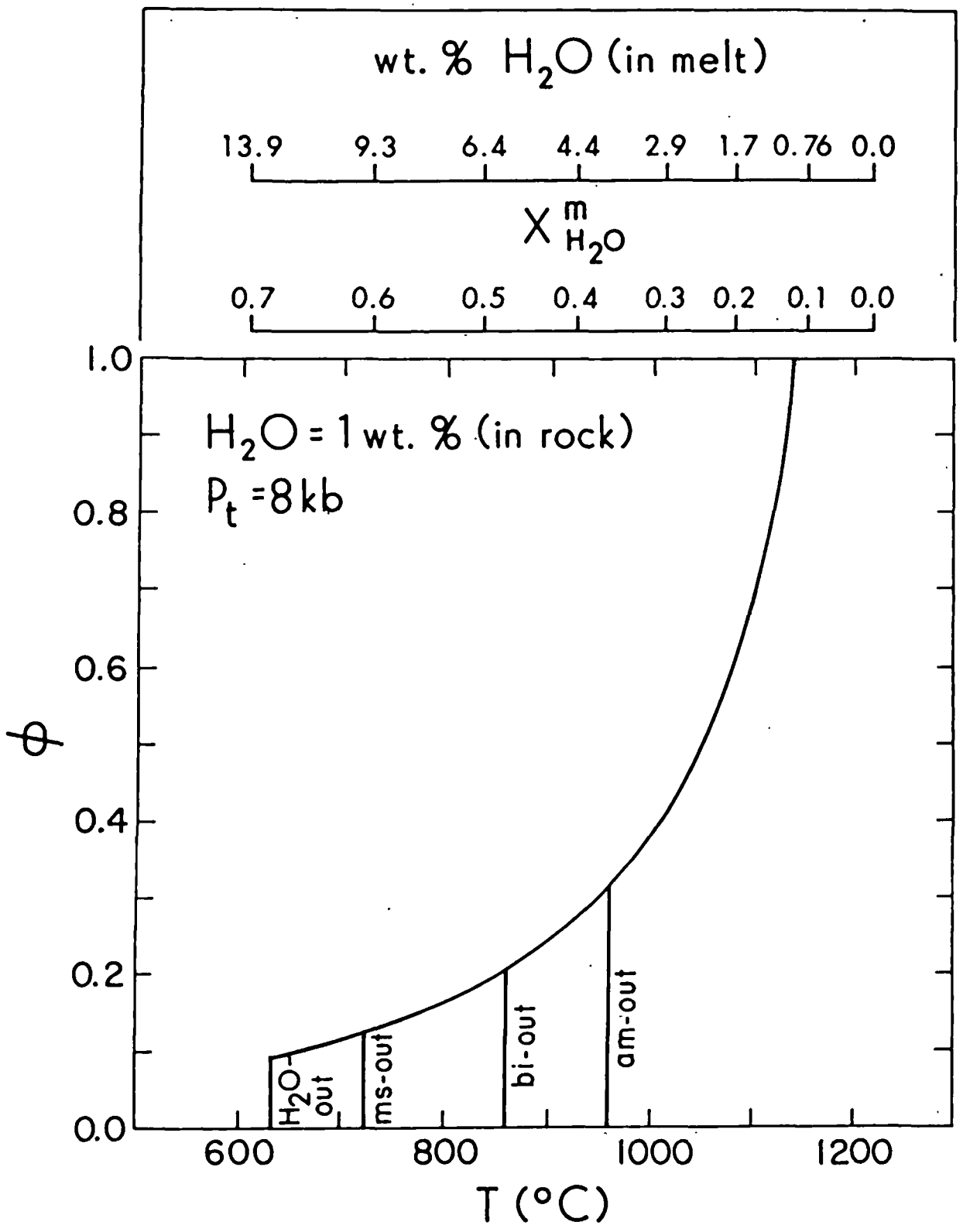
wt. % H_2O (in melt)
13.9 9.3 6.4 4.4 2.9 1.7 0.76 0.0
$X^m_{H_2O}$
0.7 0.6 0.5 0.4 0.3 0.2 0.1 0.0
H_2O = 1 wt. % (in rock)
P_t = 8 kb
1.0
0.8
0.6
0.4
0.2
0.0
ϕ
H_2O out
ms-out
bi-out
am-out
600
800
1000
1200
T (°C)

Fig. 3

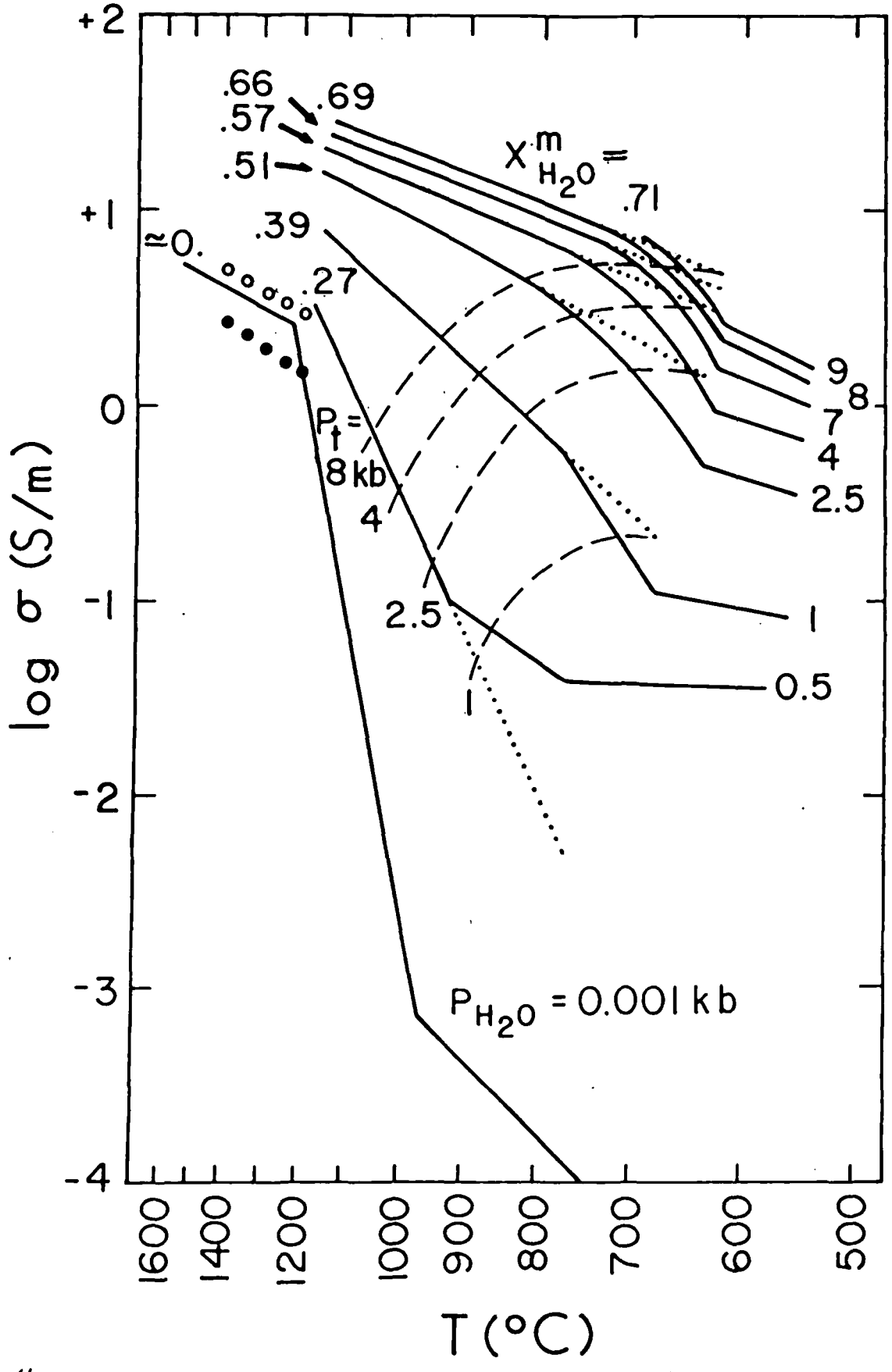
+2
+1
0
-1
-2
-3
-4
log σ (S/m)
1600
1400
1200
1000
900
800
700
600
500
T (°C)
.66
.57
.51
.69
$X^m_{H_2O}$ =
.71
≃0.
.39
.27
P_f =
8 kb
4
2.5
1
0.5
9
8
7
4
2.5
1
P_{H_2O} = 0.001 kb

Fig. 4

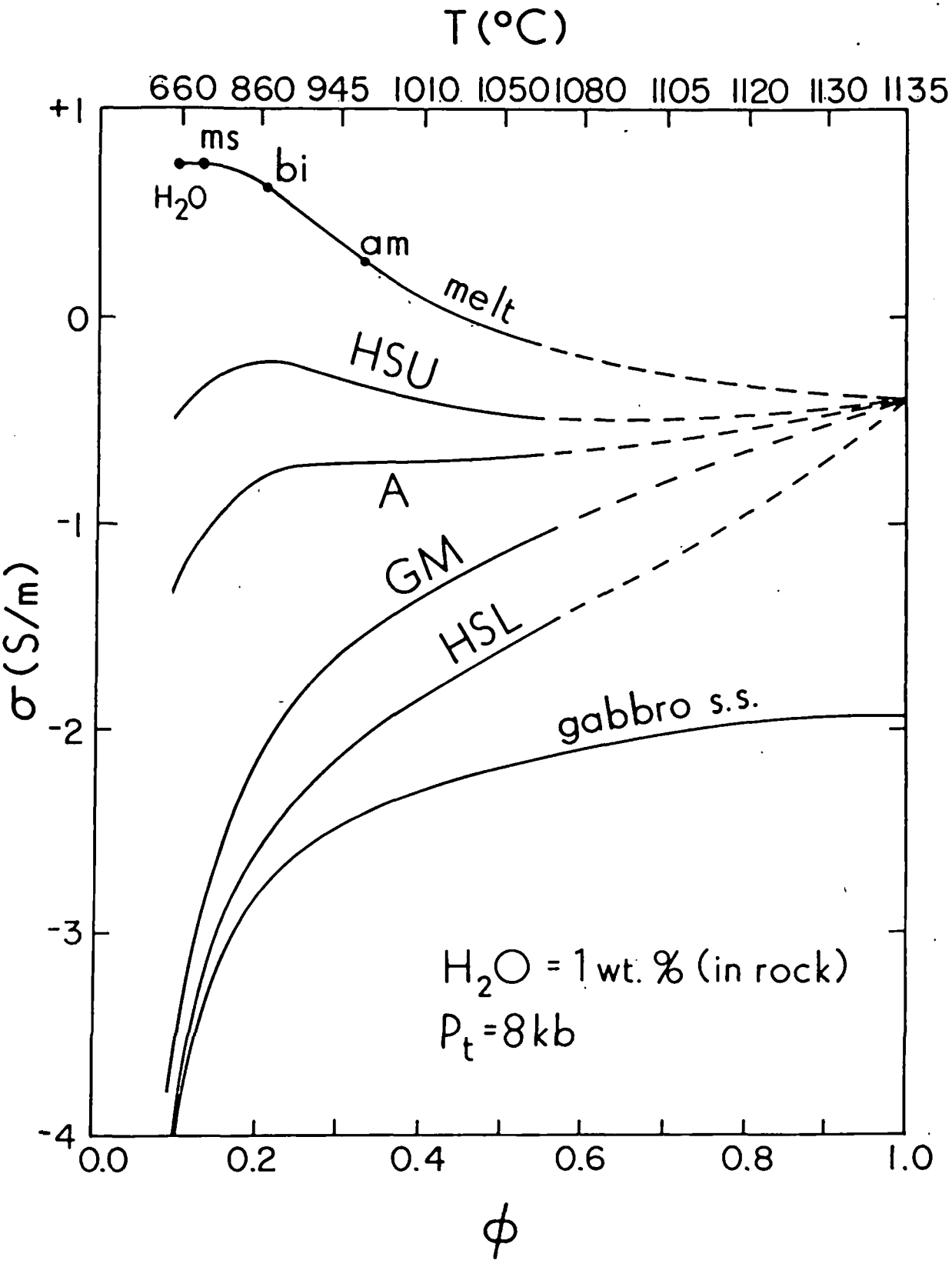
T(°C)
660 860 945 1010 1050 1080 1105 1120 1130 1135
+1
0
-1
-2
-3
-4
σ(S/m)
ms
bi
H2O
am
melt
HSU
A
GM
HSL
gabbro s.s.
H2O = 1 wt. % (in rock)
Pt = 8 kb
0.0
0.2
0.4
0.6
0.8
1.0
φ

Fig. 5

The Role of Heat in the Development of Energy and Mineral Resources in the Northern Basin and Range Province

SPECIAL REPORT NO. 13

1983

Printed by
GEOTHERMAL RESOURCES COUNCIL
P.O. Box 1350, Davis, California 95617-1350 U.S.A. (916) 758-2360

TABLE OF CONTENTS

RESISTIVITY STRUCTURE OF THE NORTHERN BASIN AND RANGE

Philip E. Wannamaker

Earth Science Laboratory/University of Utah Research Institute
420 Chipeta Way, Suite 120
Salt Lake City, Utah 84108

ABSTRACT

Trustworthy models of northern Basin and Range resistivity have been lacking mainly due to an inadequate regard for the effects of upper crustal three-dimensional (3D) inhomogeneities upon the surface electromagnetic measurements. While geomagnetic deep sounding (GDS) is relatively insensitive to upper crustal complexity, the ability of GDS to resolve structure of interest at greater depths is limited. The role of low-resistivity 3D structures near the surface has been documented most thoroughly for the magnetotelluric (MT) technique, although controlled-source electromagnetics (CSEM) using either grounded or ungrounded transmitters also is seriously complicated by inhomogeneities. The natural field methods of MT and GDS are preferred to CSEM for deep resistivity exploration due to the plane-wave nature of the source as well as to the availability of data at very low frequencies and of 2D and 3D modeling algorithms for treating upper crustal structure.

Magnetotelluric measurements in S.W. Utah have detected a low-resistivity layer from 35 to 65 km depth in the upper mantle that is proposed to reflect an accumulation of basaltic melt in peridotite. GDS experiments and various tectonic indicators suggest that this melt is controlled by adiabatic upwelling and fusion along the eastern margin of the northern Basin and Range. Similar GDS anomalies and extensional processes appear active in the western margin of this province, implying a similar resistivity structure. This would leave the northern Basin and Range interior of central Nevada as a comparatively quiescent region with an upper mantle seismic low-velocity zone whose melt interconnection, and commensurate low resistivity, remain fairly intact.

INTRODUCTION

The gains in knowledge of earth processes by investigations of electrical resistivity structure traditionally have been modest compared to those by other geoscientific methods. A major reason for this is that the electromagnetic (EM) measurements at the surface, from which one infers subsurface resistivity, in general are contaminated by complexity in the uppermost crust to a degree that is more extreme than for other geophysical techniques.

Through the course of this paper, I will examine the pitfalls in the interpretation of EM measurements in tectonically active environments, review previous surveys of resistivity structure in the northern Basin and Range, and propose a model for the Late Cenozoic evolution of deep resistivity structure and physiochemical conditions throughout the northern Basin and Range.

RESISTIVITY SURVEYS IN THE NORTHERN BASIN AND RANGE

Several key surveys of northern Basin and Range resistivity structure will be studied in this section (see Figure 1). Methods utilizing

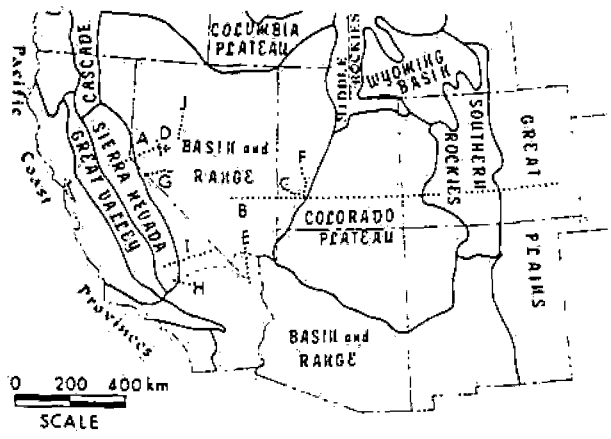

Figure 1. Physiographic provinces of the south western United States, modified from Stewart (1978). Dashed line separates Great Basin from the southern Basin and Range (Eaton, 1982). Locations are plotted for resistivity surveys discussed in text: A, Schmucker (1970); B, Porath (1971); C, MT survey at the Roosevelt Hot Springs, this paper; D, Stanley et al., 1976; E, Keller, 1971; F, Petrick et al., 1981; G, Lienert and Bennett, 1977; H, Lienert, 1979; I, Towle, 1980; J, Wilt et al., 1982.

either natural or artificial sources of EM fields have been applied. Principles of the techniques will not be reviewed here; the reader is referred to the literature cited for this purpose. I will, however, emphasize the effects on EM observations of the upper crustal three-dimensional (3D) heterogeneity so prevalent in the northern Basin and Range.

Geomagnetic Deep Sounding

Geomagnetic deep sounding (GDS), which makes use of natural magnetic field temporal variations, is less affected by upper crustal complexity than are the other EM methods I cover. The analysis of Wannamaker et al. (1983) can be extended easily to show that the secondary magnetic field transfer functions of GDS (Schmucker, 1970) are band-limited in frequency, with relatively small-scale, shallow structure like graben sediments responding over a frequency range which is higher than that of the deep regional resistivity structure of interest approximately as the square of the geometric scale factor distinguishing the two classes of structure. However, details of the separation depend on the layered host for the structures (Wannamaker et al., 1983). This separation of responses in frequency enables discrimination against surface inhomogeneity. Nevertheless, the response of the deep structure one seeks may itself be complicated; use of relatively simple 1D or 2D interpretation algorithms likely will yield models that are only qualitatively correct.

Pioneering measurements by Schmucker (1970) established geomagnetic anomalies indicating conductive upwellings beneath the Rio Grande Rift and the northwestern Basin and Range. Concerning the latter area, Schmucker places the conductive mass at a depth of 40 km in the upper mantle (Figure 2).

Much of what we know about the deep electrical resistivity of the northern Basin and Range and the Colorado Plateau is the result of geomagnetic temporal variations observed by Reitzel et al. (1970). Three components of magnetic field were recorded at periods from 20 to 200 minutes along four E-W profiles about 150 km apart, with station spacings averaging about 120 km. Porath et al. (1970) and Porath and Gough (1971) showed that anomalies in vertical and E-W horizontal fields were of internal origin (see Figure 3), with the external fields varying smoothly over the recording array. This behavior of the external fields severely limits the ability of GDS to resolve horizontal resistivity layering (Schmucker, 1970).

From these estimates of normalized anomalous fields, Porath (1971) presented a preferred, two-dimensional resistivity model, also shown in Figure 3, with a 2 Ω-m layer of varying thickness from the northern Basin and Range to the Great Plains, and with superimposed conductive ridges beneath the Wasatch Fault Belt and the Southern Rocky Mountains. This model was correlated with seismic LVZ estimates. Gough (1983) has reaffirmed the model of Porath (1971) and proposed that the conductive ridges in the upper mantle beneath western Utah and the southern Rocky Mountains reflect zones of partial melting. However, the intrinsic values of depth and resistivity are not well resolved (ibid.), especially given the assumption of purely 2D geometry. The secondary field amplitudes diminish to the south, and so presumably does the anomalous resistivity structure, but the features in Figure 3 appear to continue into northwesternmost Arizona.

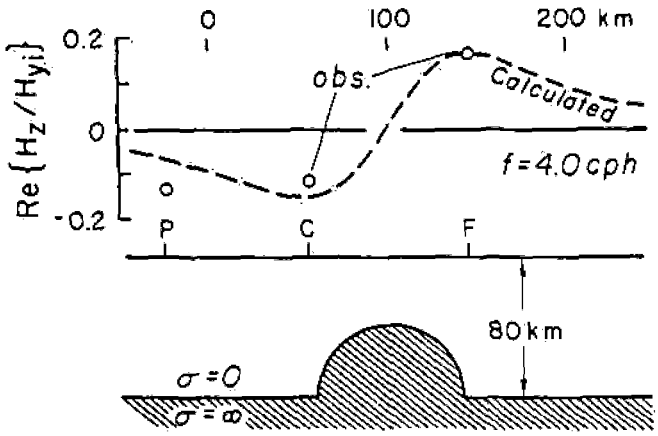

Figure 2. Observed and computed, normalized, in-phase, vertical magnetic field variation along WSW-ENE profile in western most Nevada. Also shown is simple, semi-cylindrical conductivity hump in the upper mantle which fits the observations. Urban centers located as abbreviations P (Pacific, CA), C (Carson City) and F (Fallon). Frequency is 4 cycles/hr. Adapted from Schmucker (1970).

Magnetotelluric Measurements

The magnetotelluric (MT) method, which makes use of both electric and magnetic natural field temporal variations, has been widely applied in the exploration of geothermal systems, sedimentary basins and the deep crust and upper mantle (Swift, 1967; Word et al., 1971; Vozoff, 1972; Larsen, 1975; Jupp and Vozoff, 1976; Stanley et al., 1977). While recent advances in instrumentation and data processing (Gamble et al., 1979; Weinstock and Overton, 1981; Stodt, 1983) enable accurate measurements of tensor MT responses, models of deep resistivity derived from MT responses commonly are suspect due to an unsatisfactory treatment of upper crustal lateral inhomogeneities (Wannamaker et al., 1983).

The Trouble with Upper Crustal Structure. - Serious problems with interpretation of MT soundings near electrically conductive graben sediments were first documented by Swift (1967) in his Arizona and New Mexico studies. A detailed

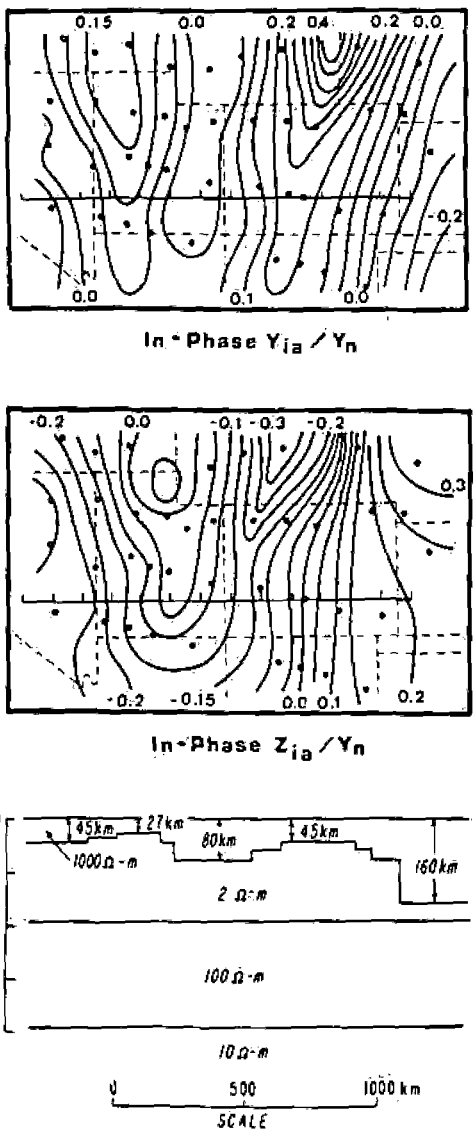

Figure 3. Normalized, anomalous, in-phase, horizontal E-W (Y_{ia}/Y_p) and vertical (Z_{ia}/Z_n) magnetic variation fields at a period of 60 minutes in the south western United States (Porath et al., 1970) along with the two-dimensional resistivity cross-section preferred by Porath (1971b) and Gough (1983) to explain the observations. The E-W profile for which the cross-section is defined is drawn on the maps of observed fields.

examination of the MT responses associated with graben alluvial fill has been performed by Wannamaker et al. (1983), who concluded that such responses are fundamentally three-dimensional in nature and that indiscriminate use of 1D or 2D modeling algorithms generally will incur serious errors.

Wannamaker et al. (1983) demonstrated in particular that two-dimensional transverse electric (TE) modeling algorithms are inappropriate for interpreting apparent resistivities, impedance phases or tipper in the northern Basin and Range identified as TE (Word et al., 1971; Vozoff, 1972). The 2D TE mode, consisting of the horizontal E-field parallel to strike and the orthogonal H-fields, involves no boundary charges and hence no current-gathering, whereas in the northern Basin and Range, all modes of MT responses due to upper crustal inhomogeneities are dominated by current-gathering.

If MT sounding data identified as TE in the presence of a 3D conductive inhomogeneity are inverted assuming a 1D model of deep resistivity structure, as I perceive has been overwhelmingly the case in the literature, then any such model will suffer systematically a compression of layer thicknesses and a downward bias in layer resistivities relative to the true 1D regional profile enclosing the inhomogeneity. This is because the TE mode apparent resistivity everywhere over and to the exterior of a conductive 3D body will be depressed throughout all frequencies relative to the apparent resistivity of the layered host containing the structure (Ting and Hohmann, 1981; Wannamaker et al., 1983).

Fortunately, accurate resistivity cross-sections through horst-graben morphology in the Great Basin can be obtained by selective application of a 2D transverse magnetic (TM) modeling algorithm (Wannamaker et al., 1983). The 2D TM mode consists of the H-field parallel to strike and the orthogonal E-fields. Boundary charges are included in both 3D and 2D TM formulations, allowing a proper treatment of current-gathering effects upon apparent resistivity and impedance phase. In defining data for transverse magnetic modeling of northern Basin and Range upper crustal structure, I recommend a uniform coordinate system based on tipper-strike (Vozoff, 1972). As with GDS transfer functions, tipper responses are band-limited in frequency (Wannamaker et al., 1983), so that one may choose an optimal frequency range for defining tipper-strike to minimize the contributions of secondary inhomogeneities much smaller than the conductive graben sediments for which one is primarily concerned in compensating.

MT Measurements at the Roosevelt Hot Springs.- A thorough accounting of upper crustal heterogeneity in the course of resolving deep resistivity has been performed on a collection of tensor MT data at the Roosevelt Hot Springs thermal area in S.W. Utah (Ward et al., 1978; Ross et al., 1982; see Figure 4). The complexly 3D nature of the MT responses directly over the thermal anomaly area prevented a rigorous quantification of any resistivity structure associated with an economic hot brine reservoir or a mid-crustal magmatic heat source for the geothermal system (ibid.). However, soundings along line B-B' in Figure 4 at distance from the thermal anomaly area, carefully modeled to remove the effects of upper crustal lateral inhomogeneities,

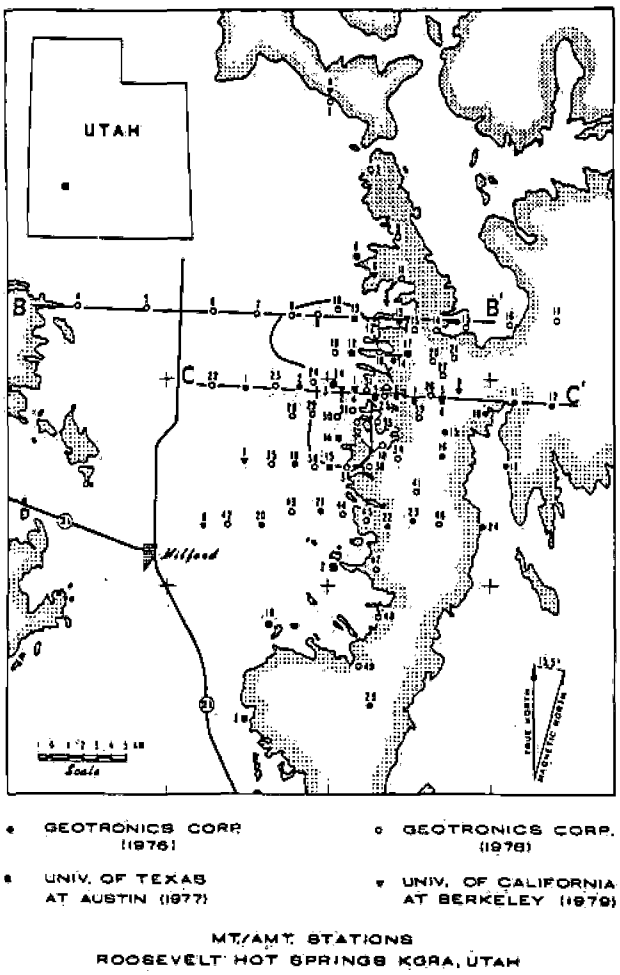

Figure 4. Magnetotelluric site location map for the Roosevelt Hot Springs thermal area. Rock outcrop bounding the Milford Valley sediments is lightly stippled while the solid curve is the 400 mWm^{-2} thermal contour (Ward et al., 1978). Station numbers referred to in text are prefixed according to the year in which they were occupied.

have yielded a regional resistivity profile for S.W. Utah to depths of about 100 km.

The observed quantities ρ_{yx} and ϕ_{yx} of line B-B', identified as TM, using a uniform coordinate direction as recommended previously, have been assembled in Figure 5 into pseudosections (Vozoff, 1972). The measured results for this line exhibit a virtually classic horst-graben response for the TM mode and bear a close resemblance to the computations of Wannamaker et al. (1983). Note especially the strong lateral gradients in ρ_{yx} and ϕ_{yx} between stations 78-8 and 78-10, which are due to the abrupt rangefront faulting bounding the graben sediments on the east side.

To interpret these MT observations, I have relied upon trial-and-error matching of results calculated from an assumed resistivity cross-section with the observed MT data of Figure 5 using a versatile and accurate 2D finite element forward program (Rijo, 1977; Stodt, 1978). Nonuniqueness in multidimensional modeling was alleviated by a high station density in each MT profile and by a wide spectrum of data at each station. In particular concerning the latter point, data at each sounding extended to sufficiently high frequencies so that both principal apparent resistivities ρ_{xy} and ρ_{yx}, as well as impedance phases ϕ_{xy} and ϕ_{yx}, have converged to common values above some frequency. For this high frequency range, the earth will likely be effectively one-dimensional, allowing one to constrain the near-surface model resistivities close to their true values. Such isotropic behavior occurs for frequencies above 1 Hz for the valley stations and above 30 Hz for the mountain sites.

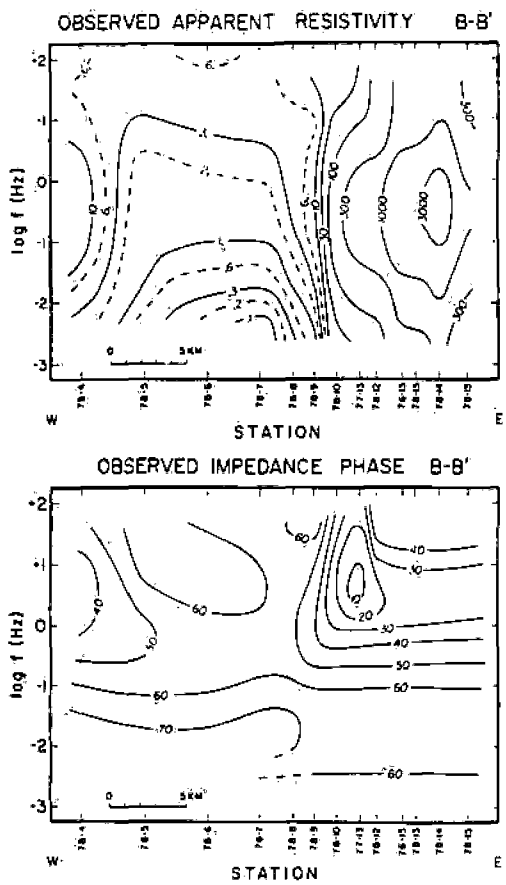

Figure 5. Observed pseudosections of ρ_{yx} and ϕ_{yx}, identified as transverse magnetic, along line B-B' of Figure 4. Contours of ρ_{yx} in Ω-m and of ϕ_{yx} in degrees.

The computed pseudosections of ρ_{yx} and ϕ_{yx} for line B-B' appear in Figure 6. Note that the computed and observed pseudosections are virtually identical; the observations have been fit to within data scatter almost everywhere. Examples of data scatter typical of sites over the Mineral Mountains will be forthcoming.

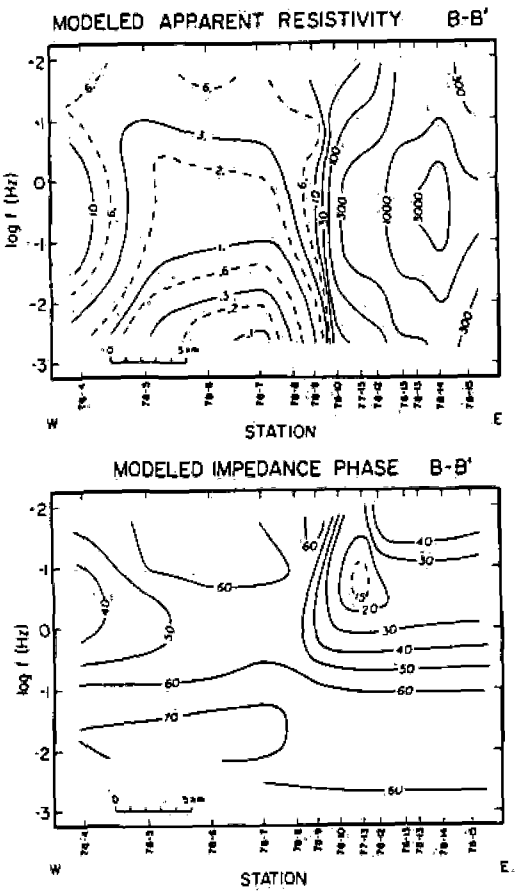

Figure 6. Best-fit pseudosections of ρ_{yx} and ϕ_{yx} obtained from transverse magnetic, finite element simulation of the observations of Figure 5. Contours of ρ_{yx} in Ω-m and of ϕ_{yx} in degrees.

The model of deep resistivity structure produced by application of the 2D TM finite element algorithm to the observations can be divided into two major parts: first, a shallow portion detailing just the extensive upper crustal lateral inhomogeneities in the upper 2 km; and second, a deep, purely layered portion extending to about 100 km which is determined by the physiochemical conditions of the crust and upper mantle below 2 km.

The upper 3 km of the finite element cross-section we have derived is shown in Figure 7. Within the Milford Valley, units within 140 m of the surface having resistivities from 3.5 to 18 Ω-m correspond to surficial clays, sands and gravels which are partially or completely water-saturated. Looking a bit deeper here, resistivities as low nearly as 1 Ω-m are caused by Pleistocene Lake Bonneville clays (Hintze, 1973, 1980), which we show residing to a maximum depth near 700 m below station 78-7. Deeper still exists a poorly resolved but substantial thickness (> 1 km) of modest resistivity material (25 Ω-m) related to pre-Bonneville alluvium and volcanics (Rowley et al., 1979). Note as well the especially steep dip of the eastern boundary faulting of the valley alluvium, inferred from the abrupt lateral gradients in ρ_{yx} and ϕ_{yx} between stations 78-9 and 78-10 in Figure 5 (cf. Wernicke and Burchfiel, 1982). The initial guess in the modeling process of this upper crustal resistivity section was guided by the refraction seismic model of Gertson and Smith (1979) and the gravity observations of Carter and Cook (1978), but the final section in Figure 7 shows important differences.

Over the Mineral Mountains, our model in Figure 7 shows resistivities of hundreds of ohm-m increasing to 3000 Ω-m over the depth interval of 2 to 3 km. This represents a decrease in porosity of the well-indurated basement rocks to well under 1%, probably due for the greater part to a decrease in fracture porosity below 2 to 3 km depth.

The 1400 Ω-m medium in Figure 7 begins the deep layered resistivity profile introduced previously and shown in its entirety in Figure 8. The best-fit model shows a maximum resistivity of 3000 Ω-m over the depth interval of 3 to 11 km. Subsequently, resistivity falls to 200 Ω-m by 35 km depth, whereupon an abrupt drop to 20 Ω-m is encountered. This low-resistivity material defines a deep, thick layer bottomed at 65 km depth by a sudden increase to a 200 Ω-m basal half-space. The fact that this deeper part of the model is purely layered is not due to poor resolution on the part of the measurements of Figure 5; the data quality for all soundings in line B-B' is good to excellent and yet the data are fit within scatter by imposing a purely 1D section for depths greater than 2 km. Furthermore, through application of a 2D TM program, the data of line C-C' in Figure 4 also are fit using the preferred deep profile of Figure 8 (Ross et al., 1982).

In Figure 9 are plotted both modes of apparent resistivity and impedance phase for station 76-13 along with several computed response curves. First, consider the solid curves passing through the observed data points of ρ_{yx} and ϕ_{yx}. These curves display the calculated response of the best-fit finite element model of Figures 7 and 8 at station 76-13, a response which seems very agreeable with the trends of the observed data points. In addition, curves of long dashes lying intermediate to the principal apparent resistivity and impedance phase observations are shown in Figure 9. The response of the best-fit one-dimensional deep resistivity profile of Figure 8 in the absence of all upper crustal lateral

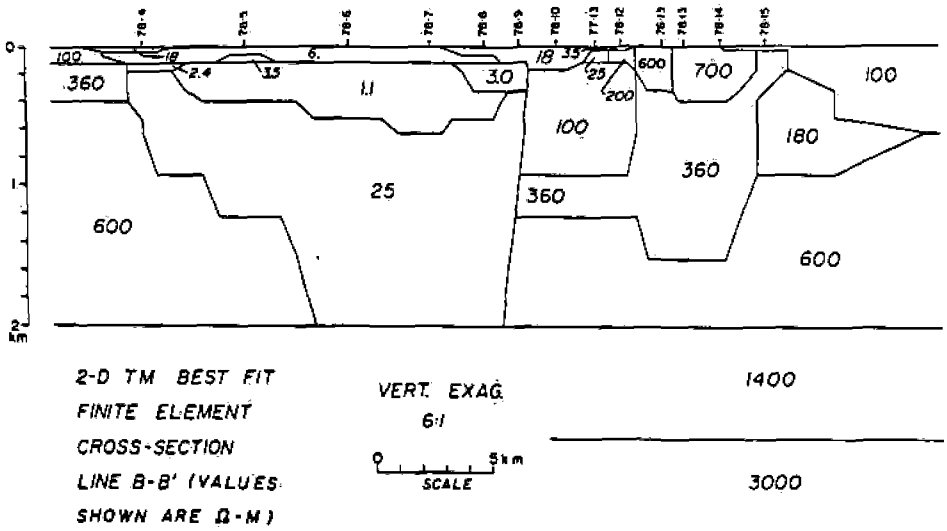

Figure 7. Best-fit, 2D TM finite element resistivity cross-section fitting the observations of line B-B' in Figure 4.

structure is represented by these latter curves. The difference between the observations and the purely 1D response illustrates again the importance of the Milford Valley in determining the MT signatures in this area. The inclusion of lateral inhomogeneities in models of deep resistivity structure is of paramount importance in tectonically disturbed regions like the Great Basin, and supercedes other considerations of the appropriateness of resistivity models vis-a-vis continuous vs. layered one-dimensional structures (Larsen, 1981; Parker and Whaler, 1981).

I turn now to resolution of detail in the deep resistivity profile of Figure 9. It is noted at the outset that, while lateral inhomogeneities, i.e., the Milford Valley, have induced anisotropy to a high degree over the Mineral Mountains, both tensor and 1D signatures in Figure 9 bear a certain mutual resemblance. In particular, the factor of ten drop in model resistivity at 35 km depth is responsible for the particularly steep gradients in the apparent resistivities and the values of impedance phases about 70° around 0.03 Hz. Also, without the abrupt rise in model resistivity at 65 km depth, the apparent resistivity data would not flatten out nor would the impedance phase data fall as strongly or rapidly as they do in Figure 9 at the lowest frequencies, especially below 0.003 Hz.

At frequencies less than 0.01 Hz in Figure 9, both ϕ_{xy} and ϕ_{yx} have converged to common values while ρ_{xy} and ρ_{yx} have shapes that are essentially identical except that they are offset by a factor of ten. Eventually, a convergence of this sort occurs as frequency falls for all stations in the Roosevelt Hot Springs area. This frequency dependence of the tensor sounding curves particularly illustrates that a one-dimensional, regional resistivity profile containing local lateral variations in structure, chiefly the Milford Valley sediments, is a viable model for the resistivity makeup here in S.W. Utah.

To strengthen confidence in the best-fit deep resistivity profile, I consider three alternates in Figure 8. The first is a profile whose log resistivity decreases linearly with depth (plotted with dots and labelled the "Steady Decrease" model in Figure 8). I arrive at a second layered sequence drawn with alternating dots and dashes in Figure 8 and called the "Shallow" regional model by shrinking the depths and resistivities of individual layers by 30% such that layer contrasts and conductivity thickness products remain constant (Madden, 1971). The last parameter resolution examination deals solely with the deep low-resistivity layer from 35 to 65 km. I maintain that this 20 Ω-m medium is not a "thin" layer (Madden, 1971), and to prove so it is replaced by a unit of equivalent conductivity-thickness product of 10 Ω-m resistivity and 15 km thickness.

The TM mode computed response curves at site 76-13 for the valley cross-section contained in each of the alternate model regional profiles appear in Figure 9. The computed apparent resistivity or impedance phase or both for each of the alternate models do not fit the observed data points over much of the frequency range, causing them to be dismissed as candidates for deep resistivity structure in this area. Recall that all soundings on profiles B-B' and C-C' are explained using the same regional profile; several other soundings in the Mineral Mountains are comparable in quality to site 76-13 and show

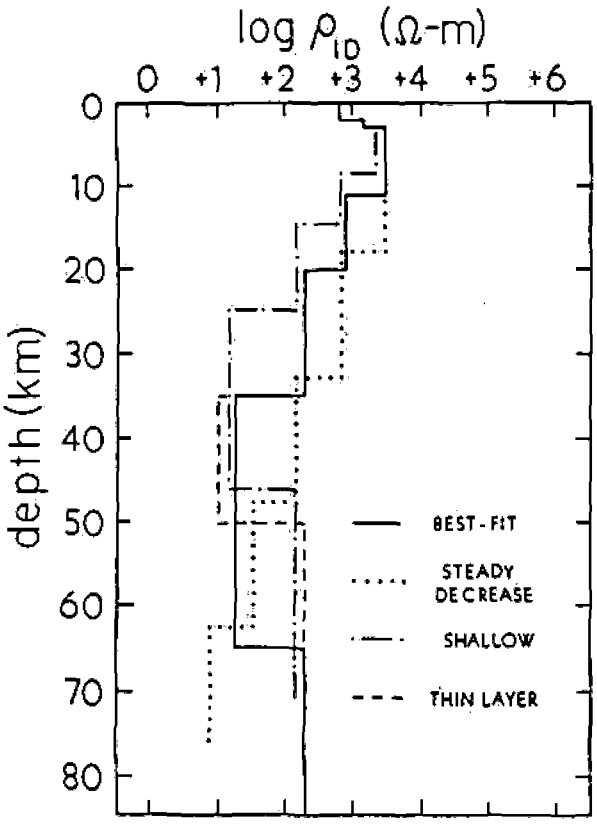

Figure 8. One-dimensional, deep resistivity profile in this area of S.W. Utah defining the lower portion of our 2D finite element model. Alternate resistivity profiles used in parameter resolution tests are drawn with dots and dashes.

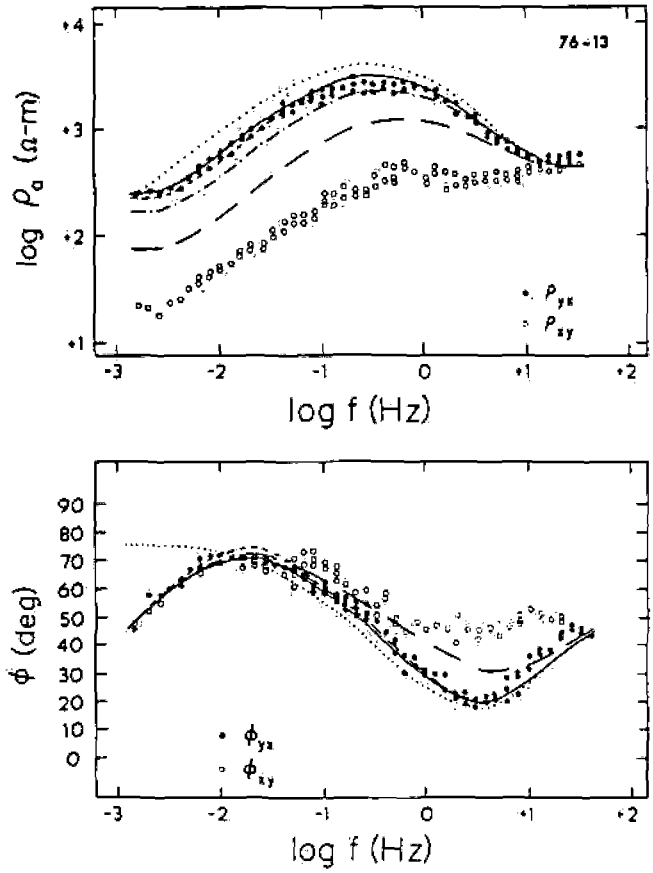

Figure 9. Observed data ρ_{xy}, ρ_{yx}, ϕ_{xy} and ϕ_{yx} for sounding 76-13 of line B-B'. Solid curve represents goodness-of-fit of computed to observed results using the best-fit resistivity cross-sections of Figures 7 and 8. Curves of dots and shorter dashes relate to correspondingly drawn alternate resistivity profiles in Figure 8 used in parameter resolution tests. Curves of long dashes appearing between the two modes of data points represent the 1D forward computation using the best-fit regional profile in Figure 8.

equally well the inadequacy of the alternate regional profiles. I presume a maximum depth of sensitivity of the data to subsurface structure of about 120 km, as imposition of low-resistivity material here causes computed phases at 0.002 Hz which exeed those of the best-fit model by about four degrees and which cannot be made to agree with the observations by increasing the resistivity of the 200 Ω-m material.

Before closing this particular study, there is one more demonstration of the hazards of 1D interpretation of MT data in regions of extension like the northern Basin and Range. In Figure 10 are reproduced the best-fit deep profile of Figure 8 as well as model profiles computed through direct 1D inversion of the tensor MT observations of Figure 9 (I used the routine of Petrick et al., 1977). The display of these observations with the computed 1D responses of the aforesaid model profiles in Figure 11 shows the goodness of fit possible by a 1D inversion algorithm to data taken in 3D environments. The deep resistivity models derived thereby are unacceptable, however; their departure from the preferred deep profile exceeds bounds that were already rejected in the rigorous parameter resolution studies of Figures 8 and 9. Moreover, due to local lateral inhomogeneity, computed layered models will vary drastically from site to site within the mountains, underscoring the unreliability of one-dimensional inversion in this environment.

Matters are even worse for 1D inversion of MT soundings taken within northern Basin and Range graben fill. Figure 12 shows layered earths computed through 1D inversion of apparent resistivities ρ_{xy} and ρ_{yx} and impedance phases ϕ_{xy} and ϕ_{yx}, identified as TE and TM (Word et al., 1971; Vozoff, 1972), for site 78-6 of Figure 4. Solid curves through the data in Figure 13 show

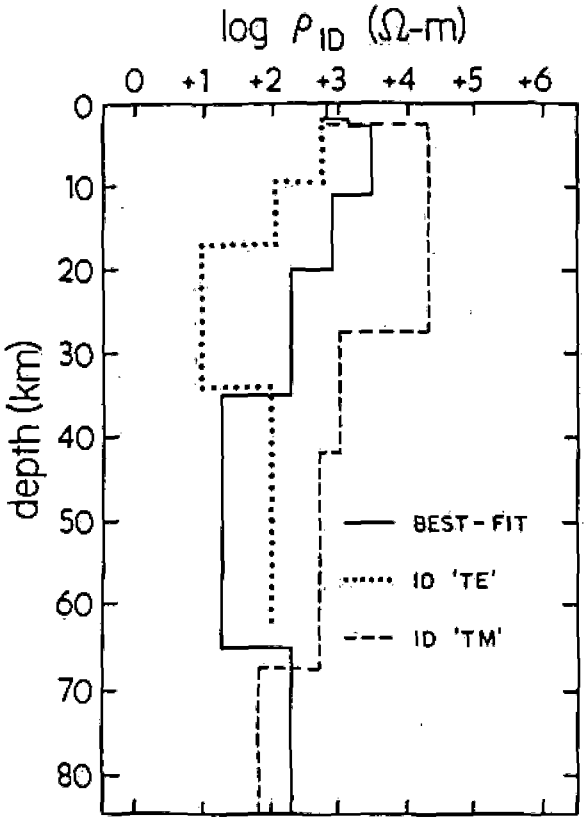

Figure 10. Best-fit regional resistivity profile for the Roosevelt Hot Springs thermal area compared to layered models obtained through 1D inversion of ρ_{xy} and ϕ_{xy} (dotted lines) and ρ_{yx} and ϕ_{yx} (dashed lines).

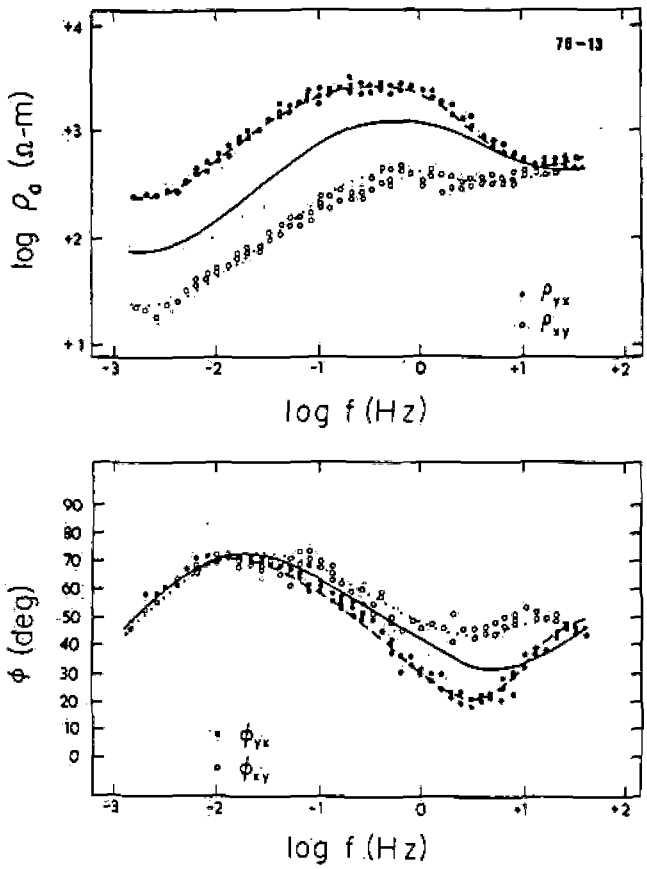

Figure 11. Observed data points of ρ_{xy}, ρ_{yx}, ϕ_{xy} and ϕ_{yx} for sounding 76-13 showing the goodness of fit that can be obtained to 3D data using a 1D inverse routine. However, the resultant layered models were dismissed as unrealistic. Solid curve appearing between data points is the 1D forward response of the best-fit regional profile.

the goodness-of-fit obtained by the inversion, with the nominally very conductive basal half-spaces resolved by the observations below 0.2 Hz. However, given the best-fit model of Figure 8 derived through a rigorous accounting for the effects of the valley sediments, the layered models at site 78-6 are obviously unrealistic. Note that the data of Figure 13 bear a close resemblance to the theoretical computations of Wannamaker et al. (1983) over their model valley. I believe that 1D models of resistivity given by Stanley et al. (1976) for the Stillwater-Soda Lakes district, which were computed from soundings taken within deep conductive alluvium of the Carson Sink area, are similarly affected. The case for low resistivities at depths as little as 5 km in that region remains to be substantiated.

Physical State at Depth in S.W. Utah. - In Figure 14, the best-fit regional profile for the Roosevelt Hot Springs is compared to laboratory experiments on the electrical properties of rocks. A crustal thickness slightly less than 30 km is assumed for this area (Keller et al., 1979; Allmendinger et al., 1983). Petrological studies and seismic velocities point to a mafic metaigneous composition near gabbro for most of the lower half of the crustal section, with relatively felsic rocks above (Smith, 1978; Padovani et al., 1982; Nash, 1983). A peridotite composition is taken for the upper mantle rocks (Wyllie, 1979).

Adopting a conductive geotherm for a regional heat flow of 2.4 HFU (1 HFU = 41.6 mWm^{-2}) (Lachenbruch and Sass, 1978; Chapman et al., 1981), the lower bound on aqueous electrolytic conduction through rock pores of Brace (1971) and the mean dry gabbro semiconductivity results of Kariya and Shankland (1983) are combined to yield the curve of dots in Figure 14. Over the depth interval 15 to 30 km, the regional profile appears somewhat less resistive than what is predicted by dry solid-state measurements. If a gabbroic

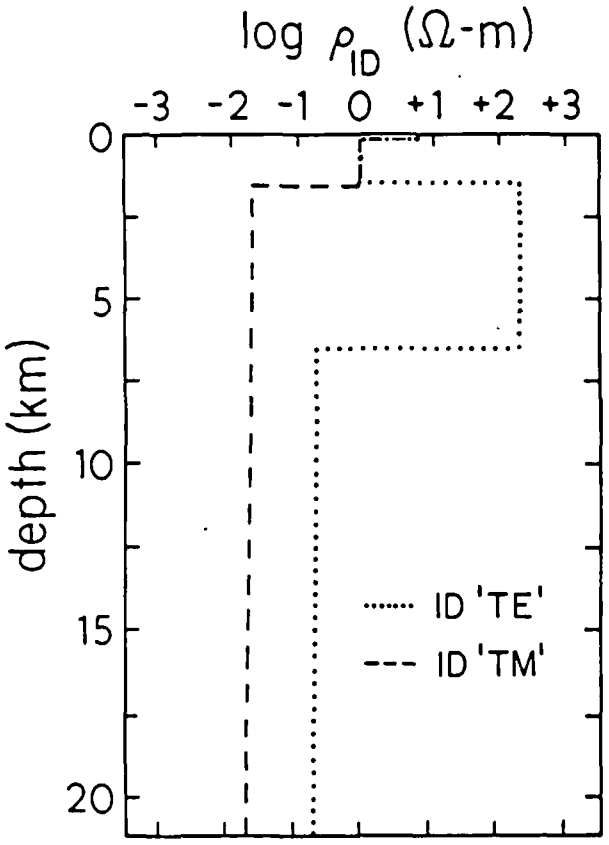

Figure 12. Layered resistivity models obtained through 1D inversion of ρ_{xy} and ϕ_{xy} (dotted lines) and ρ_{yx} and ϕ_{yx} (dashed lines) for sounding 78-6 of Figure 4. Note scale change from Figure 10.

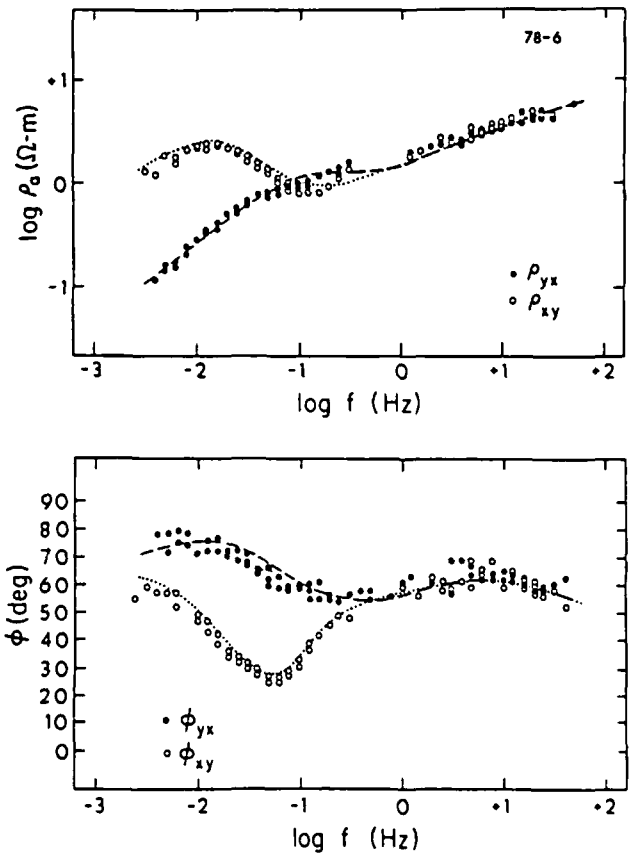

Figure 13. Observed data points of ρ_{xy}, ρ_{yx}, ϕ_{xy} and ϕ_{yx} for sounding 78-6. Curves of dots and dashes show responses of layered earth models of Figure 12.

composition is relevant then free water in this interval is improbable (Burnham, 1979a, 1979b). However, a reduction of solid-state resistivity through active deformation and non-zero partial pressure of water appears possible (Winkler, 1979; Duba and Heard, 1980; Kirby, 1983; Spear and Silverstone, 1983).

The curve of dashes in Figure 14 pertains to upper mantle rocks and results from the solid-state measurements on olivine by Duba et al. (1974) and the conductive geotherm. Of greatest importance, the shape of the solid-state curve is very different from the regional profile. In an earth where temperature increases steadily with depth, such as is the case with our conductive geotherm or even with any of the temperature profiles of Lachenbruch and Sass (1978) which incorporate convective components, the Arrhenius solid-state temperature dependence for a rock results in bulk resistivity which decreases monotonically with depth. During the discussion of parameter resolution, a deep resistivity profile that decreased steadily with depth was rejected as a candidate to explain the low-frequency MT observations in S.W. Utah; the order-of-magnitude rise of resistivity in the upper mantle in our best-fit deep model is a strict requirement.

I therefore look to partial melting in the upper mantle as the cause of the 20 Ω-m deep layer. Again imposing the conductive geotherm, the curve of dots and dashes in Figure 14 arises using a dry peridotite melting curve (Mysen and Kushiro, 1977; Wyllie, 1979; Best et al., 1980), the measurements of alkali-olivine basalt conductivity of Rai and Manghnani (1978) and the melt phase interconnection model of Waff and Bulau (1979). The large liquid fractions implied by this melting curve are of course unrealistic and result from use of a conductive temperature profile. Given that melt conductivities are strongly temperature dependent, and that the interconnection model is strictly an abstraction, I simply conclude that the melt fraction in the deep, low-resistivity layer is rather small, less than 5%. In reality, the dry peridotite solidus is advocated as a representative pressure-temperature trajectory for the depth interval of the 20 Ω-m layer (Mysen and Kushiro, 1977; Wyllie, 1979; Best et al., 1980). It is argued shortly that this trajectory may be valid to much greater depths in the region.

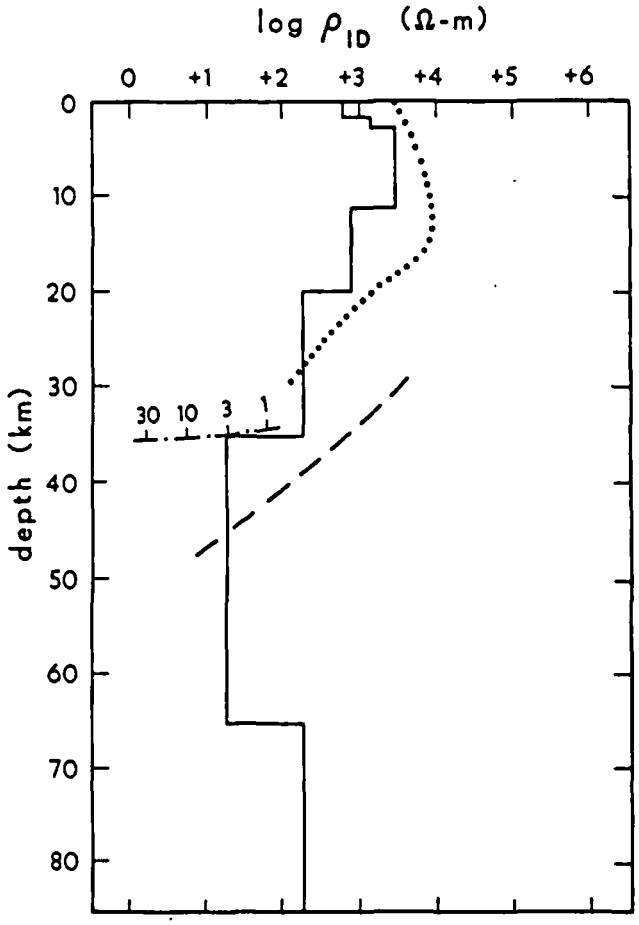

Figure 14. Best-fit, crust and upper mantle resistivity profile for southwestern Utah compared to physical model incorporating aqueous electrolytic conduction in rock pores, solid-state semiconduction in minerals and ionic conduction in partial melts. Definition of curves explained in text.

Controlled-Source EM Techniques

In controlled-source electromagnetics (CSEM), EM fields are impressed by a transmitter, either fixed-site or roving, and monitored as a function of position and/or frequency at a receiver (Grant and West, 1965; Ward, 1967). The current transmitter can be a grounded bipole, an ungrounded loop, or a very long, essentially ungrounded line source.

Effects of Upper Crustal Structure. - Ward (1983) has investigated theoretically the behavior of EM fields about typical northern Basin and Range alluvial fill for grounded bipoles and an ungrounded loop. The basin model he has chosen has a resistivity and dimensions similar to that of Wannamaker et al. (1983), except that Ward's model was enclosed simply in a 400 Ω-m half-space. The frequency of excitation was 0.03 Hz.

The difference between the total field in the presence of the valley and the half-space host field is a measure of the error in models of deep resistivity profiles derived from simple 1D inversion. For the grounded bipole source of Ward (1983) the amplitude of the horizontal magnetic field over the body rose to more than 3 times the primary field. It asymptotes to 60% of the primary field at large distances from the body. Channeling of the bipole return current through the valley fill can explain this result. Distortions of the horizontal H-field were as severe for the square loop as for the grounded bipole. The importance of this latter behavior cannot be overemphasized; total and primary fields differ to extremely large distances and to low frequencies even for ungrounded sources.

Models of Deep Resistivity from CSEM. - Experiments using galvanic resistivity methods in the northern Basin and Range and the Colorado Plateau by the U.S. Geological Survey have been summarized by Keller (1971). As Keller stated, the techniques used at the time were largely experimental and developmental, and were sensitive only to conductive graben sediments overlying a resistive rock basement.

In 1977, multifrequency dipole-dipole (3 and 6 km dipoles, separations to $n = 6$) galvanic resistivity measurements were made in southwestern Utah by the Department of Geology and Geophysics, University of Utah, in an attempt to describe any resistivity structure associated with the Pioche-Marysvale trend (Rowley et al., 1979; Petrick et al., 1981). The data, from a profile extending 33 km northward from the Roosevelt Hot Springs, were dominated to an unexpectedly severe degree by upper crustal, 3D lateral inhomogeneities, especially graben sedimentary fill. These inhomogeneities lead to a lack of fit of layered inverse calculations to observed data, as well as dubious 1D and 2D earth models (W.R. Petrick and A.C. Tripp, unpub.). A 3D inversion of these results (Petrick et al., 1981) presents a concentration of low-resistivity structure within 2 km of the surface, evidence again of variable basin fill dominating the observations.

Towle (1980), utilizing an interstate power transmission line as a long grounded bipole, has studied deep resistivity in eastern California with direct current magnetic field variations. A waiting period of 10 minutes was necessary to allow transients in the current to decay to negligible levels. Towle's data is consistent with a shallow return current concentration lying east of the Sierran Front in fractured rocks and sediments in the uppermost crust of the Basin and Range.

Assuming the same interstate power system as Towle to be an essentially ungrounded AC line source of current, Lienert and Bennett (1977) and Lienert (1979) advanced 1D models of resistivity

in eastern California and western Nevada to depths of 40 to 50 km. Included in their interpretation was 10-15 km thick layer of low resistivity (10-30 Ω-m) whose depth to top varied from 20 to 30 km (Figure 15). However, in light of Towle's experience, it appears that grounding terms were very important over the frequency range employed in the survey areas of Lienert and Bennett (1977) and Lienert (1979) (6-42 cycles/hr). Moreover, these authors did not evaluate quantitatively the effects of the 3D sedimentary basins common in their areas. It was shown by Ward (1983) that these structures can cause widespread distortions of EM fields to low frequencies even for ungrounded sources. Given these points, I do not believe their results demonstrated with certainty that a resistivity minimum exists in the lower crust.

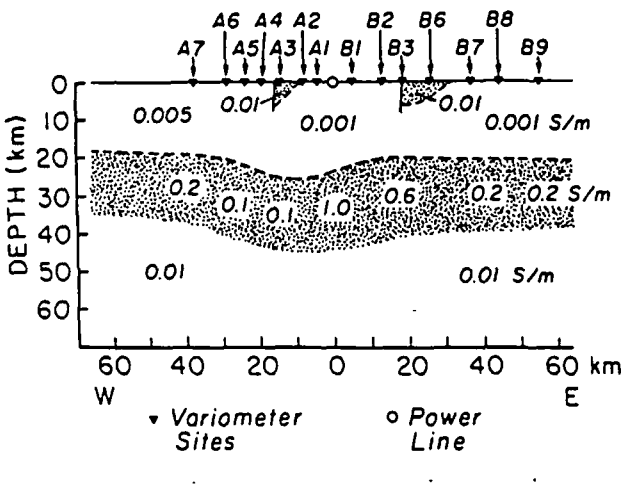

Figure 15. Cross-section of model conductivity structure beneath the Walker Lake, Nevada, district. Profile location also shown on Figure 1. Modified from Lienert and Bennett (1977).

Wilt et al. (1982) have described low-frequency CSEM soundings in the Buena Vista valley of N.W. Nevada. Through 1D inversion of the data, these authors advocate low resistivity (2-7 Ω-m) at depths of 4-7 km in basement rocks beneath the valley. A 1D inversion of a nearby MT sounding in the valley also showed relatively low resistivities (∿ 25 Ω-m) at rather shallow depths (∿ 11 km). However, Wilt et al. admit that preliminary 2D modeling suggests that 1D inversion of their CSEM data in the presence of the valley underestimated depth to conductive basement. Given the 3D model simulations of valley fill by Ward (1983) and Wannamaker et al. (1983) and the experience at the Roosevelt Hot Springs discussed previously, I take the approximate agreement between the 1D MT and 1D CSEM models at Buena Vista valley as further evidence that graben sediments seriously disrupt the CSEM observations. Again, I believe the case for widespread low resistivities at shallow depths in basement rocks of the Great Basin remains quite uncertain.

TECTONIC SIGNIFICANCE OF NORTHERN BASIN AND RANGE RESISTIVITY

The interpretation of deep resistivity at the Roosevelt Hot Springs has provided a point sampling of physiochemical conditions at depth in S.W. Utah. However, comprehension of these conditions will require consideration of the tectonic evolution of the northeastern Basin and Range during Late Cenozoic time. The model of resistivity and its implications finally are extended to the northern Basin and Range as a whole.

Evolution of Resistivity in the Northeastern Basin and Range

It is noted at the outset that the depth interval of interconnected basaltic melt corresponding to the 20 Ω-m layer in Figure 14 is significantly shallower than the seismic low-velocity zones of either the northern Basin and Range interior or the Colorado Plateau (Priestley and Brune, 1978; Thompson and Zoback, 1979), which are also interpreted to reflect partial melting in the upper mantle (Wyllie, 1979). These apparently disparate geological environments can be reconciled, with help from geomagnetic deep sounding anomalies and concepts of regional tectonic setting.

Diapirism and Melting. - Of paramount importance in fitting the deep physical state inferred in S.W. Utah to those of neighbouring regions is the well-documented, progressive concentration of extensional tectonism throughout the northeastern Basin and Range during the last 8-9 m.y. (e.g. Christiansen and McKee, 1978; Smith, 1978; Stewart, 1978; Rowley et al., 1979; Thompson and Zoback, 1979). This concentration has resulted in crustal thinning, low upper mantle velocities, bimodal volcanism and heat flow which are anomalous compared to the northern Basin and Range interior of central Nevada (Figures 16-19).

While much lithospheric extension throughout the northern Basin and Range prior to Mid-Miocene time may have been due to intrusion of calc-alkaline magmas derived ultimately from melting in the upper mantle associated with Farallon plate subduction (Zoback et al., 1981), such intrusion alone probably does not thin the crust (Gastil, 1979; Eaton, 1982). The Late Miocene to present extension defining today's horst graben morphology, however, is broadly distributed and indicates stretching and upwelling of both the crust and the upper mantle. Crustal thicknesses determined seismically hence can be used as a guide to average extension rates since the Late Miocene (see Figure 16).

If a value of 44 km for the thickness of the Colorado Plateau crust (Keller et al., 1979) can be used as a guide, then crustal thicknesses imply an average rate of extension of nearly 2% per m.y. for the northern Basin and Range interior of east-central Nevada in the last 10-12 m.y. However,

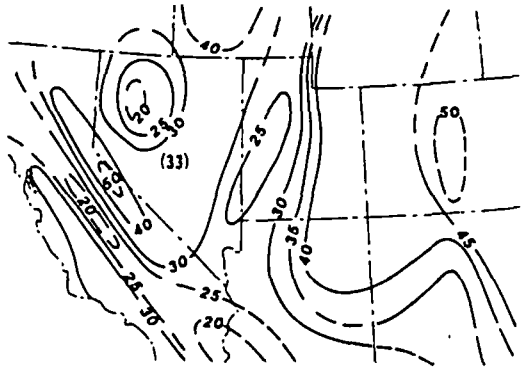

Figure 16. Crustal thicknesses in the south western United States. Contour values in kilometers. From Smith (1978), Keller et al. (1979) and Priestly et al. (1980).

about 5% per m.y. is implied for much of the northeastern Basin and Range during the last 8-9 m.y. If so, then a 1D estimate of upward velocity v of material at depth (related linearly to extension rate s and depth z through v = sz; Lachenbruch and Sass, 1978) ranges from about 1 ½ km/m.y. at 35 km through 5 km/m.y. at 100 km to over 7 km/m.y. at 160 km.

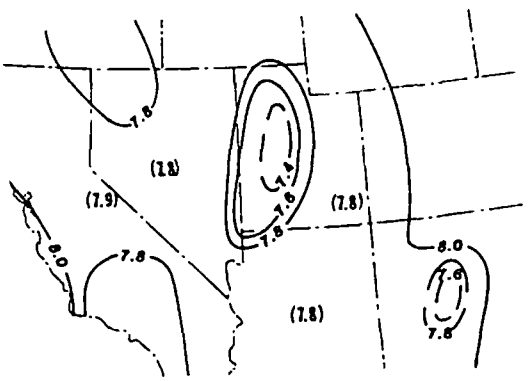

Figure 17. Uppermost mantle compressional (P_n) velocities. Contour values in km/s. From Smith (1978) and Keller et al. (1979).

While contributing a great deal to surface heat flow and temperatures within the lithosphere (Lachenbruch and Sass, 1978), extension rates tell something about the thermal state at greater depths as well. Consider for simplicity a spherical diapir in the upper mantle of radius 50 km, a representative E-W length scale for the region of enhanced tectonism defining the northeastern Basin and Range. For the thermal state of a rising diapir to be largely adiabatic (Oxburgh, 1980), its ascent time must be less than its thermal conduction time constant (Spera, 1980). If the hypothetical spherical diapir has been rising with a velocity v = 5 km/m.y. from a depth of 100 km or so during the last 8 m.y., then a distance of roughly 40 km would have been covered. In covering this distance, the diapir ascent rate merely must exceed about 0.40 km/m.y. (Spera, 1980), much less than v, for the aforesaid thermal inequality to be met. One may conclude that large volumes rising here in the upper mantle tend to retain much of their sensible heat during transport.

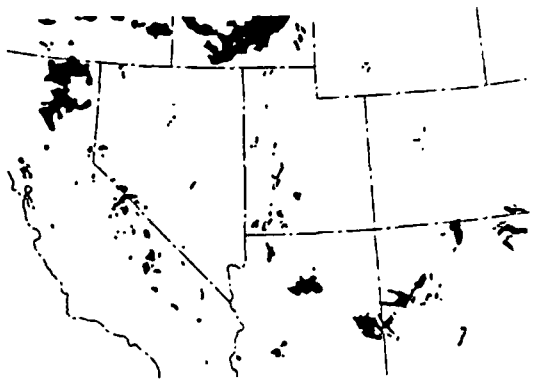

Figure 18. Distribution of volcanics less than 5 m.y. old. From Christiansen and McKee (1978), Ward et al. (1978) and Luedke and Smith (1978a, 1978b, 1981).

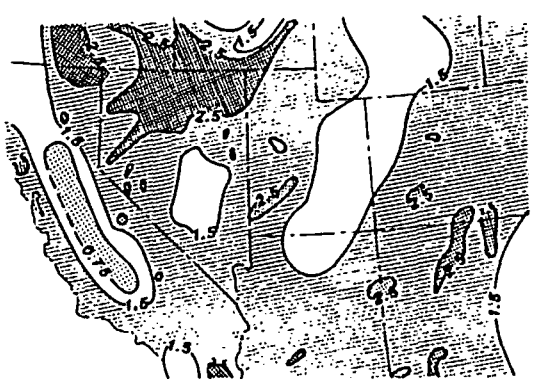

Figure 19. Surface heat flow contours in heat flow units. From Sass et al. (1981) and Bodell and Chapman (1982).

As a mass at depth rises adiabatically, its temperature trajectory may intersect the peridotite solidus so that melting will proceed (Yoder, 1976). Upon crossing the solidus, the temperature within the ascending diapir is buffered by the melting behavior of peridotite (Oxburgh, 1980). In particular, the great size of the latent heat of fusion relative to the heat capacity of peridotite along with the nearly invariant nature of basalt production serve to keep the temperature gradient within the diapir well within 1 °C/km of the solidus during adiabatic ascent (Yoder, 1976; Mysen and Kushiro,

1977; Oxburgh, 1980; Turcotte, 1982). The degree of melting is inevitably subdued through heat loss to the earth's surface from the top of the diapir (Spera, 1980).

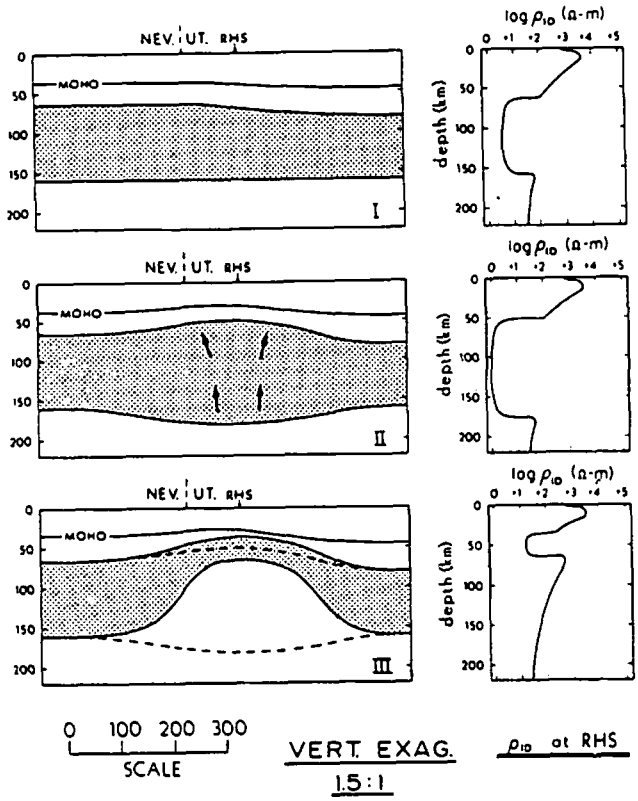

Figure 20. Schematic, highly simplified, three-stage model of evolution of resistivity structure in the eastern Great Basin. The region of continuous interconnection of melt in the upper mantle is defined by stippling and the predicted deep resistivity profile beneath the eastern Great Basin at each stage is drawn at the right side of diagram.

With this brief discussion of diapirism, I advance a schematic and highly simplified model for the Late Cenozoic evolution of deep resistivity in the northeastern Basin and Range. The model is depicted in Figure 20 in three stages: I, by about 10 m.y. ago, extensional activity responsible for the present horst-graben morphology had spread throughout the northern Basin and Range. Attendant upwelling of mantle peridotite had resulted in widely distributed, fundamentally basaltic volcanism, presumably involving the mechanism of decompression just described, along with a layer of partial melt of low melt fraction (~ 5%) which did not differ greatly from that defining the present seismic low-velocity zone of central Nevada; II, by 8 m.y. ago, the well-documented concentration of extension in the northeastern Basin and Range was underway. Accelerated diapiric uprise of mantle material leads to a further amplification of the thickness and degree of melting of the LVZ. The extent of the amplification is difficult to gauge, as it depends on the degree to which the geotherm just above and just below the former LVZ was superadiabatic (Oxburgh, 1980); III, the melt fraction in the magnified zone of fusion can build up only to a point, after which much of it drains buoyantly upward. This convection of basalts, which in effect are superheated with respect to the environment into which they rise, advances the front of melting to 35 km depth and helps establish the realm of interconnected melt corresponding to the 20 Ω-m layer of Figure 14 by warming the host peridotite during passage.

The model of present distribution of partial melting in the upper mantle of the northern Basin and Range and western Colorado Plateau in Figure 20 is similar to that of Thompson and Zoback (1979). The latter authors utilize the resistivity model of Porath (1971), however, to suggest that interconnected melt exists to a depth of about 160 km beneath the northeastern Basin and Range. Nevertheless, the magnetotelluric data preclude such an interconnection below about 65 km and the resolution by geomagnetic deep sounding of such details is doubtful (Gough, 1983). Given the chemistry of certain basaltic lavas in the northeastern Basin and Range (Wyllie, 1979; Best et al., 1980) and our model of diapiric upwelling, some melting events are probable at depths well below 65 km - they just don't result in a broad zone of interconnected liquid. On the other hand, the uniqueness of the model of Thompson and Zoback beneath the northeastern Basin and Range must be questioned.

I suggest that the zone of interconnected melt below S.W. Utah lies where it is because the very much reduced rigidity of the crystalline peridotite matrix at greater depths (Darot and Gueguen, 1981) promotes both the formation of vertical fissures under tensile stress (Spera, 1980) and the ductile collapse of the crystalline matrix as the melt leaves to enter the fissures (Stolper et al., 1981; Turcotte, 1982). In addition, any melt percolating up from great depth along intergranular passageways (Turcotte, 1982) would be impeded from rising beyond the zone of our low resistivity layer by the increasingly stiff rheology of peridotite.

Thermal State at Depth in the Eastern Great Basin. - Previously, I assigned a temperature trajectory through the deep low-resistivity layer that was coincident with the dry peridotite solidus (nominally that of Wyllie, 1979). Based upon compositions of basalts in S.W. Utah, such a thermal profile seems appropriate to depths near 100 km (op. cit.). In fact, if the abstraction of adiabatic diapiric uprise in the northeastern Basin and Range is favored, a dry solidus trajectory may be definitive to a depth exceeding 160 km.

In Figure 14, a conductive geotherm based

upon a regional heat flow of 2.4 HFU for S.W. Utah predicted fusion of dry peridotite at essentially the same depth as the top of the model low-resistivity layer. However, with the high extension rates proposed for the northeastern Basin and Range, the foregoing coincidence should not be (Lachenbruch and Sass, 1978). As a simple example, purely solid-state stretching at a rate of 5% per m.y. is consistent with a depth of melting of nearly 40 km, but a surface heat flux reaching 3 HFU is to be expected (ibid.).

One would conclude on this basis that the crust and upper mantle of northeastern Basin and Range has not reached a steady thermal state. The onset of extension is fundamentally an increase of heat flux into the lithosphere, and adjustment of surface heat flow to this form of thermal disturbance may take longer than the 8 m.y. inferred as the interval of concentrated extension in the northeastern Basin and Range (Lachenbruch and Sass, 1978; Rowley et al., 1979). By coincidence, a conductive geotherm based on present surface heat flow and a non-equilibrium convective geotherm considering the concentration of extension in the northeastern Basin and Range do not differ greatly.

Application of Interpretation to Other Areas

Attenuated crustal thicknesses in northwestern Nevada (Figure 16), the pronounced extension near Yerrington interpreted by Proffett (1977) and the concentration of rifting, heat flow and volcanism in western Nevada and southeastern California (Figure 16-19) indicate that the western margin of the northern Basin and Range experiences an enhanced degree of extension relative to the northern Basin and Range interior. The similarity in tectonic styles between the eastern and western margins of the northern Basin and Range suggests that a deep electrical structure corresponding to Stage III of Figure 20 is likeliest for the northwestern Basin and Range. The deep resistivity investigation by Schmucker (1970) permits this conclusion, but does not uniquely favor it given the limited resolution.

Another tectonic environment which probably fits into the framework of Figure 20 is the Rio Grande Rift and nearby regions. Of particular interest is the continuation of this rift zone northward into Colorado. As described by Williams (1982), extensional deformation and volcanism diminishes in this direction although some Late Tertiary mafic volcanism persists into Wyoming. In light of the modest degree of extension, I propose that the continuation of the Rio Grande Rift into Colorado may be a good place to search for deep electrical structure representing Stage II in Figure 20. The northward increase in geomagnetic deep sounding anomalies in this area (Figure 3) is furthermore suggestive of this notion, but magnetotelluric profiling with a proper multidimensional interpretation is needed to assess accurately the deep resistivity section here.

CONCLUSIONS

In active extensional environments, significant temperature perturbations may exist, possibly with interconnected melt phases, creating lateral and vertical contrasts in resistivity of an order-of-magnitude or greater. Unluckily, such environments also are attended to a large degree by upper crustal lateral inhomogeneities, especially graben sedimentary fill, whose resistivity contrast with the surrounding rock host is at least as high as that of the structures of interest at depth, and whose proximity to the surface obscures the interpretation of deep targets using electromagnetic measurements.

However, there is generally a strong preferred orientation of lithospheric deformation and upper mantle processes, and thus of the distribution of lateral resistivity inhomogeneities, in rift environments that is perpendicular to the direction of spreading. For the magnetotelluric method, a 2D transverse magnetic mode algorithm is most suitable for removing the distortion of MT soundings by such upper crustal structures and hence for assessing the resistivity of the deeper crust and upper mantle in extensional regimes. Equivalent 2D algorithms are not available for most controlled sources, although they are sorely needed.

An appropriately rigorous modeling technology has been applied to a collection of MT soundings in S.W. Utah and yielded an accurate profile of deep resistivity to depths exceeding 100 km. A feature required by the data is a low-resistivity (nominally 20 Ω-m) layer residing from about 35 to 65 km in the upper mantle beneath the Roosevelt Hot Springs. No low-resistivity layer in the middle to lower crust has been detected, however, nor do I think the case has yet been made on the basis of EM observations for such a layer to be widespread in the northern Basin and Range (cf. Eaton, 1982; Jiracek et al., 1983).

The present-day deep resistivity structure of southwestern Utah derives from the evolution of the northeastern Basin and Range through Late Cenozoic time. The low-resistivity layer interpreted in the upper mantle here is a manifestation of diapiric uprise and melting events occurring over an interval that extends to much greater depths than does the layer itself, perhaps in excess of 160 km. Both the resistivity structure and the timing and amplitude of extensional activity suggest that temperatures in the deep crust and uppermost mantle here exceed those which would be inferred from surface heat flow. Similar processes appear to be occurring in the northwestern Basin and Range, leaving central Nevada as a fairly quiescent region whose low-resistivity layering in the upper mantle, ironically, may be relatively pronounced. Unfortunately, deep resistivity surveys are lacking in the northern Basin and Range interior.

ACKNOWLEDGEMENTS

Thoughtful reviews and criticisms of this work by Drs. J.R. Bowman, D.S. Chapman, G.W. Hohmann, W.P. Nash, D.L. Nielson, W.T. Parry, W.R. Sill, C. M. Swift, Jr., and S.H. Ward are gratefully recognized. Technical assistance came from Sandra Bromley, Doris Cullen and Joan Pingree.

This work was supported by NSF contract EAR 8116602 and DOE/DGE contract DE-AC07-80ID12079.

REFERENCES

Allmendinger, R. W., Sharp, J. W., Von Tish, D., Serpa, L., Brown, L., Kaufman, S., Oliver, J., and Smith, R. B., 1983, Cenozoic and Mesozoic structure of the eastern Basin and Range province, Utah, from COCORP seismic-reflection data: Geology, 11, p. 532-536.

Best, M. G., McKee, E. H., and Damon, P. E., 1980, Space-time-composition patterns of Late Cenozoic mafic volcanism, southwestern Utah and adjoining areas: Am. J. Sci., 280, p. 1035-1050.

Bodell, J. M., and Chapman, D. S., 1982, Heat flow in the north-central Colorado Plateau: J. Geop. Res., 87(B4), p. 2869-2884.

Brace, W. F., 1971, Resistivity of saturated crustal rocks to 40 km based on laboratory measurements, In The Structure and Physical Properties of the Earth's Crust, ed. by J. G. Heacock, AGU Mono. 14, p. 243-256.

Burnham, C. W., 1979a, The importance of volatile constituents, In The Evolution of the Igneous Rocks: Fiftieth Anniversary Perspectives, ed. by H. S. Yoder, Jr., Princeton Univ. Press, p. 439-482.

_____, 1979b, Magmas and hydrothermal fluids, In Geochemistry of Hydrothermal Ore Deposits, ed. by H. L. Barnes, John Wiley and Sons, New York, p. 71-136.

Carter, J. A., and Cook, K. L., 1978, Regional gravity and aeromagnetic surveys of the Mineral Mountains and vicinity, Millard and Beaver Counties, Utah: ESL Report 77-11, 178 p.

Chapman, D. S., Clement, M. D., and Mase, C. W., 1981, Thermal regime of the Escalante Desert, Utah, with an analysis of the Newcastle geothermal system: J. Geop. Res. 86(B12), p. 11735-11746.

Christiansen, R. L., and McKee, E. H., 1978, Late Cenozoic volcanic and tectonic evolution of the Great Basin and Columbia intermontane region, In Cenozoic Tectonics and Regional Geophysics of the Western Cordillera, ed. by R. B. Smith and G. P. Eaton, GSA Mem. 152, p. 283-311.

Darot, M., and Gueguen, Y., 1981, High-temperature creep of forsterite single crystals: J. Geop. Res., 86(B7), p. 6219-6234.

Duba, A. G., Heard, H. C., and Schock, R. N., 1974, Electrical conductivity of olivine at high pressure and under controlled oxygen fugacity: J. Geop. Res., 79(11), p. 1667-1673.

Duba, A. G., and Heard, H. C., 1980, Effect of hydration on the electrical conductivity of olivine: EOS Transactions, 61(17), p. 404.

Eaton, G. P., 1982, The Basin and Range province: origin and tectonic significance: Ann. Rev. Earth Plan. Sci., 10, p. 409-440.

Gamble, T. D., Goubau, W. M., and Clarke, J., 1979, Magnetotellurics with a remote reference: Geophysics, 44(1), p. 53-68.

Gastil, R. G., 1979, A conceptual hypothesis for the relation of differing tectonic terranes to plutonic emplacement: Geology, 7, p. 542-544.

Gertson, R. C., and Smith, R. B., 1979, Interpretation of a seismic refraction profile across the Roosevelt Hot Springs, Utah and vicinity: ESL Report DOE/ID/78-1701.a.3, 116 p.

Gough, D. I., 1983, Electromagnetic geophysics and global tectonics: J. Geop. Res., 88(B4), p. 3367-3378.

Grant, F. S., and West, G. F., 1965, Interpretation Theory in Applied Geophysics: McGraw-Hill Book Company, Toronto, 584 p.

Hintze, L. F., 1973, Geologic history of Utah: Brigham Young Univ. Geology Studies, 20, pt. 3, 181 p.

_____, 1980, Geologic map of Utah: Utah Geological and Mineralogical Survey, Salt Lake City.

Jiracek, G. R., Mitchell, P. S., and Gustafson, E. P., 1983, Magnetotelluric results opposing magma origin of crustal conductors in the Rio Grande rift: Tectonophysics, 94, p. 299-326.

Jupp, D. L., and Vozoff, K., 1976, Discussion on "The magnetotelluric method in the exploration of sedimentary basins" by K. Vozoff: Geophysics, 41(2), p. 325-328.

Kariya, K. A., and Shankland, T. J., 1983, Interpretation of electrical conductivity of the lower crust: Geophysics, 48(1), p. 52-61.

Keller, G. V., 1971, Electrical studies of the crust and upper mantle, In the Structure and

Physical Properties of the Earth's Crust, ed. by J. G. Heacock, AGU Mono. 14, p. 107-125.

Keller, G. R., Braile, L. W., and Morgan, P., 1979, Crustal structure, geophysical models and contemporary tectonism of the Colorado Plateau: Tectonophysics, 61, p. 131-147.

Kirby, S. H., 1983, Rheology of the lithosphere: Reviews of Geophysics and Space Physics, 21(6), p. 1458-1487.

Lachenbruch, A. H., and Sass, J. H., 1978, Models of an extending lithosphere and heat flow in the Basin and Range province, In Cenozoic Tectonics and Regional Geophysics of the Western Cordillera, ed. by R. B. Smith and G. P. Eaton, GSA Mem. 152, p. 209-250.

Larsen, J. C., 1975, Low frequency (0.1-6.0 cpd) electromagnetic study of the deep mantle electrical conductivity beneath the Hawaiian Islands: Geop. J. Roy. Ast. Soc., 43, p. 17-46.

_____, 1981, A new technique for layered earth magnetotelluric inversion: Geophysics, 46(9), p. 1247-1257.

Lienert, B. R., 1979, Crustal electrical conductivities along the eastern flank of the Sierra Nevadas: Geophysics, 44(11), p. 1830-1845.

Lienert, B. R., and Bennett, D. J., 1977, High electrical conductivities in the lower crust of the northwestern Basin and Range: an application of inverse theory to a controlled-source deep-magnetic-sounding experiment, In The Earth's Crust, ed. by J. G. Heacock, AGU Mono. 20, p. 531-552.

Luedke, R. G., and Smith, R. L., 1978a, Map showing distribution, composition, and age of Late Cenozoic volcanic centers in Arizona and New Mexico, U.S.G.S. Miscellaneous Investigations Series, Map 1-1091-A.

_____, 1978b, Map showing distribution, composition, and age of Late Cenozoic volcanic centers in Colorado, Utah, and southwestern Wyoming, U.S.G.S. Miscellaneous Investigations Series, Map 1-1091-B.

_____, 1981, Map showing distribution, composition, and age of Late Cenozoic volcanic centers in California and Nevada, U.S.G.S. Miscellaneous Investigation Series, Map 1-1091-C.

Madden, T. R., 1971, The resolving power of geoelectric measurements for delineating resistive zones within the crust, In The Structure and Physical Properties of the Earth's Crust, ed. by J. G. Heacock, AGU Mono. 14, p. 95-105.

Mysen, B. O., and Kushiro, I., 1977, Compositional variations of coexisting phases with degree of melting of peridotite in the upper mantle: Am. Min., 62, p. 843-865.

Nash, W. P., 1983, Silicic volcanism along the eastern margin of the Basin and Range province: Utah and Idaho: GSA Abstracts with Programs, p. 402.

Oxburgh, E. R., 1980, Heat flow and magma genesis, In Physics of Magmatic Processes, ed. by R. B. Hargraves, Princeton Univ. Press, p. 161-200.

Padovani, E. R., Hall, J., and Simmons, G., 1982, Constraints on crustal hydration below the Colorado Plateau from V_p measurements on crustal xenoliths: Tectonophysics, 84, p. 313-328.

Parker, R. L., and Whaler, K. A., 1981, Numerical methods for establishing solutions to the inverse problem of electromagnetic induction: J. Geop. Res., 86(B10), p. 9574-9584.

Petrick, W. R., Pelton, W. H., and Ward, S. H., 1977, Ridge regression inversion applied to crustal resistivity sounding data from South Africa: Geophysics, 42(5), p. 995-1005.

Petrick, W. R., Sill, W. R., and Ward, S. H., 1981, Three-dimensional resistivity inversion using alpha centers: Geophysics, 46(8), p. 1148-1162.

Porath, H., 1971, Magnetic variation anomalies and seismic low-velocity zone in the western United States: J. Geop. Res., 76(11), p. 2643-2648.

Porath, H., and Gough, D. I., 1971, Mantle conductive structures in the western United States from magnetometer array studies: Geop. J. Roy. Ast. Soc., 22, p. 261-275.

Porath, H., Oldenburg, D. W., and Gough, D. I., 1970, Separation of magnetic variation fields and conductive structures in the western United States: Geop. J. Roy. Ast. Soc., 19, p. 237-260.

Priestley, K., and Brune, J. N., 1978, Surface waves and the structure of the Great Basin of Nevada and western Utah: J. Geop. Res., 83 (B5), p. 2265-2272.

Priestley, K., Orcutt, J. A., and Brune, J. N., 1980, Higher-mode surface waves and structure of the Great Basin of Nevada and western Utah: J. Geop. Res., 85(B12), p. 7166-7174.

Proffett, J. M., Jr., 1977, Cenozoic geology of the Yerrington district, Nevada, and implications for the nature and origin of Basin and Range faulting: GSA Bull., 88, p. 247-266.

Rai, C. S., and Manghnani, M. H., 1978, Electrical conductivity of basalts to 1550°C, In Proceedings of Chapman Conference on Partial Melting in the Earth's Upper Mantle, ed. by H. J. B. Dick, Oreg. Dept. Geol. Min. Ind., Bull. 96, p. 219-232.

Reitzel, J. S., Gough, D. I., Porath, H., and Anderson, C. W., III, 1970, Geomagnetic deep soundings and upper mantle structure in the western United States: Geop. J. Roy. Ast. Soc., 19, p. 213-235.

Rijo, L., 1977, Modeling of electric and electromagnetic data: Ph.D. Thesis, Dept. of Geology and Geophysics, Univ. of Utah.

Ross, H. P., Nielson, D. L., and Moore, J. N., 1982, Roosevelt Hot Springs geothermal system, Utah - case study: Am. Assoc. Petr. Geol. Bull., 66(7), p. 879-902.

Rowley, P. D., Steven, T. A., Anderson, J. J., and Cunningham, C. G., 1979, Cenozoic stratigraphic and structural framework of southwestern Utah: U.S.G.S Professional Paper 1149, 22 p.

Sass, J. H., Blackwell, D. D., Chapman, D. S., Costain, J. K., Decker, E. R., Lawver, L. A., and Swanberg, C. A., 1981, Heat flow from the crust of the United States, in Physical Properties of Rocks and Minerals, ed. by Y. S. Touloukian and C. Y. Ho, McGraw-Hill/CINDAS Data Series on Material Properties, II-2, New York, p. 503-548.

Schmucker, U., 1970, Anomalies of geomagnetic variations in the southwestern United States, Bull. Scripps Inst. Oceanography, 13, 165 p.

Smith, R. B., 1978, Seismicity, crustal structure and intraplate tectonics of the interior of the western Cordillera, In Cenozoic Tectonics and Regional Geophysics of the Western Cordillera, ed. by R. B. Smith and G. P. Eaton, GSA Mem. 152, p. 111-144.

Spear, F. S., and Silverstone, J., 1983, Water exsolution from quartz: implications for the generation of retrograde metamorphic fluids: Geology, 11(2), p. 82-85.

Spera, F. J., 1980, Aspects of magma transport, In Physics of Magmatic Processes, ed. by R. B. Hargraves, Princeton Univ. Press, p. 265-324.

Stanley, W. D., Wahl, R. R., and Rosenbraum, J. G., 1976, A magnetotelluric study of the Stillwater-Soda Lakes, Nevada, geothermal area: U.S.G.S. Open-File Report 76-80, 38 p.

Stanley, W. D., Boehl, J. E., Bostick, F. X., Jr., and Smith, H. W., 1977, Geothermal significance of magnetotelluric soundings in the Snake River Plain - Yellowstone region: J. Geop. Res., 82(17), p. 2501-2514.

Stewart, J. H., 1978, Basin and Range structure in western North America: a review, In Cenozoic Tectonics and Regional Geophysics of the Western Cordillera, ed. by R. B. Smith and G. P. Eaton, GSA Mem. 152, p. 1-31.

_____, 1980, Geology of Nevada: Nevada Bureau of Mines and Geology Special Pub. 4, 136 p.

Stodt, J. A., 1978, Documentation of a finite element program for solution of geophysical problems governed by the inhomogeneous 2-D scalar Helmholtz equation: NSF Program Listing and Documentation, ESL, 66 p.

_____, 1983, Bias removal for conventional magnetotelluric data: ESL report, in press, Salt Lake City.

Stolper, E., Walker, D., Hager, B. H., and Hays, J. F., 1981, Melt segregation from partially molten source regions: the importance of melt density and source region size: J. Geop. Res., 86(B7), p. 6261-6272.

Swift, C. M., 1967, A magnetotelluric investigation of an electrical conductivity anomaly in the southwestern United States: Ph.D. thesis, Massachusetts Institute of Technology, 211 p.

Thompson, G. A., and Zoback, M. L., 1979, Regional geophysics of the Colorado Plateau: Tectonophysics, 61, p. 149-181.

Ting, S. C., and Hohmann, G. W., 1981, Integral equation modeling of three-dimensional magnetotelluric response: Geophysics, 46(2), p. 182-197.

Towle, J. N., 1980, Observations of a direct current concentration on the eastern Sierran front: evidence for shallow crustal conductors on the eastern Sierran front and beneath the Coso Range: J. Geop. Res., 85(B5), p. 2484-2490.

Turcotte, D. L., 1982, Magma migration: Ann. Rev. Earth Plan. Sci., 10, p. 397-408.

Vozoff, K., 1972, The magnetotelluric method in the exploration of sedimentary basins: Geophysics, 37(1), p. 98-141.

Waff, H. S., and Bulau, J. R., 1979, Equilibrium fluid distribution in an ultramafic partial melt under hydrostatic stress conditions: J. Geop. Res., 84(B11), p. 6109-6114.

Wannamaker, P. E., Hohmann, G. W., and Ward, S. H., 1983, Magnetotelluric responses of three-dimensional bodies in layered earths: submitted to Geophysics.

Ward, S. H., 1967, Electromagnetic theory for geophysical application, In Mining Geophysics, II, Society of Exploration Geophysics, Tulsa, p. 10-196.

Ward, S. H., 1983, Controlled source electrical methods for deep exploration: Geop. Surv., in press.

Ward, S. H., Parry, W. T., Nash, W. P., Sill, W. R., Cook, K. L., Smith, R. B., Chapman, D. S., Brown, F. H., Whelan, J. A., and Bowman, J. R., 1978, A summary of the geology, geochemistry and geophysics of the Roosevelt Hot Springs thermal area, Utah: Geophysics, 43(7), p. 1515-1542.

Weinstock, H., and Overton, W. C., Jr., 1981, SQUID applications in geophysics: SEG, Tulsa, 208 p.

Wernicke, B., and Burchfiel, B.C., 1982, Modes of extensional tectonics: J. Struc. Geol., 4(2), p. 105-115.

Williams, L. A. J., 1982, Physical aspects of magmatism in continental rifts, In Continental and Oceanic Rifts, ed. by G. Palmasson, AGU Geodynamics Series, 8, p. 193-222.

Wilt, M. J., Goldstein, N. E., Haught, J. R., and Morrison, H. F., 1982, Deep electromagnetic soundings in central Nevada: Expanded abstract of paper presented at the 52nd annual meeting of the SEG, Dallas, TX.

Winkler, H. C. F., 1979, Petrogenesis of metamorphic rocks: Fifth ed., Springer-Verlag, New York, 348 p.

Word, D. R., Smith, H. W., and Bostick, F. X., Jr., 1971, Crustal investigations by the magnetotelluric impedance method, In The Structure and Physical Properties of the Earth's Crust, ed. by J. G. Heacock, AGU Mono. 14, p. 145-167.

Wyllie, P. J., 1979, Petrogenesis and the physics of the earth, In The Evolution of the Igenous Rocks: Fiftieth Anniversary Perspectives, ed. by H. S. Yoder, Jr., Princeton Univ. Press, p. 483-520.

Yoder, H. S., Jr., 1976, Generation of basaltic magma: National Academy of Sciences, Washington, 265 p.

Zoback, M. L., Anderson, R. E., and Thompson, G. A., 1981, Cenozoic evolution of the state of stress and style of tectonism of the Basin and Range province of the western United States: Phil. Trans. Roy. Soc. Lond., A 300, p. 407-434.

June 9, 1987

MEMO TO:

All parties interested in ESL/UofU MT system development

FROM:

John A. Stodt

RE:

Comparison of Electromagnetic Instruments, Inc. (EMI) portable MT system with current ESL/UofU MT system and planned upgrades. Status of the upgrade project. Directions for future upgrades.

Stan has recently received a description of the new EMI MT-1 portable MT system which he has made available to me for assessment and comparison with our current system and its planned upgrades. The purpose of this memo is twofold, first to compare the EMI system with our own system and planned upgrades, second to appraise everyone of the nature of the upgrades currently under way and to indicate desirable follow on work for which additional funding must be secured.

EMI MT-1 System Description

The EMI MT-1 system is configured as four modules; the B-Field sensors/preamps and Power Supply (BF-4B or Bf-5 or BF-6, and BFPS-1), the E-Field Signal Conditioner (EFSC-1) and electrodes, an Acquisition and Processing Unit (APU-12 or APU-16), and a suitable IBM PC compatible system computer. Analog signals are brought into the APU, which consists of:

a) CIM 800 CMOS computer, 160K RAM, RS-232 interface
b) multiplexer and 12 or 16 bit A/D (APU-12 or APU-16)
c) digital interface board
d) analog interface board
e) Signal Acquisition Boards (SAB), one for each channel.

The APU can accomodate up to 10 channels of analog inputs and presents an RS-232 interface for connection to the external system computer which, for example, can be an IBM PC compatible portable laptop such as the Toshiba Model 1100+.

The CIM 800 computer controls low level data acquisition functions and buffers sampled data for transmission to the system computer. Its operation is in turn controlled by the system computer. The system computer provides control for the APU, acquires data from the APU, and can display or process data to obtain MT parameters.

The MT-1 system has low and high frequency modes of operation. In the low frequency mode (.001 Hz - 40 Hz), input signals are conditioned by the SAB, multiplexed, and converted to digital 512 point time series which are buffered in the APU before being sent to the system computer for processing. In the high frequency mode (2 Hz - 20 KHz) a 12 bit dynamic heterodyne conversion scheme is used wherein input data is multiplied in the SAB by sine and cosine waveforms of preselected frequencies to give running estimates of the Fourier coefficients. The Q of the data window selected for processing can range from 1 to 2000. An automatic system calibration of the APU can be run in high frequency mode just prior to collection of data. Time series can be stored in low frequency mode with the addition of a suitable storage device to the basic MT-1 system at the expense of greater power consumption. Only Fourier coefficients are available in high frequency mode.

Power consumption is stated as less than 20 Watts for the APU and sensors when configured for 10 channel operation. Power consumption of the system computer must be added to this figure.

The MT-1 APU is delivered with battery packs suitable for up to 8 hours of continuous operation. The EFSC-1 signal conditioner can sustain up to 3 days continuous operation.

ESL/UofU MT System Description

Current system configuration.

Our MT system is currently based on an in house computer system built with a DEC PDP-11/23 processor and an 8 Mbyte Winchester disk. Seven channels of data can be acquired simultaneously, allowing remote reference operation. A recording truck houses the computer system and an eight channel chart recorder. Preamplified analog signals are brought to the recording truck over approximately 100 m of cable. This allows approximately 200 m of separation between the reference and local data sites. We currently use an H-field reference. At the truck, the analog signals pass through line receivers to Programmable Filter (PF) cards (one per channel) for final signal conditioning prior to digitization with a 14 bit A/D converter. The PF cards, sampling, and A/D conversion are controlled by the computer. The E-field measurements are conditioned and preamplified at the measurement site with a programmable signal conditioner with differential inputs. Line drivers send the conditioned signals to the recording truck. Power for the E-field signal conditioner and line drivers is currently supplied from the recording truck over the same cable used to send the signals back to the truck. Configuration information is sent form the recording truck to the E-field signal conditioner over the same cable, allowing remotely controlled setup.

The H-field measurements are currently obtained with Geotronics coils donated to us by Mobil Oil Co. The local site coils contain preamplifiers and signal conditioning at the coil heads; the amplified signals are delivered over a short cable to a box containing line drivers, which in turn deliver the signals to the recording truck. The coils at the reference site do not have preamplifiers and signal conditioning at the coil heads; instead, the raw signals from the coils are delivered over a short cable to a box containing preamplifiers and signal conditioning. Line drivers in the box deliver the conditioned signals to the recording truck. Both sets of H-field sensors have a High and a Low gain setting which is switch selectable from the recording truck. Both sets of H-field sensors are currently battery powered, with several days of operation possible before recharging is necessary.

Power for the recording truck (and, consequently, the E-field signal conditioner) is supplied by a trailer mounted motor-generator. A large amount of effort has been expended (translate: money, time, lost opportunity to collect data) to isolate this power source from the measurements. With the exception of the H-field sensors, power requirements for the current system are large because no attempt was made in the original design to address battery powered operation. The E-field signal conditioner requires about 40 watts, and the recording truck equipment, including the chart recorder, requires several hundred watts. Air conditioning is required in the recording truck on hot days to maintain the equipment at reasonable operating temperatures at this level of power dissipation. Data below 2 Hz is acquired, processed, and archived in real time by an algorithm based on decimation processing. Up to ten levels of decimation can be handled in the current program. This allows data to be collected over a nine octave band in a single run. In practice, data are normally acquired in two bands, a mid-band (2 Hz - 0.1 Hz) and a low band (0.25 Hz - 0.0005 Hz). These bands are currently acquired in separate runs due to different signal conditioning requirements. Data is acquired continuously in the selected band until the operator is satisfied with data quality and terminates a run.

A separate program and strategy are used to collect data above 2 Hz because the current system can no longer process all incoming data in real time above 2 Hz, and because the character of the data becomes impulsive at the higher frequencies. Data are acquired a pair of frequencies at a time starting at the knee of the anti-alias filter, using 12th and 16th harmonic sine and cosine correlations. The operator switches the anti-alias filter knee (and consequently the sampling rate) under program control to acquire data at a different pair of frequences. Data can usually be acquired over a two to three octave bandwidth before it is necessary to readjust the gain settings for further data

collection. We are presently limited to an upper frequency of 125 Hz due to the speed of our current A/D converter.

Both the low and high frequency data collection algorithms incorporate initial data quality assessment based on amplitudes of the incoming signals, followed by sorting procedures based on multiple coherence function evaluations applied to subsets of the incoming data to exploit nonstationary behavior of the field measurements. The data quality assessment and multiple coherence sorting are performed in real time as the data are collected.

Current upgrading program.

A remote H-field reference capability was successfully added to the system last year and is part of the current upgrade program. Our reference is made from equipment donated by Mobil Oil Co. and modified for integration into the system, as discussed above.

We also replaced our motor-generator and reworked the power delivery to the recording truck, using one five wire cable in place of two separate three wire cables for delivery of generator and Uninterruptible Power Supply (UPS) backed power. Additional transformer isolation of the generator power was incorporated to reduce noise. We now have a much more reliable motor-generator system, and the use of one power cable instead of two has reduced setup time and the potential for creation of additional noise sources due to an inappropriate placement of separate power cables.

Unfortunately, we have had to spend time trying to work around the poor design of the donated Mobil Oil Co. equipment. Dale has spent several weeks reworking the reference field amplifiers and power distribution in an attempt to reduce crosstalk between the channels arising from poor design. Additional field tests were also required to verify correct operation after modifications were made.

The items discused in the previous two paragraphs were not budgeted in the current upgrade program but were necessary to support ongoing operations. Consequently, our ability to complete the planned upgrade program within the original budget has been jeopardized, primarily in the area of salary support for Dale.

Although we have a functioning MT system, it suffers from a number of deficiencies which I am trying to correct with Dale's help. Within our current budget we will not be able to remake the system completely into the state of the art instrument I would like to build, but we will improve the system substantially with the following changes:

1) Convert to battery powered operation at the measurement sites and incorporate digital data communications from both the local and reference measurement sites to the recording truck. We had initially planned to do this with fiber optic links but have abandoned this approach in favor of a new transceiver/modem product (ESTeem wireless modem) which will provide error checked packetized radio communications and networking over ranges up to 30 miles under favorable conditions (manufacturer's claim). Note that this is a major change, requiring ALL analog processing and A/D conversion to be done at the measurement sites. This will require low power diskless computer subsystems to be built to control the hardware for data collection. This hardware must be controlled remotely from the recording truck via the digital communications links.

2) Shift from DEC PDP-11 technology to IBM PC technology. This is a move from a high cost, high power requirement hardware environment to a low cost, low power requirement hardware environment. The appropriate hardware and software products to provide a CONVENIENT and CHEAP development environment to produce stand alone low power diskless subsystems with PC-based technology became available about the 3rd quarter of last year.

3) Design and build low power 16 bit A/D converters and Sample/Hold cards. Currently available commercial "16 bit" A/D cards have high power requirements and do not typically give full 16 bit resolution.

4) Abandon the use of Winchester disks in the field, and use static RAM disks instead.

5) Abandon the eight channel mechanical strip chart in favor of an electronic strip chart device compatible with the IBM PC.

6) Modify the E-field signal conditioner for battery operation and for control from the PC based computer subsystem. Modify our H-field sensor/preamp subsystems for operation and control from the PC based computer subsystem.

7) Incorporate notch filters on the PF cards. This is the only reasonable location within our current system to provide notch filters for the H-field measurements. We currently have no notches available for the H-field measurements.

8) Modify the E-field signal conditioner analog cards and the PF cards to simplify their operation and calibration. Remove the Q-Bus interface from the PF cards and substitute static I/O line controls to manipulate programmable hardware.

9) Develop a simplified calibration scheme for the modified hardware.

10) Construct an appropriate battery charging system to service the instrument batteries.

When these changes are completed our system will be configured as follows. Equipment at the recording truck will consist of an IBM PC AT computer and appropriate expansion cards to provide serial ports for communications, a static RAM disk, and the electronic strip chart capability mentioned above. The system will have floppy disks and a battery backed static RAM disk (no Winchester disk). One or two ESTeem wireless modems will provide communications to the local and reference measurement sites. The recording truck will still be powered by a motor generator, which will also be used to drive a battery charging system to service spare sets of instrument batteries while data is being collected. Note that the instrumentation at the measurement sites will not be physically connected to the recording truck and its power source. We will have the potential to operate the local and reference sites with separ-ations of as much as 60 miles under favorable conditions (if manufacturer's claims for the ESTeem wireless modems are accurate).

Instrumentation at the measuring sites will consist of an ESTeem wireless modem (with battery power source) connected via RS-232 link to a signal conditioning and processing box. This box will contain a diskless computer subsystem to control data collection, PF cards from our current system modified to operate in the new environment, the Sample/Hold and 16 bit A/D cards described above, and separate power supplies to operate the digital and analog hardware in the processing box, and the sensors connected to it. The signal conditioning and processing box is being designed to handle a maximum of seven channels of data because this number is convenient given our current packaging. The box is also being designed with a sensor interface flexible enough to handle any of our sensors, to provide interchangability and minimize the problem of back up in case of hardware failure. Although each signal conditioning and processor box will handle up to seven channels of data individually, we will only have the capability to process a total of seven channels of data from all measurement sites at the conclusion of the current upgrading program because we only have seven PF cards available to modify.

Our current E and H field sensor/preamp combinations will be modified to integrate with and be controlled from the processor box. The E-field signal conditioner must be modified additionally for battery powered operation.

I anticipate at least initially providing essentially the same operating modes for data collection in the new system as is available in the current system. This is not because I don't have any more ideas for improvements, but rather because remaking the current system control, processing, and calibration software

for the new environment will occupy the bulk of my time on this upgrade.

Major Differences Between the EMI and ESL/UofU(upgraded) Systems:

1) The EMI system has a high frequency mode which uses heterodyne detection to collect data in the range from 2 Hz to 20 kHz. This has proved to be a very good way to collect AMT data and gives the EMI system the potential to be used as an active source EM receiver, if appropriate synchronization and transmitter control can be provided. A new instrument project would be required for us to develop a similar capability, either in a separate instrument or as an option to be integrated with our current MT system.

2) For data collection below 40 Hz, the EMI system uses FFT processing with 512 point data sequences. This provides estimates over a 4 to 5 octave bandwidth from an individual run. Our system uses decimation processing and can produce estimates over a 9 octave bandwidth in a single run. In addition to allowing data collection over a wider bandwidth, I believe decimation processing allows better exploitation of nonstationary behavior of the field measurements. I speculate that even the rudimentary quality assessment and sorting schemes I have implimented in our present system are at least as sophisticated, if not more so, than any other schemes currently in use for data assessment and selection. These schemes have proven to be a major advantage of our system over others currently in use.

3) The EMI APU box is designed to acquire ten channels of data from analog inputs. The system is supplied with 50 m cables which implies a station separation of 100 m maximum. The EMI brochure states that longer cables could be supplied but the maximum usable length has not been determined. Line drivers at the sensors are mentioned as a possibility to increase station spacing using direct analog connections, at the expense of greater power consumption. The disadvantages of this standard configuration for remote reference operation with wide station spacings are obvious. The EMI brochure refers to analog or digital telemetry, or clocks, as other possibilities for remote reference operation. Analog telemetry limits dynamic range to about 50 dB (equivalent to between 8 and 9 bits of resolution), while operation with clocks, or with digital telemetry using either radios or a fiber optic link, would require two APUs. In addition, operation with clocks would sacrifice the ability to process, reduce, and assess the data in real time.

Our upgraded system is being designed for remote reference operation using digital radio telemetry. Two primary advantages of this approach are that the measurement sites are disconnected from the recording truck and its power source, and it is possible to work with much larger separations between base and reference

stations than is feasible with wire or fiber optic links. One disadvantage of radio telemetry is that of potential licensing problems for work outside the USA. Our system could be reconfigured to operate with fiber optic links in this case, with some additional work.

4) The EMI E-field signal conditioner is designed with two single ended inputs sharing a common ground. Low and high pass filtering is performed prior to amplification of up to 40 dB, whereupon the analog signal is optically isolated from subsequent system hardware. We (Dale, Steve, and I) are very suspicious of this type of design for the front end processing of E-field measurements and offer the following discussion:

a) The use of single ended inputs allows signal conditioning to be performed prior to amplification at the expense of sacrificing the common mode rejection available by using differential amplifiers at the inputs. Conversely, a differential input configuration can provide 80-100 dB attenuation of common mode noise, but allows only minimal signal conditioning (e.g., a low pass filter integrated with the differential amplifier) prior to amplification to retain a high level of common mode rejection. In our opinion, the advantages of high common mode rejection far outweigh the advantages of substantial signal conditioning prior to amplification.

b) The single ended input configuration is more susceptible to introducing noises which are correlated between channels into the measurements. Examples are the electrode noise of the common electrode, and the noise generated due to bias current noise from the amplifiers of either channel passing back through non-zero electrode impedances. Note that thermal effects in either amplifier can cause fluctuations in bias current noise which could introduce additional correlated noise into both channels.

c) The optical isolation of the analog signal is apparently an attempt to avoid common mode system noise. However, it is difficult to design optical isolation to operate linearly over a wide dynamic range. Steve estimates 40 to 60 dB maximum dynamic range (7 to 10 bits) for linear operation, and Dale was skeptical even of these figures. Another potential problem is that of capacitive coupling across the optical isolation. Note that the EMI brochure shows that the APU system ground is brought out to the signal conditioner and represents a potential RF noise source which could couple capacitively across the optical isolation. Another potential problem which optical isolation does not solve is that of common mode noises other than those produced from ground loops in the system; see item b) above.

5) The EMI MT system APU uses a CIM 800 computer as a controller. The CIM 800 is based on a Z80 microprocessor and has a maximum of 160 K of RAM memory. In contrast, our upgraded system processing boxes will be controlled with CMOS IBM PC-XT compatible computers

running MS-DOS from a static RAM disk. This configuration gives us a number of advantages, including:

a) Compatibility with a wide variety of readily available expansion board hardware products designed for the IBM PC.
b) Greater memory capacity, 640K for the IBM vs 160K for the CIM.
c) Faster, more powerful microprocessor.
d) Compatibility with high level language development tools (e.g., FORTRAN and C compilers, debuggers, real time multitasking libraries, communications libraries, etc.) to create or modify applications.

These advantages allow greater flexibility and speed in applications development and modification.

6) Finally, I address the issue of portability. The EMI system has been designed for maximum portability of the entire system, using battery power throughout. Our upgraded system will not be portable in its entirety, but is designed with a different view toward portability. Specifically, Dale and I are making the measurement site instrumentation as portable and as flexible as the current budget will allow while working within the constraints imposed by our existing hardware, but have retained the use of a mobile motor-generator power source and a recording truck from which an operator coordinates data acquisition, for our standard system configuration. This configuration offers a number of advantages, namely:

a) The operator and recording truck equipment are protected effectivly from sudden changes in the weather. A comfortable operating environment (i.e., air conditioning in hot weather and heat in cold weather) can be provided for the field crew, which I believe is important during extended field operations to reduce fatigue and the mistakes it induces.
b) The motor-generator provides a power source for recharging batteries to allow continuous field operations.
c) Greater in field processing and analysis capabilities can be provided because the requirements of low power and portability are less stringent for the equipment at the recording truck.
d) Simultaneous data acquisition from multiple measurement sites can be coordinated continuously from the recording truck.
e) The advantages provided by the recording truck/motor-generator combination are realized while retaining most of the advantages of a truly portable system, if the measurement site equipment is made as portable as possible and digital radio links are used for communications.

At the completion of our current upgrading program, a complete five channel measurement at a given site will require the following hardware:

a) Hx, Hy, and Hz sensors and primary signal conditioning (Geotronics coils/preamps + junction box, or coils + preamp/junction box).
b) Ex and Ey sensors and primary signal conditioning (Five PbCl pots and connecting wire, and an E-field signal conditioning box).
c) Signal conditioning and processing box. Contains signal conditioning cards, sample/hold and sequencing card, computer subsystem with 16 bit A/D converter, and power supplies/batteries.
d) ESTeem wireless modem, power source (e.g., 20 AH 12V battery), and antenna.
e) Miscellaneous cabling.

The most unwieldy components in this list are the Geotronics coils, and our current E-field connecting wire and set of five PbCl pots. The other components will be similar in size and weight to the EMI system's APU, EFSC-1, and BFPS-1 components, with the exception of the greater battery reserves required to operate the ESTeem modem and to meet the power requirements of our other hardware. Although we are working to minimize the power requirements while modifying our current hardware for the upgrade, the original designs were not made with battery powered operation as a primary consideration. Complete redesign of our analog hardware would be benificial, but is not possible within our current budget.

Note that our signal conditioning and processing box is designed with a serial interface, which could just as well be connected to a portable computer for control. This configuration would provide a mode of operation essentially identical to that of the EMI system, except that our data processing is different and our signal conditioning and processing box will handle seven channels maximum. Seven channels is sufficient to provide a reference, but not two simultaneous stations, using one signal conditioning and processing box. It should be apparent from this discussion that we will be close to having developed a portable MT system at the conclusion of our current upgrade program. Portability could be enhanced further as follows:

a) Replace our current E-field and H-field sensor systems with more portable components.
b) Redesign our analog hardware with low power operation a primary consideration.
c) Repackage the system professionally, rather than using odd sized army surplus boxes and donated Mobil Oil Co. packaging as a cost saving measure, as we are currently doing.

Future Upgrades of the ESL/UofU MT System:

Although we will have a substantially improved MT system at the conclusion of our current upgrade program, there are a number of items left unaddressed which would improve the system further. Efforts at improvement can be divided into three general categories; a) designs to increase the signal to noise ratio of the system, b) designs to improve operational efficiency, including portability, and c) improvements in processing algorithms to produce more accurate estimates of the transfer functions from available data.

We are, of course, always looking for lower noise components and better designs to improve the system's signal to noise ratio. A new amplifier has become available which could potentially improve our system and we will evaluate its use in future upgrades. However, our most pressing problems in this area appear to be with our H-field measurements at the reference site. Recall from previous discussions that the preamplifiers for our local H-field measurements are packaged with the coils, while the preamplifiers for our reference H-field measurements are packaged in a separate box and are each connected to a coil with approximately 30 feet of cable. Experience with this configuration indicates that the reference H-field measurements are far more susceptible to electromagnetic interference than are the local H-field measurements. One solution is to redesign the H-field preamplifier and package the new design with the reference coils. In addition, the local site preamps should be replaced with the new design. The current local site H-field preamplifiers should be redesigned, rather than copied, to correct deficiencies in the old Mobil Oil Co. design. This approach will require a significant outlay of time and money. Before such an expenditure is made, it is worthwhile to consider replacement options for both the local and reference site H-field sensors to improve portability as well as operational characteristics. At least four replacement options should be explored: a) EMI coils, b) Phoenix Geophysics coils, c) AET (Geotronics) coils, and d) ring core fluxgate magnetometers. Other possibilities include any new SQUID sensors developed based on the new high temperature superconducting materials recently discovered, and any new sensors based on fiber optic technology. I don't know of any commercial sensors developed and currently available which use these two technologies, however.

Operational efficiency and portability of our upgraded system could be enhanced substantially through redesign of the analog hardware. The changes in hardware described below are primarily aimed at improving operational efficiency in the field in order to boost production.

Our current system allows an MT sounding over the frequency range from 125 Hz to .0005Hz to be acquired in approximately 1.5 days under the best circumstances. However, it is not uncommon to spend between 2 and 3 days acquiring data at a single site.

There are two primary factors which impede more efficient data collection with our system:

a) The setup time required with our current system is large. This time will be reduced substantially at the completion of the current upgrade program. In particular, we will trade the time required to establish wire links to the local and reference sites for the time required to erect simple dipole antennas for radio communications. In addition, the recording truck and reference locations can potentially be chosen to allow communications between a number of MT station locations so that only one set of measurement site hardware need be moved to collect data at a new site. Although these developments should improve our ability to collect data expeditiously, further developments to improve setup time are possible.
b) Data in separate bands must be acquired sequentially with our system. This mode of operation is a particular handicap to the efficient acquisition of high quality data in both the mid and low bands because of the nonstationary behavior of the MT signals. I believe the time spent acquiring high quality data at a site would be reduced substantially if data could be acquired simultaneously in both the mid and low bands, thus maximizing the chances of recording data at times of high signal activity in each band.

Setup time could be further reduced if more manageable E-field and H-field sensor combinations could be identified and incorporated with the system, if all analog hardware were redesigned with low power operation and simplified operation as primary considerations, and if better (i.e. lighter, more compact) packaging was implimented. The capability to record data simultaneously in the mid and low bands could be implimented in our upgraded system by redesigning the PF cards to provide two separate signal paths for conditioning appropriate to the mid and low bands. Two sets of sample and hold amplifiers could be used to acquire the data in the separate bands. The timing for sampling and subsequent sequencing of the A/D converter would also require redesign to multiplex the measurements. Operating software would obviously have to be reworked to provide for simultaneous data reduction.

I believe better processing algorithms can be developed to improve estimation of impedances from the measured data. In particular, I believe that decimation and FFT processing can be combined advantageously to provide more flexible processing. In addition, the complete set of recommendations I outlined in the 1982 DOE reports and in my dissertation have not been implimented fully in our current system due to space limitations in the RT-11 environment. These recommendations included weighted averaging at the spectral level, and separate processing for "XY" mode, "YX" mode, and Tipper based on analysis of three separate dual input single output linear system models, each with Hx and Hy inputs,

and with Ex, Ey, or Hz as the output. We currently apply lower and upper amplitude cutoff criteria to incoming data, and subsequently sort the screened data according to multiple coherence criteria developed for sensitivity to the "XY" and "YX" modes, but weighted averaging and separate treatment of the Tipper functions have not been implimented.

It is becoming increasingly apparent that a very serious and sometimes nearly ubiquitous problem exists in the processing of MT data with regard to the recognition and rejection of data contaminated by source effects, introduced by proximity to cultural or natural sources. The methods reported recently by Chave, et al., (1987) appear to provide some discrimination. I believe further progress can be made in this area with proper application of matrix norm theory to the linear equation sets which are generated to solve for the transfer functions. The idea behind this approach is to identify and use only those data sets which are consistent with a linear model having time invariant transfer functions.

Finally, I mention the possibility of developing a separate long period instrument for low frequency MT measurements, and of developing instrumentation to improve our collection of AMT data. It may be worthwhile to consider a separate very portable AMT system rather than trying to integrate these measurements with our MT system. A separate system would provide additional flexibility. For example, it could be designed to work as a CSAMT receiver and transmitter controller as well as a passive AMT system. It could provide the ability to make AMT measurements as part of site selection and preparation for subsequent MT measurements.

I am currently developing proposals to address future hardware development based on the information provided in this memo. Discussion and comments are welcome.